Case Studies in Small Animal Diagnostic Imaging

Alexane Durand

Degrees

Submitted in fulfilment of the requirements for the

Degree of Master of Veterinary Medicine

University of Glasgow

School of Veterinary Medicine

Month 2013

Summary

A set of 15 cases with a variety of clinical problems were analysed with specific reference to imaging tools and interpretation.

Table of Contents

Summary i

Table of Contents ii

List of Figures iii

Table of Appendix viii

List of Abbreviations ix

Declaration xi

Acknowledgements xii

Clinical cases xiii

Case 1. Hiatal Hernia 14

Case 2. Vascular Ring Anomaly 21

Case 3. Severe Ileitis 28

Case 4. Histiocytic sarcoma 37

Case 5. Extra Hepatic Porto-Systemic Shunt 45

Case 6. Thoracic Mass causing Budd-Chiari-like Syndrome 52

Case 7. Sub-lumbar Foreign Body 61

Case 8. Feline Conn's Syndrome 69

Case 9. Mechanical ileus 78

Case 10. Parasitic pneumonia 87

Case 11. Gallbladder Rupture secondary to Biliary Mucocoele 97

Case 12. Bronchial Carcinoma 104

Case 13. Ependymal Cyst 115

Case 14. Oesophageal Foreign Body 124

Case 15. Bilateral Radial Hemimelia 130

Appendix 136

Appendix 1 - Diagnostic Imaging Equipment 137

List of Figures

Figure 1.1 - Dorso-ventral thoracic radiograph....20
Figure 1.2 - Right lateral thoracic radiograph....20
Figure 1.3 - Left lateral thoracic radiograph....20
Figure 1.4 - Right lateral abdominal radiograph....20
Figure 1.5 - Left lateral abdominal radiograph....20
Figure 2.1 - Transverse CT angiogram image demonstrating the marked dilation of the cranial thoracic oesophagus (Arterial phase)....27
Figure 2.2 - Transverse CT angiogram image showing the narrowing of the oesophagus at the level of the vascular ring anomaly (Arterial phase)....27
Figure 2.3 - Dorsal MPR CT image showing the dextraposition of the aorta (Arterial phase)....27
Figure 2.4 - Transverse CT angiogram image showing the separated origins of the bicarotid trunk and the right subclavian artery (Arterial phase)....27
Figure 2.5 - Sagittal MPR CT image of the aortic arch, showing the separated origins of the bicarotid trunk and the right subclavian artery (Arterial phase)....27
Figure 3.1 - Right lateral abdominal radiograph....36
Figure 3.2 - Longitudinal ultrasound image of distal ileum....36
Figure 3.3 - Transverse ultrasound image of distal ileum....36
Figure 3.4 - Longitudinal ultrasound image of distal ileum (Follow up)....36
Figure 3.5 - Transverse ultrasound image of distal ileum (Follow up)....36
Figure 4.1 - Medio-lateral view of the L stifle....43
Figure 4.2 - Medio-lateral view of the L stifle....43
Figure 4.3 - Caudo-cranial view of the L stifle....43
Figure 4.4 - Dorso-ventral thoracic radiograph....43
Figure 4.5 - Right lateral thoracic radiograph....43
Figure 4.6 - Left lateral thoracic radiograph....43
Figure 4.7 - Transverse ultrasound image of the left cranial tibial muscle....44
Figure 4.8 - Longitudinal ultrasound image of the left cranial tibial muscle....44
Figure 4.9 - Proximal ultrasound aspect of the left cranial tibial muscle....44
Figure 4.10 - Longitudinal ultrasound image of the left stifle (distal part on the left)....44
Figure 5.1 - Ultrasound images with Power Doppler examination of the portosystemic shunt joining the left side of the caudal vena cava....51
Figure 5.2 - Ultrasound image of the portosystemic shunt....51

Figure 6.1 - Ultrasound image demonstrating abdominal effusion 59
Figure 6.2 - Ultrasound image showing the pulmonary mass pushing the diaphragm ... 59
Figure 6.3 - Ultrasound image showing the compression of the caudal vena cava by the pulmonary mass 59
Figure 6.4 - Dorso-ventral thoracic radiograph 59
Figure 6.5 - Right lateral thoracic radiograph 59
Figure 6.6 - Left lateral thoracic radiograph 59
Figure 6.7 - Transverse CT image of the right-sided cavitary pulmonary mass (Lung window) 60
Figure 6.8 - Transverse CT image showing mineralisations of the pulmonary mass (Soft tissue window) 60
Figure 6.9 - Transverse CT image showing mineralisations of the pulmonary mass and fluid line delineation (Soft tissue window) 60
Figure 6.10 - Delay post contrast transverse CT image showing compression of the caudal vena cava (Soft tissue window) 60
Figure 7.1 - Right lateral caudal abdominal radiograph 68
Figure 7.2 - Ultrasound image of the right inguinal area showing fluid accumulation (Microconvex transducer) 68
Figure 7.3 - Ultrasound image of the right inguinal area showing fluid accumulation (Linear transducer) 68
Figure 7.4 - Transverse CT image of the right sublumbar hypoattenuating lesion and subcutaneous cellulitis (Soft tissue window) 68
Figure 7.5 - Transverse CT image of right sublumbar emphysema and thigh cellulitis (Soft tissue window) 68
Figure 7.6 - Transverse CT image of right thigh cellulitis (Soft tissue window) 68
Figure 8.1 - Ultrasound image demonstrating marked left adrenomegaly with heterogeneous parenchyma 76
Figure 8.2 - Power Doppler ultrasound image of the left enlarged adrenal gland and adjacent aorta (Ao) 76
Figure 8.3 - Ultrasound image of the normal right adrenal gland 76
Figure 8.4 - Ultrasound image of the left renal pelvic mineralisations, with acoustic shadowing 76
Figure 8.5 - Right lateral radiograph of the body 76
Figure 8.6 - Left lateral radiograph of the body 76

Figure 8.7 - Transverse post-contrast CT image showing the left adrenal mass adjacent to but not invading the caudal vena cava and aorta (Soft tissue window) 77
Figure 8.8 - Dorsal oblique MPR post-contrast CT image of the left adrenal mass adjacent to the caudal vena cava (Soft tissue window) 77
Figure 8.9 - Sagittal MPR post-constrast CT image of the left adrenal mass adjacent to the caudal vena cava (Soft tissue window) 77
Figure 9.1 - Right lateral abdominal radiograph 85
Figure 9.2 - Left lateral abdominal radiograph 85
Figure 9.3 - Dorso-ventral abdominal radiograph 85
Figure 9.4 - Right lateral thoracic radiograph 85
Figure 9.5 - Ultrasound image showing gastric fluid dilation, with small hyperechoic structures floating within the lumen 85
Figure 9.6 - Ultrasound image showing marked duodenal fluid dilation 85
Figure 9.7 - Ultrasound image showing marked small intestinal fluid dilation 86
Figure 9.8 - Ultrasound image demonstrating small intestinal dilation proximally to the foreign body 86
Figure 9.9 - Ultrasound image of the small intestinal foreign body, with strong distal acoustic shadowing 86
Figure 9.10 - Ultrasound image demonstrating moderate mesenteric lymphadenomegaly. 86
Figure 10.1 - Right lateral thoracic radiograph 95
Figure 10.2 - Right lateral thoracic radiograph, follow up 3 weeks later 95
Figure 10.3 - Left lateral thoracic radiograph 95
Figure 10.4 - Left lateral thoracic radiograph, follow up 3 weeks later 95
Figure 10.5 - Dorso-ventral thoracic radiograph 95
Figure 10.6 - Dorso-ventral thoracic radiograph, follow up 3 weeks later 95
Figure 10.7 - Transverse CT image demonstrating consolidation of the ventral cranial lung lobes (Lung window) 96
Figure 10.8 - Transverse CT image showing alveolar pattern and ground glass opacities at the periphery of the cranial lung lobes (Lung window) 96
Figure 10.9 - Transverse CT images showing A 96
Figure 10.10 - Transverse CT image demonstrating bronchial wall thickening and bronchiectasis (Lung window) 96
Figure 10.11 - Transverse CT image showing alveolar pattern within the caudal lung lobes (Lung window) 96

Figure 10.12 - Transverse CT image demonstrating nodular alveolar pattern within the caudal lung lobe (Soft tissue window) 96
Figure 11.1 - Ultrasound image demonstrating biliary mucocoele 103
Figure 11.2 - Ultrasound image of the irregular heterogeneous mass adjacent to the gallbladder 103
Figure 11.3 - Ultrasound image of the irregular heterogeneous mass adjacent to the gallbladder 103
Figure 11.4 - Ultrasound image of the irregular heterogeneous mass adjacent to gallbladder 103
Figure 11.5 - Ultrasound image demonstrating the marked amount of abdominal free fluid (Post-operative) 103
Figure 12.1 - Right lateral thoracic radiograph 113
Figure 12.2 - Dorso-ventral thoracic radiograph 113
Figure 12.3 - Right lateral view of the caudal abdomen 113
Figure 12.4 - Ventro-lateral view of the abdomen 113
Figure 12.5 - Transverse CT image showing consolidation of the R middle and accessory lung lobes and associated bronchiectasis (Soft tissue window) 114
Figure 12.6 - Transverse CT image showing consolidation of the R middle and accessory lung lobes and associated bronchiectasis (Lung window) 114
Figure 12.7 - Transverse CT image showing pulmonary consolidation and mineralisations (Soft tissue window) 114
Figure 12.8 - Transverse CT image demonstrating bronchial wall thickening and bronchiectasis (Lung window) 114
Figure 12.9 - Transverse CT image of the pulmonary nodule ventrally to the bifurcation of the right cranial and middle main bronchi (Lung window) 114
Figure 12.10 - Transverse CT image demonstrating subpleural thickening at the dorsal aspect of the left caudal lung lobe (Lung window) 114
Figure 13.1 - T2w sagittal image of the cyst-like lesion at the level of the 4th ventricle (Mid brain) 122
Figure 13.2 - T1w sagittal post-contrast image of the cyst-like lesion at the level of the 4th ventricle showing peripheral rim enhancement (Mid brain) 122
Figure 13.3 - T2w dorsal image of the cyst-like lesion at the level of the 4th ventricle 122
Figure 13.4 - T1w dorsal post-contrast image of the cyst-like lesion at the level of the 4th ventricle showing peripheral rim enhancement 122

Figure 13.5 - T2w transverse image of the cyst-like lesion at the level of the 4th ventricle 123
Figure 13.6 - FLAIR transverse image of the cyst-like lesion at the level of the 4th ventricle 123
Figure 13.7 - T1w transverse image of the cyst-like lesion at the level of the 4th ventricle 123
Figure 13.8 - T1w transverse post-contrast image of the cyst-like lesion at the level of the 4th ventricle showing peripheral enhancement 123
Figure 13.9 - T2w transverse image showing moderate dilation of the lateral ventricles 123
Figure 14.1 - Right lateral thoracic radiograph 129
Figure 14.2 - Dorso-ventral thoracic radiograph 129
Figure 14.3 - Ventro-dorsal abdominal radiograph 129
Figure 14.4 - Right lateral abdominal radiograph 129
Figure 15.1 - Medio-lateral radiograph of the right forearm 135
Figure 15.2 - Medio-lateral radiograph of the left forearm 135

Table of Appendix

Appendix 1 - Diagnostic Imaging Equipment…...……137

List of Abbreviations

/L: per Liter

µ: Micro

3D MPR: 3-Dimensional Multiplanar Reconstruction

Acc: Accessory lung lobe

Alb: Albumin

ALKP: Alkaline Phosphatase

ALT: Alanine Aminotransferase

Ao: Aorta

aPTT: Activated Partial Thromboplastine Time

AST: Aspartate Aminotransferase

BAL: Broncho-Alveolar Lavage

CE-MRA: Contrast-Enhanced Magnetic Resonance Angiography

CdVC: Caudal Vena Cava

cm: Centimeters

CNS: Central Nervous System

CrVC: Cranial Vena Cava

CSF: Cerebrospinal Fluid

CT: Computed tomography

DWI: Diffusion Weighted Imaging

FCoV: Feline Coronavirus

FeLV: Feline leukaemia virus

Fig: Figure

Figs: Figures

FIV: Feline Immunodeficiency Virus

FLAIR: Fluid Attenuated Inversion Recovery

fPLI: feline Pancreatic Lipase Immunoreactivity

g: Grams

GALT: Gut-Associated Lymphoid Tissue

GFAP: Glial Fibrillary Acidic Protein

GGT: Gamma-Glutamyl Transferase

Glob: Globulin

Hb: Haemoglobin

HS: Histiocytic Sarcoma

HTC: Haematocrit

KCCT: Kaolin Cephalin Clotting Time

kV: Kilovolt

L: Left

Ladr: Left adrenal mass

LCd: Left caudal lung lobe

Liv: Liver

mAs: Milliampers Second

MHz: Megahertz

mm: Millimeters

mmol: Millimole

MRI: Magnetic Resonance Imaging

N: No

O: Yes

Oe: Oesophagus

PCR: Polymerase Chain Reaction

pmol: Picomole

PO: Per Os

PSS: Porto-Systemic Shunt

PT: Prothrombine Time

PV: Portal vein

R: Right

RBC: Red Blood Cells

RK: Right Kidney

Spl: Spleen

STIR: Short Tau Inversion Recovery

T: Trachea

T1w: T1-weighted

T2w: T2-weighted

TP: Total Protein

U: International Unity

US: Ultrasound

WBC: White Blood Cells

Declaration

I, Alexane Durand, declare that the work in this thesis is original, was carried out solely by myself or with due acknowledgements. It has not been submitted in any form for another degree or professional qualification.

Acknowledgements

I am immensely thankful to the whole Diagnostic Imaging team of the Small Animal Hospital, University of Glasgow, who has been allowing me to improve my work and knowledge for the last year and a half, and has assisted me in the completion of this work: Gill and Nicky for their daily work, helpfulness, advice and cheerfulness, Marlene for her support, friendship and kindness, Gawain, Alison and Susan for their knowledge, teaching and guidance, and especially Martin for his critical suggestions and supervision throughout the realisation of this work.

I express my deep sense of gratitude to Dr Juliette Sonet, from the Diagnostic Imaging Department of the Veterinary Teaching Hospital, University of Lyon, who gave me solid foundation in diagnostic imaging and brought me to this stage.

I extend many thanks to Dr Isabelle Bublot, Cardiology Department of the Veterinary Teaching Hospital, University of Lyon, for her friendship and support during my veterinary and postgraduate studies, and to Dr Jean-Luc Cadore, Internal Medicine Department, and Dr Isabelle Goy-Thollot, Emergency and Critical Care Department, of the Veterinary Teaching Hospital, University of Lyon, for their teaching and their care to help me in my professional projects.

Clinical cases

Case 1. Hiatal Hernia

Signalment and History

A 2-year-old male Boston Terrier presented with a persistently poor appetite. Infrequently normal, the dog most often just grazed food. Excitement occasionally induced vomiting or regurgitating. Before presentation, an increased frequency of vomiting had been noted, either mucus or food. The owners changed the diet to sensitivity pet food and the dog was treated with ranitidine (Zantac®, Boehringer-Ingelheim) and sucralfate for 3 weeks with little response. The dog also snored, with snuffling sounds and panted when walking. He was fully vaccinated, and had been treated for endo- and exoparasites.

Clinical Signs

a) Mild abdominal discomfort
b) Moderate to severe stertor and stridor while breathing with no stress
c) Bilateral stenotic nares

Ultrasound Examination

1. **Equipment** - See Appendix 1
2. **Restraint** - The dog was sedated and placed in dorsal recumbency for the general abdominal ultrasonography.

Ultrasound report

The spleen was decreased in size, mildly hypoechoic and displaced dorso-cranially compared to normal. The pancreas was subjectively mildly more hypoechoic than expected but without thickening of the parenchyma or hyperechoic surrounding fat. Excessive gas and content were present in the gastro-intestinal tract preventing a complete examination, and the stomach was difficult to evaluate.

Radiographic Examination

1. **Equipment** - See Appendix 1
2. **Restraint** - The dog was sedated with midazolam 0.2mg/kg (Hypnovel®, Roche Products Ltd.) and ketamine 5mg/kg (Ketaset®, Fort Dodge Animal Health). Positioning was achieved using wedges of dressing material and rope ties.

Area	View	kV	mAs	Grid
Thorax	Dorso-ventral (Fig.1.1)	64.5	10	O
	Right Lateral (Fig.1.2)	66	12.5	O
	Left Lateral (Fig.1.3)	47	4	O
Abdomen	Right Lateral (Fig.1.4)	66	6.3	O
	Left Lateral (Fig.1.5)	66	10	O

Radiographic Appraisal

The images are well processed and the majority of the views are well positioned and centred. The dorso-ventral view (Fig.1.1) is slightly centred on the left side and the left lateral view (Fig.1.3) is moderately over-collimated dorsally to evaluate the vertebral column and related soft tissue. The right lateral radiograph of the thorax (Fig.1.2) is moderately overexposed. Primary markers and exposure setting are present. Secondary L (left) and R (right) markers have been added to the dorso-ventral thoracic radiograph and the right lateral abdominal radiograph (Fig.1.4) respectively. The radiographs are of diagnostic quality.

Radiological Report

On both projections of the abdomen (Figs.1.4 and 1.5), small intestinal loops and transverse colon are displaced cranially, and some small intestinal loops are filled with gas without visible dilation. The stomach and spleen are not visible in the abdomen and a mild decrease in cranial abdominal serosal details is noted. A mixed soft tissue and gas opacity cavitated structure is visible superimposed on the dorsal part of the diaphragmatic silhouette, from the dorso-cranial part of the abdomen to the dorso-caudal part of the thorax. The prostate is visible on both views, but its size is within normal limits. The vertebral bodies of the caudal sacrum and the coccygeal vertebrae show bone remodelling and sclerosis.

The large rounded mixed soft tissue and gas opacity cavitated structure of about 65 x 75 mm, visible on abdominal radiographs (Figs.1.4 and 1.5), is seen superimposed on the dorso-caudal lung field, the dorsal aspect of the diaphragmatic silhouette and slightly in the dorso-cranial aspect of the abdomen, on both thoracic lateral views (Figs.1.2 and 1.3), extending cranially to the 6^{th} intercostal space and caudally to the 11^{th} intercostal space. On the dorso-ventral view (Fig.1.1) this structure can be seen projecting slightly to the left of midline of the caudal mediastinum/cranial abdomen. This appearance is consistent with a gas-filled viscera structure, most likely the stomach, as it is not visible in the cranial abdomen on lateral views. On the right lateral view of the chest (Fig.1.2), the cranial thoracic oesophagus is moderately distended by gas opacity, associated with a mild ventral displacement of the caudal trachea. The vertebral bodies of T5, T8 and

T9 are wedge–shaped, associated with a decrease in the surrounding intervertebral spaces, moderate kyphosis at T8/9 and mild spondylosis. T10 is a butterfly vertebra.

Diagnosis

Hiatal hernia with displacement of a significant proportion of the stomach. Congenital vertebral malformations.

Further Investigations

Evaluation of the soft palate and larynx was performed under anaesthesia. A stage I laryngeal collapse (everted laryngeal saccules) was identified. The length of the soft palate was considered excessive being indicative of elongated soft palate. The larynx function was normal.

Haematology showed a regenerative moderate anaemia (RBC=3.78x10^6/µL, Hb=8.4g/L, HCT=26.4%) and a mild neutrophilia (WBC=15.03x10^9/L with neutrophils= 12,625x10^9/L).

Coagulation tests were within normal limits.

Biochemistry showed a mild hypoalbuminemia (24g/L).

Outcome

The dog underwent bilateral vertical wedge rhinoplasty, palatoplasty, and bilateral sacculectomy as well as reduction of the hiatal hernia with gastropexy and oesophagopexy. A full thickness gastric biopsy was taken and sent for histopathological analysis, which was consistent with a normal gastric wall.

The dog recovered well from surgery and was discharged 2 days later. A course of sucralfate and omeprazole was started. The owner was advised to feed him with moist balls of food for the next two weeks, not to place any stress on the surgical site, and to control exercise.

A follow up examination was performed 2 weeks after surgery. The dog was bringing up some dense froth sporadically. This was always first thing in the morning, not every day, and it could happen 2 days in a row and then not happen for a week. Otherwise he was in good form and was eating without difficulties. The owners had noticed a very marked improvement and the dog was now keen on eating and bright. His general physical examination was within normal limits. A chronic gastritis or oesophagitis was suspected regarding the clinical signs; therefore the treatment on sucralfate was continued for a further month and on omeprazole for 3 months.

Discussion

Hiatal hernia is defined as the protrusion of abdominal contents through the oesophageal hiatus of the diaphragm into the thorax. Four types of hiatal hernia are described. Type I or sliding hiatal hernia (also called axial or oesophageal hiatal hernia) is the most common form diagnosed in dogs and cats. It is characterised by a displacement of the terminal oesophagus, the gastro-oesophageal junction and part of the stomach through the oesophageal hiatus into the thoracic cavity. The three other types are much more rare in small animals. In type II or paraoesophageal hiatal hernia, the distal segment of the oesophagus and the gastro-oesophageal junction remains in place, but a portion of the fundus slides through the hiatus alongside the thoracic oesophagus. Type III is a combination of types I and II and in type IV, the most severe form, herniation of a large part of the stomach and other abdominal organs (including spleen, colon, and jejunum) into the thoracic paraoesophageal sac is noted.[1,2,3,4]

Hiatal hernia is mainly observed in young dogs (congenital form), occurring secondary to incomplete fusion of the diaphragm during early embryonic development, with Chinese Shar Peis and English Bulldogs being the most commonly affected breeds.[1,2] Cats are also affected, with domestic shorthair breed overrepresented.[1] Hiatal hernia can be observed occasionally in adults as a consequence of a traumatic event or in association with severe upper respiratory disease[5,6] (acquired form), including brachycephalic syndrome and laryngeal paralysis.[1,2,4,6] Increased inspiratory effort associated with upper airway obstructive syndrome causes an increase in negative intra-oesophageal and intrapleural pressure resulting in hiatal hernia.[2,6] In those cases, the resolution of the upper airway obstruction might resolve spontaneously the secondary associated hiatal hernia.[6] In cases of congenital hiatal hernia, brachycephalic airway obstruction syndrome may worsen the hiatal hernia and exacerbate clinical signs related to the herniation.[2,6] Type I hiatal hernia can also be an incidental finding and it may be that many animals have asymptomatic hiatal herniation as seen in humans.[2]

Clinical signs can be constant or, more commonly, intermittent due to the herniated organs moving back and forth from the abdominal to thoracic cavities.[2] In congenital hiatal hernia, clinical signs may be observed immediately after weaning onto solid/dry food and are usually seen before one year of age. The most common clinical signs include regurgitation, hypersalivation, vomiting, slow growth, anorexia, coughing and dyspnoea.[1,2,3,4] Gastrointestinal signs are generally more prominent compared to respiratory signs, the latter attributed to secondary aspiration pneumonia and/or lung compression by herniated viscera, or less often pleural effusion[4]. All these signs are also

often encountered in other conditions such as reflux oesophagitis and megaoesophagus. These latter two conditions may be associated with or be consequences of hiatal hernia, and their presence is associated with a worse prognosis.[2]

Diagnosis is based on survey radiographs, with the presence of, most often, a gas-filled intra-thoracic soft tissue structure containing gastric rugal folds - not always visible - within the caudo-dorsal thorax adjacent to the diaphragm.[1,2,3,4,5,6] Possible additional thoracic radiographic abnormalities seen with hiatal hernia include megaoesophagus, absence of the right crus of the diaphragmatic border and lobar alveolar consolidation due to aspiration pneumonia. It is frequently necessary to perform a positive contrast oesophagram/gastrogram, with the aid of fluoroscopy, to facilitate the detection of intermittent herniation, the diagnosis of which is challenging.[1,2,5,6] Definitive diagnosis of reflux oesophagitis requires oesophageal endoscopy and biopsy. Abdominal ultrasonography may be useful in the diagnosis of hiatal herniation in some cases when gastric and/or splenic displacement can be visualised and it avoid the risk of aspiration associated with the use of contrast medium in a potentially dysphagic or regurgitating patient.[2]

The two main treatment options are medical therapy and surgery.[1,2,3] Medical therapy is recommended initially and includes prokinetics, antacids, and cytoprotective agents, as well as elevated feeding.[1] The goals of medical management are to resolve reflux oesophagitis and associated megaoesophagus. If aspiration pneumonia is present, as a complication of regurgitation, it must be treated with appropriate antibiotics. If clinical signs persist with medical management, surgical treatment is recommended to achieve reduction of the hernia and restoration of normal lower oesophageal sphincter function. Surgical management is generally a combination of gastropexy, oesophagopexy, and plication of dorsal and/or ventral aspects of the oesophageal hiatus, after hiatal hernia reduction. The prognosis of hiatal hernia is variable and depends on the chronicity of clinical signs, the degree and type of herniation, and the method of medical and/or surgical treatment[4], however a good outcome is generally observed in dogs with congenital hernia.

References

1-Guiot LP, Lansdowne JL, Rouppert P, Stanley BJ. Hiatal hernia in the dog: a clinical report of four Chinese Shar Peis. **J Am Anim Hosp Assoc** 2008; 44(6): 335-341.

2-Keeley B, Puggioni A, Pratschke K. Congenital oesophageal hiatal hernia in a pug. **Irish Vet J** 2008; 61(6): 389-393.

3-Rahal SC, Mamprim MJ, Muniz LM, Teixeira CR. Type-4 esophageal hiatal hernia in a Chinese Shar-Pei dog. **Vet Radiol Ultrasound** 2003; 44(6): 646-647.

4-Gordon LC, Friend EJ, Hamilton MH. Hemorrhagic pleural effusion secondary to an unusual type III hiatal hernia in a 4-year-old Great Dane. **J Am Anim Hosp Assoc** 2010; 46(5): 336-340.

5-Arndt JW, Marks SL, Kneller SK. What is your diagnosis? Hiatal hernia due to laryngeal squamous cell carcinoma. **J Am Vet Med Assoc** 2006; 228(5): 693-694.

6-DeSandre-Robinson DM, Madden SN, Walker JT. Nasopharyngeal stenosis with concurrent hiatal hernia and megaesophagus in an 8-year-old cat. **J Feline Med Surg.** 2011; 13(6): 454-459.

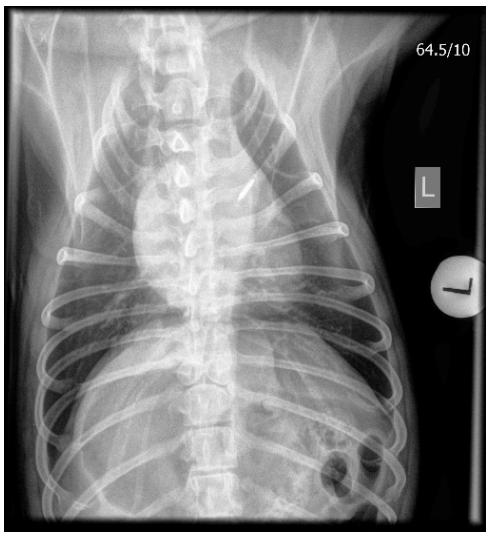

Figure 1.1 - Dorso-ventral thoracic radiograph

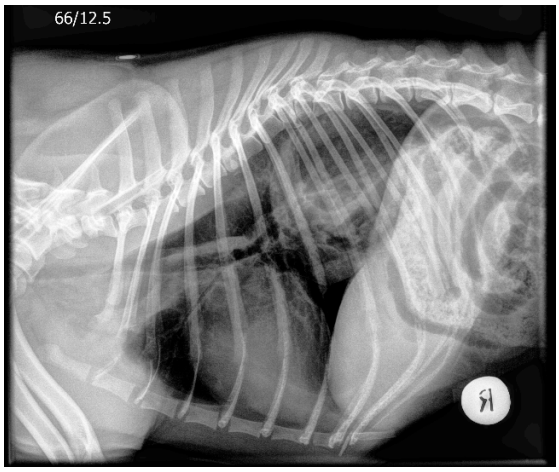

Figure 1.2 - Right lateral thoracic radiograph

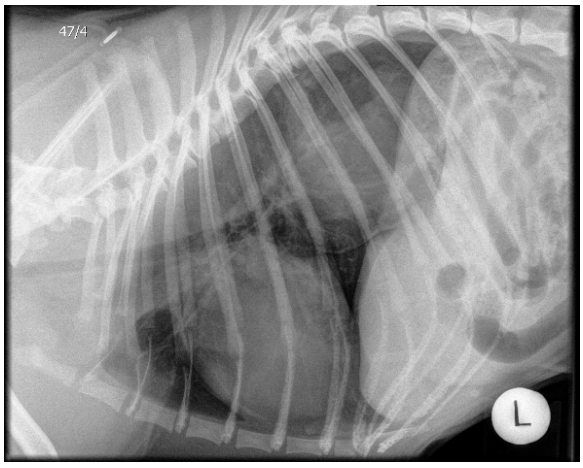

Figure 1.3 - Left lateral thoracic radiograph

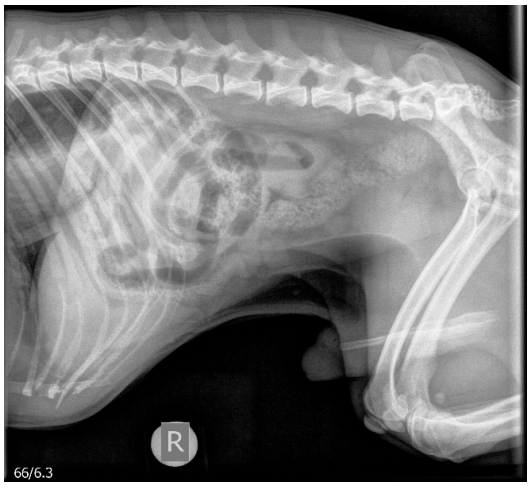

Figure 1.4 - Right lateral abdominal radiograph

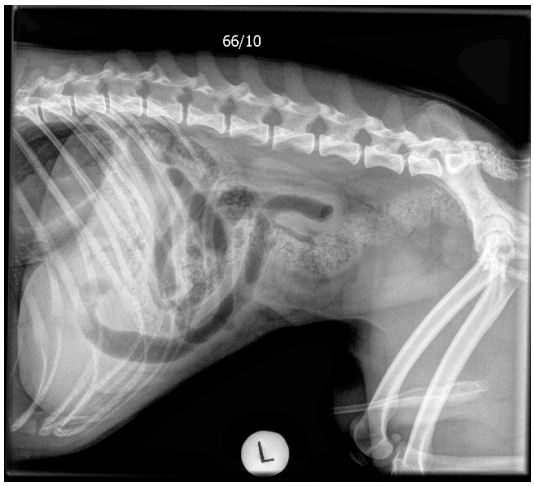

Figure 1.5 - Left lateral abdominal radiograph

Case 2. Vascular Ring Anomaly

Signalment and History

A 4-month-old male Great Dane, vaccinated and dewormed, has been fed with pureed puppy food since he was 10 weeks old. He started to regurgitate large amounts of compacted undigested food at the time he began to eat dry food (e.g. dog biscuits), at 3 months. Otherwise he was energetic and bright, putting on weight and eating well. Radiographs with swallowing of contrast medium, taken at the general practice, showed a dilation of the cranial part of the thoracic oesophagus, cranially to the cardiac silhouette, associated with an accumulation of contrast medium within. His diet was switched back to pureed food and puppy milk, before being referred. No coughing or sneezing was reported.

Clinical Signs

The physical examination was unremarkable.

Swallowing Study – Fluoroscopic examination

1. **Equipment -** See Appendix 1
2. **Restraint -** The dog was conscious, restraint with leash and fed with a mixture of barium and wet food during the study.

Swallowing Study Report

An accumulation of the swallowed food in a focal oesophageal dilation, cranial to the cardiac silhouette, was visible, before entering the caudal oesophagus. A moderate focal narrowing of the oesophagus just caudal to the dilation was noted. The motility observed in the cranial thoracic oesophagus was reasonable as material could be seen moving through with reasonable ease. Peristalsis caudally was within normal limits, although an occasional moderate gastric reflux was visible.

Diagnosis

Thoracic oesophageal stenosis with cranial oesophageal dilation, consistent with a vascular ring anomaly. Intermittent gastric reflux.

Advanced Imaging Modality – Computed Tomography Examination

1. **Equipment -** See Appendix 1
2. **Restraint -** The dog was anaesthetized, intubated and placed in ventral recumbency.

Computed Tomography Report

A CT angiography of the thorax was performed (Figs.2.1 to 2.5). First of all, a plain CT of the thorax was obtained and images were reformatted with bone and soft tissue filter. 2ml/kg of ioversol (*Optiray 300, Mallinckrodt Pharmaceuticals, UK*) was injected intravenously, with a pump injector at a rate of 5ml/s. Arterial phase, venous phase and delayed phase CT of the thorax were obtained 5 seconds, 30 seconds and 3 minutes after injection of contrast medium respectively. The images demonstrate marked gas dilation of the oesophagus from the inlet of the thorax to the cranial aspect of the base of the cardiac silhouette (Fig.2.1) followed by a narrowing at this level (Fig.2.2), then a moderate dilation of the oesophagus caudally. A dextraposition of the aorta relative to the trachea (Fig.2.3) is noted. The brachiocephalic trunk is not visible. Indeed, the common carotid artery arises from the ventral part of the aortic arch, whereas the right subclavian artery arises slightly dorsally to the common carotid artery (Fig.2.4 and 2.5). The left subclavian artery cannot be followed fully, even after multiplanar reconstruction of the images, as its course disappears dorsal to the dilated oesophagus. It seems to arise slightly more dorsally to the right subclavian artery. These features are consistent with a type I vascular ring anomaly, persistence of the fourth right aortic arch.

A marked interstitial pattern is visible at the ventro-medial aspect of the left cranial lung lobe and slightly at the ventral part of the right middle lung lobe. These features are most likely consistent with atelectasis, although foci of aspiration pneumonia cannot be completely excluded.

A flattening of the spinal cord at the level of C3-C4 is noted, which may be due to the animal positioning, although a vertebral anomaly, linked to the breed, cannot be completely excluded.

Outcome

The dog underwent exploratory left intercostal thoracotomy. The ligamentum arteriosum was identified loosely constricting the oesophagus. Oesophageal dilation was noted rostral to the constriction. The ligamentum arteriosum was ligated, resected and some small fibrous tissue bands, identified constricting the oesophagus, were cut. No other vascular anomaly was noted. A chest drain was placed before the wound was closed. The dog recovered well from surgery, he was eating and drinking well with an elevated food bowl and no episode of regurgitation was noticed. The chest drain was removed the day following surgery and the dog was discharged 3 days later.

A follow-up examination was performed 6 months after surgery. The dog has regurgitated occasionally when eating dry food and treats since surgery. Otherwise he was doing well, and a soaked diet in a raised bowl twice daily was continued.

Discussion

Vascular ring anomalies are relatively uncommon congenital cardiovascular disorders resulting in varying degrees of oesophageal and/or tracheal compression in dogs and cats. Dorso-lateral abnormal vascular structures and the heart base ventrally form a ring entrapping the oesophagus, however the ring may be incomplete in some cases and clinically irrelevant.[1,2] Persistence of the right fourth aortic arch (the right dorsal aorta remains patent whereas the left dorsal aorta regresses abnormally) accounts for up to 95% of vascular ring anomalies in dogs, and usually results in significant oesophageal compression from the left ligamentum arteriosum.[1,2,3,4,5] However various other vascular anomalies resulting in tracheo-oesophageal compression have also been reported, such as aberrant left or right subclavian arteries, double aortic arch, right-sided ligamentum arteriosum, persistent of the left cranial vena cava or aberrant intercostal arteries. Multiple locations of oesophageal compression may occur in case of concurrent cardiovascular abnormalities.[1,3,5] Aberrant left subclavian artery is the most frequently reported defect associated with persistence of the right aortic arch, occurring in approximately 33% of cases. The anomalous origin of the left subclavian artery may cause a second site of oesophageal compression, however most often no compression or clinically insignificant compression is observed.[1,5] Connection of the ligamentum arteriosum from the main pulmonary artery to an aberrant left subclavian artery rather than the aortic arch causing oesophageal compression has also been reported in dogs with persistence of the right aortic arch. Patent ductus arteriosus is also associated to vascular ring anomaly in about 10% of patients.[3,5]

Breed predisposition and genetic heritability for some types of vascular ring anomalies have been found in German Shepherds, Greyhounds, Irish Setters, German Pinscher and Boston Terriers.[2,5,6] The heritability of a persistent right aortic arch has not been described in cats.[4]

A presumptive diagnosis of vascular ring anomaly is commonly made from the history of the patient and results of clinical and radiographic examinations. The most common clinical sign referable to a vascular ring anomaly is regurgitation because of focal oesophageal dilation cranial to constriction at the level of ring. It is generally observed in puppies or kittens when they start to eat dry food at the time of weaning. Affected

animals are often thin and smaller than their littermates. Respiratory signs, such as dyspnoea, may be encountered secondary due to associated aspiration pneumonia. If the ductus arteriosus is patent, clinical signs indicative of volume overload and cardiovascular compromise can develop.[3,4,5,7]

Dilation of the oesophagus cranial to the base of the cardiac silhouette, with ventral and left displacement of the trachea, is the most common radiographic sign, which is a high indicator for a presumptive diagnosis of vascular ring anomaly.[1,3,4] Positive contrast oesophagography is also useful to demonstrate oesophageal constriction at the base of the heart with varying degrees of oesophageal dilatation extending cranially.[7] Areas of marked interstitial to alveolar pattern within the ventral part of the cranial or middle lung lobes may be also visible in patients with secondary aspiration pneumonia. Standard radiographs are also essential in the follow-up of aspiration pneumonia or recurrent postoperative regurgitation.[2] However, even if thoracic radiography is affordable and readily available, it does not consistently provide definitive evidence of a vascular ring anomaly, nor the type of malformation or the 3-dimensional (3D) relationships with adjacent structures.

Complete evaluation of the oesophageal function with fluoroscopic oesophagography is important as some patients with localized oesophageal compression have a generalized dysmotility that will negatively affect the prognosis. Oesophageal motility, and the magnitude and clinical significance of compression(s), can only be assessed with swallowing studies in conscious animals. However, the risk of barium, or other contrast medium, regurgitation and subsequent lung aspiration must be taken in consideration, particularly in dogs with significant oesophageal dysmotility.[2]

Additional arch abnormalities cannot be readily detected with thoracic radiography or echocardiography, which could influence pre-surgical planning. Computed tomography (CT) angiography is used to better characterize a suspected vascular ring anomaly, assess the different vascular malformations and localise tracheo-oesophageal sites of compression. Although anaesthesia is required, CT provides a non-invasive means of acquiring 3D images with a relatively short acquisition time, providing high resolution anatomic information for procedure planning. Furthermore, post-processing techniques are available to remove or enhance overlying structures.[3,5,8] Air added to the oesophagus prior to CT angiography, through an inflated balloon catheter, provides valuable information on the exact localization of the oesophagus, its shape, and the number of compressive sites.[2] Oesophageal compression is best displayed in transverse images, and transverse, sagittal and 3-dimensional volume-rendered images are most suitable to

demonstrate the spatial relationships of the aorta with adjacent organs on computed tomography.[3] In the normal dog, the aorta is ventral and to the left relative to the trachea. The brachycephalic trunk, at the origin of the common carotid arteries and right subclavian artery, arises ventrally from the normal aortic arch, whereas the left subclavian artery arises slightly more dorsally. In cases of persistent right aortic arch, the aorta is on the right side of the trachea and passes dorsally to it, causing a leftward and ventral displacement of the trachea.[5,8] The site of the ligamentum arteriosum, connecting the descending right aortic arch to the main pulmonary artery, can be assessed at the level of the oesophageal constriction, however the ligamentum arteriosum itself is generally not visible on CT images. Several concurrent vascular anomalies can be visualised, such as the separated origins of a bicarotid trunk and the right subclavian artery and/or an aberrant left subclavian artery, arising from the distal aortic arch or the proximal descending aorta, coursing dorsally to the oesophagus and trachea. A mild dilation of the proximal portion of the aberrant subclavian artery near its origin of the aorta may be observed in dogs, and a diverticulum at the same level in cats, analogous to the human Kommerell's diverticulum, presumed to be a remnant of the left fourth aortic arch.[3,5]

In cases of persistent right aortic arch with left ligamentum arteriosum, a left thoracotomy is required for ligation and transection of the ligamentum arteriosum. However, other less frequent types of anomalies may require a different surgical approach. Furthermore, as multiple aberrant vessels may contribute to oesophageal compression, those may be missed during surgery if not properly identified preoperatively.[2,3] When an aberrant left subclavian artery is present, recommendations can also include division and anastomosis to the left carotid artery to prevent subclavian steal syndrome, characterized by reversal of flow in the vertebral or internal thoracic arteries following occlusion of the subclavian artery that leads to neurologic signs or ischemia of the left forelimb.[3,5]

Significant clinical improvement usually follows corrective surgery in most patients (>90%); however, oesophageal hypomotility and regurgitation may persist. In these instances, affected animals are managed with elevated feedings as described for idiopathic megaoesophagus. The best prognosis for return of normal oesophageal function is obtained with early diagnosis and prompt surgical intervention.

References

1-Bottorff B, Sisson DD. Hypoplastic aberrant left subclavian artery in a dog with a persistent right aortic arch. **J Vet Cardiol** 2012; 14(2): 381-385.

2-Joly H, D'Anjou MA, Huneault L. Imaging diagnosis – CT angiography of a rare vascular ring anomaly in a dog. **Vet Radiol Ultrasound** 2008; 49(1): 42-46.

3-Henjes CR, Nolte I, Wefstaedt P. Multidetector-row computed tomography of thoracic aortic anomalies in dogs and cats: patent ductus arteriosus and vascular rings. **BMC Vet Res** 2011; 7: 57.

4-Tremolada G, Longeri M, Polli M, Parma P, Acocella F. Persistent right aortic arch and associated axial skeletal malformations in cats. **J Feline Med Surg** 2013; 15(2): 68-73.

5-Saunders AB, Winter RL, Griffin JF, Thieman Mankin KM, Miller MW. Surgical management of an aberrant left subclavian artery originating from a left patent ductus arteriosus in a dog with a right aortic arch and abnormal branching. **J Vet Cardiol** 2013; 15(2): 153-159.

6-Menzel J, Distl O. Unusual vascular ring anomaly associated with a persistent right aortic arch and an aberrant left subclavian artery in German pinschers. **Vet J** 2011; 187(3): 352-355.

7-White RN, Burton CA, Hale JSH. Vascular ring anomaly with coarctation of the aorta in a cat. **J Small Anim Pract** 2003; 44(7): 330-334.

8-Pownder S, Scrivani PV Non-selective computed tomography angiography of a vascular ring anomaly in a dog. **J Vet Cardiol** 2008; 10(2): 125-128.

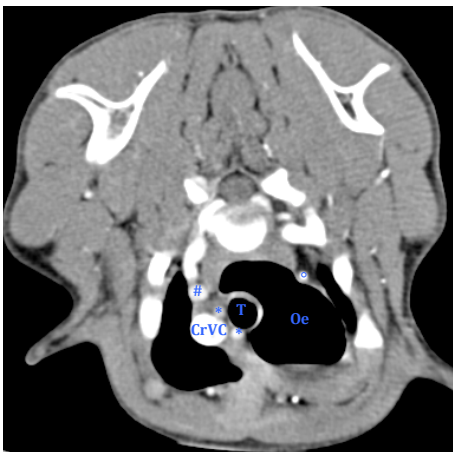

Figure 2.1 - Transverse CT angiogram image demonstrating the marked dilation of the cranial thoracic oesophagus (Arterial phase)

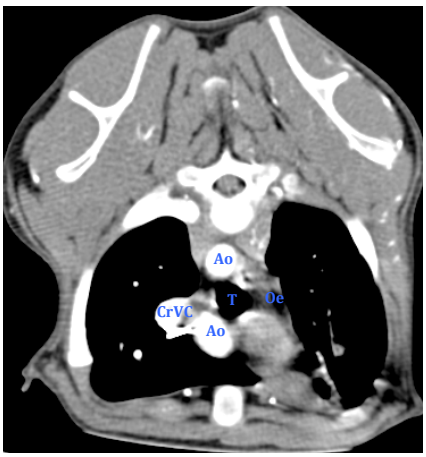

Figure 2.2 - Transverse CT angiogram image showing the narrowing of the oesophagus at the level of the vascular ring anomaly (Arterial phase)

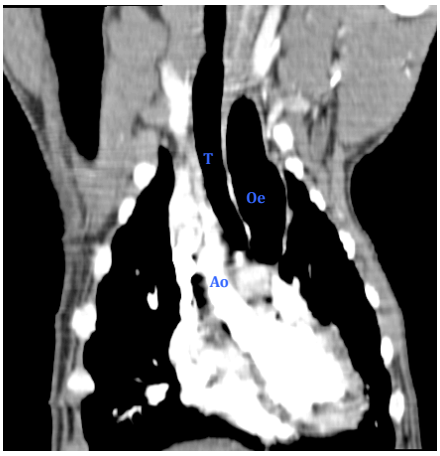

Figure 2.3 - Dorsal MPR CT image showing the dextraposition of the aorta (Arterial phase)

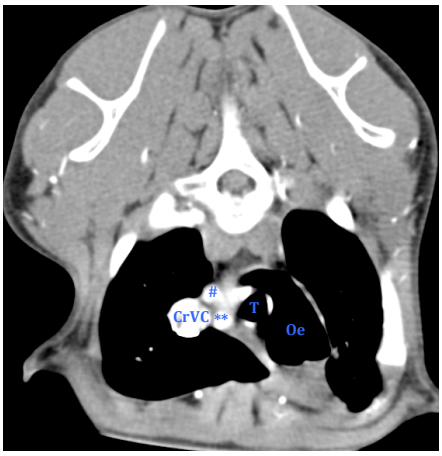

Figure 2.4 - Transverse CT angiogram image showing the separated origins of the bicarotid trunk and the right subclavian artery (Arterial phase)

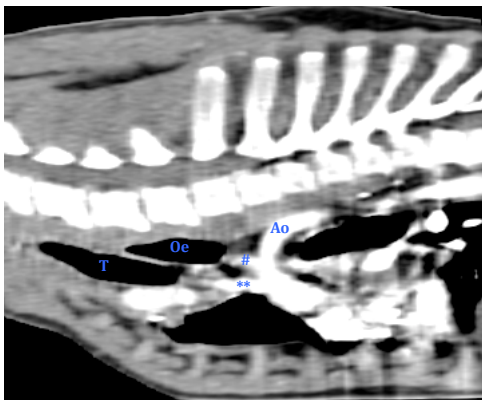

Figure 2.5 - Sagittal MPR CT image of the aortic arch, showing the separated origins of the bicarotid trunk and the right subclavian artery (Arterial phase)

Ao: Aorta; CrVC: Cranial Vena Cava; Oe: Oesophagus; T: Trachea; #: Right subclavian artery; °: Left subclavian artery; **: Bicarotid trunk; *: Common carotid artery.

Case 3. Severe Ileitis

Signalment and History

An 8-year-old male West Highland White Terrier was presented for further investigation of a fortnight history of vomiting, diarrhoea, lethargy and weight loss. At the onset of the clinical signs, the dog had vomited stones. Supportive treatment was initiated at the referring veterinary surgeon, consisting of intravenous fluid-therapy, ranitidine (Zantac®, Boehringer Ingelheim) and maropitant citrate (Cerenia®, Pfizer).

Clinical Signs

a) Quiet, but alert and responsive
b) Moderate abdominal discomfort
c) Possibly small liver size on palpation

Radiographic Examination

1. **Equipment** - See Appendix 1
2. **Restraint** - The dog was sedated. Positioning was achieved using wedges of dressing material.

Area	View	kV	mAs	Grid
Abdomen	Right Lateral (Fig.3.1)	61.5	6.30	O

Radiographic Appraisal

Only the right lateral view of the abdomen (Fig.3.1) is available. It is well positioned, centred and exposed. A thin radio-opaque line is visible in the middle of the film perpendicular to the length of the film, consistent with a processing fault due to a dusty detector. A primary marker is present covered by a secondary added R marker. Exposure settings have been added. The radiograph is of diagnostic quality.

Radiographic Report

A small amount of gas is visible in some small intestinal loops, without any visible dilation. The caecum is filled by a moderate amount of gas. A mild decrease in the cranial abdominal contrast, between the stomach and the caecum, is noted, consistent with focal steatitis or small volume of localised free fluid. A very small mineralized structure is visible in the cranial mid abdomen, at the distal aspect of one 13^{th} rib, consistent with mineralization of a 13^{th} costo-chondral joint or a non-obstructive mineralized ingesta. New bone production is visible at the ventral aspect of the vertebral bodies of L7/S1, consistent with spondylosis.

Abdominal Ultrasound Report

A focal pronounced circumferential thickening of the entire wall of the terminal ileum (Figs.3.2 and 3.3) was visible, most marked in the muscular and the submucosal layers. The thickening was moderately asymmetric in the very distal ileum, at the level of the ileo-colic junction (thickness up to 8.2 mm). An alteration of the wall layering was noticed without complete loss. No sign of intestinal obstruction was visible. The surrounding fat was hyperechoic, although no mesenteric or ileo-colic lymphadenopathy was seen. The medial iliac lymph nodes were moderately enlarged (thickness about 8mm), associated with a moderately hypoechoic parenchyma and well-defined margins.

Differential Diagnoses

Marked focal circumferential but asymmetrical thickening of the distal ileum wall associated with surrounding steatitis, consistent with marked focal inflammatory/infectious process, granuloma or neoplastic infiltration (e.g. lymphoma, carcinoma, sarcoma, leiomyoma, leiomyosarcoma).

Further Investigations

Haematology showed mild lymphopaenia ($0.63x10^9$/L) and eosinopaenia (0.079 x 10^9/L) compatible with stress leukogram.

Biochemistry showed mild hypocalcaemia (2.2mmol/L), hypophosphatemia (1.19mmol/L) and hypoalbuminaemia (27g/L).

Canine Pancreatic Lipase Immunoreactivity snap test was negative.

Campylobacter upsaliensis (80%) was isolated after culture of a faecal sample, which could have been the underlying cause of the clinical signs. However healthy carrier animals are common. A profuse culture of *Clostridium perfringens* and a sparse culture of beta-haemolytic *Escherichia coli* were also recovered from the sample.

Outcome

The dog was discharged with a treatment course of maropitant citrate (Cerenia®, Pfizer) and metronidazole (Flagyl®, Sanofi-Aventis) and a support intestinal diet, while waiting for the sensitivity of the *Campylobacter* isolates. One week after discharge the dog was doing well and back to normal. The total calcium was rechecked and appeared to be lower than previously (1.67mmol/L), although the ionized calcium was within normal limits (1.2mmol/L). A course of enrofloxacin was started to treat the *Campylobacter*, as these bacteria were not sensitive to metronidazole.

A follow-up examination was performed one month later. The dog seemed to be doing well, however constant diarrhoea was observed since previous follow up. Faeces were well formed initially but became very watery and varied in colour, from light to dark brown. The dog was inconsistently bright or dull and lethargic during the day. The dog had vomited bright yellow froth 3 times, since the previous examination, and seemed frequently uncomfortable. Ionised calcium was lower than previous values (1.14mmol/L).

The ultrasound scan was repeated. A marked focal symmetric thickening of the wall of the distal part of the ileum was still visible (about 7.3mm), associated with a more marked asymmetric thickening of its ventral wall (about 9.4mm), just proximal to the junction with the colon (Figs.3.4 and 3.5). This was moderately thicker compared to previous scan. An alteration of the wall layering was still present at the level of the asymmetric thickening. Hyperechogenicity of the surrounding fat was still evident. A moderate enlargement of the ileo-colic lymph nodes was noticed (thickness about 6.5mm). Final needle aspirate of the ileum and lymph nodes was note performed because of the lack of safe acoustic window. A mild heterogeneity of the parenchyma of the spleen was present associated with small ill-defined hypoechoic and hyperechoic areas, consistent with a reactive splenitis, extramedullary haematopoiesis, lymphoid hyperplasia or congestion, although a neoplastic infiltration could not be completely excluded.

The dog underwent exploratory surgery. An approximately 5cm firm complex mass was found at the ileo-colic junction, including the intestines at this level, an adhesion of a proximal loop of ileum, the ileo-caecal lymph nodes and mesentery. Mesenteric lymphatic vessels traveling to this area were markedly engorged. An enterotomy was performed at the level of the mass and severely thickened intestinal walls causing substantial narrowing of the lumen were visible. Full thickness biopsies of ileum, ileo-colic junction and ileo-colic lymph nodes were taken. Two layers of simple interrupted sutures was made because of the marked friable state of the wall. The jejunum appeared thickened and diffusely oedematous with prominent lymphatics and gut-associated lymphoid tissue (GALT) patches. Hepatic, splenic and full thickness jejunal biopsies were also performed. The liver appeared covered with diffuse small round dark red to purple speckles associated with several focal areas of pale yellowish to white tissue. The dog recovered well from surgery and was discharged 4 days later. The dog was doing well 15 days after surgery.

Histopathological results were consistent with a severe extensive transmural ileitis with nodular histiocytic aggregates, serosal and mesenteric fibrosis, muscular degeneration and mucosal oedema, probably linked to a previous insult, such as a transiting foreign body. No evidence of malignancy could be identified. The biopsy of the jejunum showed slightly swollen smooth muscle cells. The changes within the liver and the spleen were non-specific.

Discussion

Gastrointestinal diseases are common conditions in dogs and cats, however clinical signs are non-specific and often do not aid in differentiating inflammatory intestinal lesions from intestinal tumours. Vomiting, diarrhoea (often chronic), melena, anorexia, abdominal pain, weight loss and lethargy are the most common clinical signs in both inflammatory and neoplastic diseases. On physical examination an abdominal mass or thickened intestinal loops may be palpated in both conditions.[1,2] In order to establish an appropriate treatment, differentiating inflammatory from neoplastic infiltration of the gastrointestinal tract is imperative. Ultrasonography is the gold standard diagnostic imaging tool used to assess the gastrointestinal tract. Gastro-intestinal wall thickening and layering, degree, symmetry and distribution of gastrointestinal wall changes, echogenicity of the mucosa, gastrointestinal motility and regional lymph nodes appearance can be assessed to distinguish gastrointestinal inflammation from neoplasia.[1,2] Care should be taken in the interpretation of measurements of wall thickness. Indeed, in normal dogs a significant increase in the jejunum and duodenum wall thickness is observed as the body weight increases, and the duodenum wall thickness is significantly thicker than the jejunal wall thickness.[3] Therefore, an abnormal wall thickness is considered to be greater than 6mm in the duodenum and greater than 4.7mm in the jejunum in dogs.[3,4]

Gastrointestinal inflammatory conditions include inflammatory bowel diseases (e.g. lymphoplasmacytic enteritis most commonly, eosinophilic enteritis, rarely granulomatous enteritis), protein-losing enteropathy and lymphangiectasia, food-responsive disease, antibiotic responsive diarrhoea, chronic infection (e.g. giardia, histoplasma, pythium, mycobacterium, toxoplasma, prototheca, bacterial infection) or changes induced by a traumatic event (e.g. foreign body).[1,5] Inflammatory disease often leads to a mild to moderate transmural, generally diffuse, thickening of the intestinal wall with preserved layering.[1,2,6] The relative thickness of the layers may also change while the total wall thickness remains normal in cases of chronic inflammatory

infiltrates. Changes in the mucosal echogenicity (e.g. increased echogenicity, mucosal striations, mucosal speckles) may be encountered in inflammatory process, such as inflammatory bowel disease, protein-losing enteropathy or lymphangiectasis.[5] Hyperechoic striations are reported to have a sensitivity of 75% and a specificity of 96% for dogs with protein-losing enteropathy, whereas hyperechoic speckles are non-specific for diagnosing inflammatory bowel disease.[5] In some instances, focal or segmental changes may be seen. Indistinct or complete loss of wall layering may also be observed with inflammatory processes, most commonly if ulcerative enteritis, fibrosis, oedema, haemorrhage and/or severe lymphoplasmacytic infiltration of the intestinal wall are present.[1,2,5] In one study[2], only 6.5% of dogs with enteritis had intestinal wall thickness equal to or exceeding 1cm and all were diagnosed with severe haemorrhagic, oedematous, necrotizing, fibrotic and/or suppurative enteritis. In the same study[2], 11% of dogs with enteritis had a loss of wall layering and all were diagnosed with severe, necrotizing, suppurative, granulomatous enteritis and/or intestinal wall perforation. These severe transmural changes are most likely responsible for the severity of the wall thickening and the loss of wall layering.[2] Other uncommon inflammatory conditions such as gastrointestinal pythiosis or histoplasmosis may also have severe focal or extensive wall thickening with loss of layering and/or intestinal masses. However, measurements of intestinal wall thickness are neither specific nor sensitive for diagnosing inflammatory intestinal disease[4], and ultrasonographic findings are non-specific for a particular disease process[5,6], except for hyperechoic mucosal striations, which are quite suggestive of lymphangiectasia, but not pathognomonic. Furthermore, inflammatory processes of the gastrointestinal tract do not always induce changes that can be detected with ultrasonography, and biopsy of the wall, by endoscopy or exploratory laparotomy, is required to confirm the diagnosis and assess the severity of lesions.[1,5] An insufficient number of infiltrating cells to cause an enlargement of the wall but nevertheless significant enough to result in clinical signs, or villus atrophy accompanying inflammation and reducing wall thickness may explain an ultrasonographically normal wall thickness in animals with histopathological evidence of inflammation and clinical signs. Mucosal echogenicity may be a better parameter for detecting inflammatory bowel disease than intestinal wall thickness in dogs with chronic diarrhoea[5], however normal-appearing intestinal wall on ultrasound does not rule out the presence of inflammation.[4,5,6,7]

The most common intestinal wall tumours in dogs are adenocarcinomas, lymphomas, leiomyomas, and leiomyosarcomas, whereas haemangiomas are rare but can occur. In

cats, the most common causes of neoplastic intestinal disease are lymphomas, mast cell tumours, and adenocarcinonomas.[1] A marked focal intestinal wall thickening, which may be eccentric or concentric, associated with a loss of wall layering, is the typical ultrasonographic finding in case of gastrointestinal neoplasia.[1,2] Neoplastic infiltrative wall thickness is significantly greater than that of nonspecific inflammatory disease.[1,2] In one study of 150 dogs[2] the mean wall thickness in dogs with non-specific enteritis was reported to be 0.6cm compared 1.5cm in dogs with neoplastic infiltration. In the same study, only 15% of dogs with intestinal neoplasia had wall thickness less than 1cm, however all these dogs but one had a loss of wall layering, which was present in 99% of all dogs with intestinal tumour (vs. 11% in dogs with non specific inflammatory process). Loss of wall layering identified ultrasonographically has a 50-times greater likelihood of a diagnosis of neoplasia than of a nonspecific inflammatory process and is the most reliable predictive factor for an intestinal tumor.[1,2] Gastrointestinal lymphoma is the most common neoplastic cause of diffuse infiltration and wall thickening that can appear similar to inflammatory disease, particularly in cats, but commonly occurs as a solitary, hypoechoic intestinal mass with transmural loss of wall layering. A significant association between muscularis thickening and feline T-cell lymphoma has been reported[1], but due to the overlap of diseases associated with muscularis thickening and lymphadenopathy in cats full-thickness intestinal biopsies are indicated for a definitive diagnosis.

Hepatic, splenic, gastric, pancreaticoduodenal, jejunal, colic and lumbar aortic lymph nodes drain the gastrointestinal tract and should be assessed during routine ultrasonographic examination, especially in case of gastrointestinal disease. Normal lymph nodes appear as small oval shaped homogeneous and smoothly marginated structures slightly hypoechoic or isoechoic to the surrounding mesentery. Jejunal lymph nodes are the largest and longest lymph nodes in normal dogs and their height in healthy dogs may be up to 8.2 mm.[1] Lymph nodes may be enlarged in inflammatory disease, but typically maintain a normal shape and echogenicity, whereas metastatic lymph nodes are typically markedly enlarged, rounded, and hypoechoic in cats and dogs. The median lymph node thickness was reported to be 1cm in dogs with non-specific enteritis vs. 1.9cm in dogs with gastrointestinal neoplasia.[2] However, infectious diseases often lead to more severe lymph node enlargement with features similar to those of metastatic infiltration. Necrotic or haemorrhagic lymph nodes appear larger, more heterogeneous and irregular, independent of the underlying cause.[1] Percutaneous ultrasound-guided

fine needle aspiration of enlarged lymph nodes, under sedation or anaesthesia, is a useful tool to obtain a definitive diagnosis.

Awareness of features of both gastrointestinal inflammatory and neoplastic infiltration is important for the accurate interpretation of the ultrasonographic findings, however overlaps in the ultrasonographic appearances of inflammatory and neoplastic infiltrations make a definitive diagnosis difficult. Full-thickness intestinal biopsy remains the gold standard for differentiating inflammatory from neoplastic disease. Ultrasound-guided fine needle aspiration of gastrointestinal masses or enlarged lymph nodes may be an interesting less invasive tool which can lead to a definitive diagnosis, especially in case of suspected neoplasia.[7]

References

1-Gaschen L. Ultrasonography of small intestinal inflammatory and neoplastic diseases in dogs and cats. **Vet Clin North Am Small Anim Pract** 2011; 41(2): 329-344.

2-Penninck D, Smyers B, Webster CR, Rand W, Moore AS. Diagnostic value of ultrasonography in differentiating enteritis from intestinal neoplasia in dogs. **Vet Radiol Ultrasound** 2003; 44(5): 570-575.

3-Delaney F, O'Brien RT, Waller K. Ultrasound evaluation of small bowel thickness compared to weight in normal dogs. **Vet Radiol Ultrasound** 2003; 44(5): 577-580.

4-Rudorf H, van Schaik G, O'Brien RT, Brown PJ, Barr FJ, Hall EJ. Ultrasonographic evaluation of the thickness of the small intestinal wall in dogs with inflammatory bowel disease. **J Small Anim Pract** 2005; 46(7): 322-326

5-Gaschen L, Kircher P, Stüssi A, Allenspach K, Gaschen F, Doherr M, Gröne A. Comparison of ultrasonographic findings with clinical activity index (CIBDAI) and diagnosis in dogs with chronic enteropathies. **Vet Radiol Ultrasound** 2008; 49(1): 56-64.

6-Gaschen L, Kircher P. Two-dimensional grayscale ultrasound and spectral Doppler waveform evaluation of dogs with chronic enteropathies. **Clin Tech Small Anim Pract** 2007; 22(3): 122-27.

7-Leib MS, Larson MM, Grant DC, Monroe WE, Troy GC, Panciera DL, Rossmeisl JH, Werre SR. Diagnostic utility of abdominal ultrasonography in dogs with chronic diarrhea. **J Vet Intern Med** 2012; 26(6): 1288-1294.

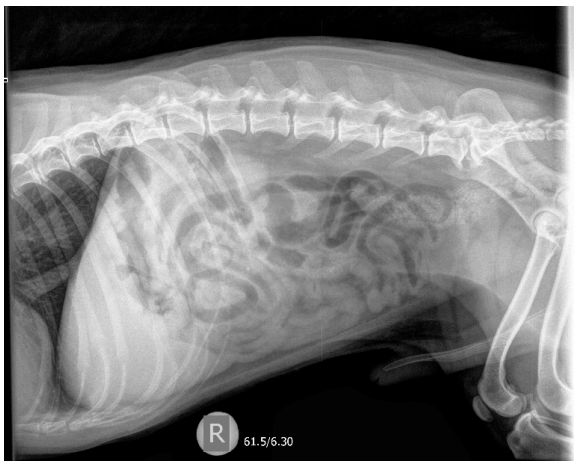

Figure 3.1 - Right lateral abdominal radiograph

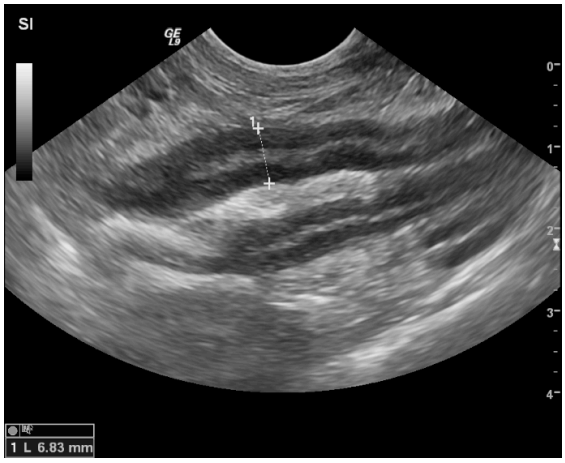

Figure 3.2 - Longitudinal ultrasound image of distal ileum

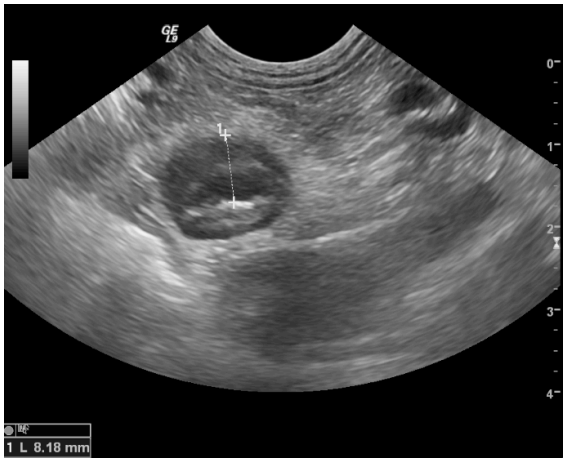

Figure 3.3 - Transverse ultrasound image of distal ileum

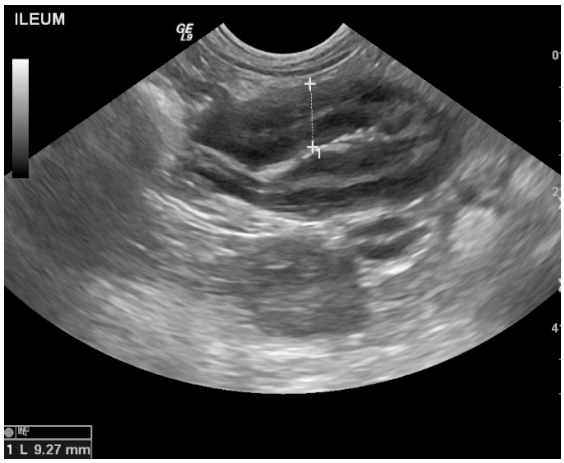

Figure 3.4 - Longitudinal ultrasound image of distal ileum (Follow up)

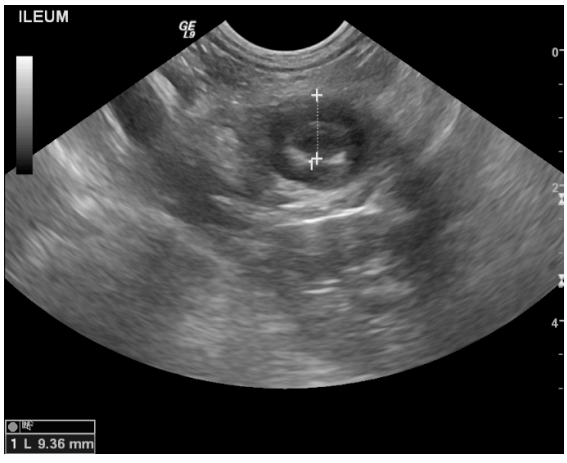

Figure 3.5 - Transverse ultrasound image of distal ileum (Follow up)

Case 4. Histiocytic sarcoma

Signalment and History

A 6-year-old female neutered Flat Coated Retriever was presented with an acute onset of a moderate left hind limb lameness of 2-3 weeks duration associated with a toe-touching stance. Treatment with meloxicam (Metacam®, Boehringer-Ingelheim) improved the condition only slightly.

Clinical Signs

a) Moderate left hind limb lameness (4/10)
b) Pain on manipulation of the left stifle with peri-articular swelling
c) Atrophy of the quadriceps muscle group on the left limb
d) Examination under sedation revealed a soft tissue mass extending distally from the proximal end of the cranial tibial muscle

Radiographic Examination

1. **Equipment** - See Appendix 1
2. **Restraint** - The dog was sedated and positioning was achieved using wedges of dressing material and rope ties.

Area	View	kV	mAs	Grid
Left stifle	Caudo-Cranial (Fig.4.1)	55	4	N
	Medio-Lateral (Fig.4.2)	55	4.5	N
	Medio-Lateral (Fig.4.3)	55	4.5	N
Thorax	Dorso-Ventral (Fig.4.4)	70	12.5	O
	Right Lateral (Fig.4.5)	64.5	10	O
	Left Lateral (Fig.4.6)	64.5	10	O

Radiographic Appraisal

Two medio-lateral views of the left stifle were available; one slightly more centred on the femur (Fig.4.2) and the other one slightly more centred on the tibia (Fig.4.3). A moderate rotation of the femur is noted on the 1st medio-lateral radiograph (Fig.4.2), but it is well centred. Other radiographs are well positioned and centred. A radio-opaque line, perpendicular to the length of the film at the level of the femoral condyle, is visible on the 2nd medio-lateral radiograph (Fig.4.3), most likely due to a dusty detector – processing default. All radiographs are well exposed. Primary markers are present on all views, although a secondary L marker has been added to the 2nd medio-lateral radiograph, as the primary one is half outside the field of view. Exposure settings are

present on the 1st medio-lateral and caudo-cranial (Fig.4.1) views. The radiographs are of diagnostic quality.

All the thoracic radiographs are well centred. The dorso-ventral view (Fig.4.4) of the thorax is slightly rotated; all other views are well positioned. Both lateral radiographs of the chest (Figs.4.5 and 4.6) are slightly overexposed. A linear radio-opaque line, parallel to the length of the films is visible in all views, due to a dusty detector – processing default. Primary markers are present on all views, superimposed on thoracic soft tissue. The thoracic radiographs are of diagnostic quality.

Radiological Report

There is a loss of the parapatellar fat pad with marked soft tissue swelling within the joint indicative of severe effusion (Figs.4.1 and 4.2). Loss of the caudal fascial plane and most especially in the cranio-lateral aspect of the crus, is suggestive of joint distension and periarticular swelling (Figs.4.1 to 4.3). Fairly well defined radiolucent areas are visible in the medial fabella. Small focal radiolucent areas are also visible in the caudal aspect of the medial femoral and lateral tibial condyles, which could be consistent with lytic change. A slightly altered contour of the proximal third of the fibular diaphysis is noticed associated with slightly irregular thickening of the cortex, which may be associated with adjacent soft tissue swelling. Mild new bone production is observed at the trochlear ridges, the distal aspect of the patella and the lateral tibial plateau most likely consistent with mild degenerative changes. The area of popliteal lymph node is unclear, so it cannot be assessed properly.

A very mild diffuse bronchial pattern is visible on thoracic radiographs (Figs.4.4 to 4.6), most likely consistent with the age. A mild increased opacity of the lung field is noted on the dorso-ventral view (Fig.4.4), most likely consistent with the expiratory status. No obvious sign of metastasis is visible. Very mild new bone formation is noted at the caudal aspect of both humeral heads consistent with mild degenerative changes.

Differential Diagnosis

Polyostotic lytic changes with associated soft tissue swelling centred on the stifle, consistent with soft tissue neoplasia (e.g. histiocytic sarcoma, haemangiosarcoma, less likely synovial cell sarcoma), diffuse infectious/inflammatory disease (e.g. myositis, cellulitis, septic arthritis, fabellar osteomyelitis) or arthropathy (e.g. haemarthrosis, cruciate disease, arthritis).

Further Investigations

Ultrasonography of the left stifle was performed. A selection of US images is included with this report (See Figs.4.7 to 4.10, page 43). A swelling of the muscles distal to the stifle was noticed and this appeared irregular, disorganized with patchy mixed echogenicity. Multiple hypoechoic nodules with a hyperechoic background were visible within. Similar changes were present in the distal quadriceps muscle. No fluid accumulation, periosteal reaction or change in the bone surface was noted. Differential diagnosis included muscle neoplasia most likely (e.g. histiocytic sarcoma, haemangiosarcoma, fibrosarcoma).

Fine needle aspiration of the muscle mass was performed and cytology was consistent with histiocytic sarcoma. No bacterium was isolated after culture of the aspirate, even after enrichment.

Fine needle aspiration of the left popliteal lymph node was performed for the regional staging. No aberrant cells were detected.

Abdominal ultrasonography under sedation was performed for general staging. A small hypoechoic nodule about 3mm in diameter was visible in the spleen and a fine needle aspiration of it was performed but no aberrant cells were seen. The rest of the ultrasound examination of the abdomen was unremarkable.

Biochemistry revealed a mild elevation of the aspartate aminotransferase (AST = 107 U/L) possibly secondary to muscle damage. Haematology revealed no significant abnormality.

Outcome

The dog underwent left hind limb amputation by coxo-femoral disarticulation 3 days later. He made a very rapid and smooth recovery after surgery and was discharged three days post-surgery. Histopathological examination of the left hind limb mass confirmed histiocytic sarcoma.

At follow-up visit 15 days after surgery, the dog was doing well and coping well with 3 legs. No swelling or discharge of the wound was noticed. After discussion, the owners decided to not pursue any chemotherapy options due to financial constraints. They have been advised to monitor the surgical site for any changes, which may indicate local recurrence, or tachypnea, dyspnoea or exercise intolerance that could indicate pulmonary metastasis.

Discussion

Malignant proliferations of histiocytic cells were first reported in the dog in the late 1970s[1]. Histiocytic sarcoma (HS), subcategorized as localized or disseminated, is thought to arise from myeloid dendritic antigen-presenting cells. Previously the term malignant histiocytosis was used for disseminated HS, described as an involvement of multiple organs, with sites of predilection including lung, spleen, bone marrow, liver, and lymph nodes, although a large number of other anatomical sites has been reported. In contrast, localized HS is a single primary lesion, with or without regional lymph node metastasis, typically involving the lung, skin, subcutaneous and muscular tissues, bones, or joints. However, localized HS can metastasize beyond the regional lymph node, and disseminated HS may be a terminal stage of localized HS with systemic metastases. A third clinical manifestation of HS is recognised as haemophagocytic HS, thought to arise from macrophages of the splenic red pulp and bone marrow, characterized by diffuse splenomegaly, anaemia and thrombocytopenia.[1,2,3,4]

A predisposition in Bernese Mountain Dogs, with a highest prevalence for the disseminated form, is recognized, male appearing to be more affected than female. Rottweilers, Flat-Coated Retrievers, Golden Retrievers and Labrador Retrievers are also overrepresented, however the localised musculoskeletal form is most often reported in these breeds.[1,4,5] In a study of HS in thirty-seven Flat-Coated Retrievers, thirty-four presented a swelling or mass in a muscle group or surrounding a joint[3].

Dogs are commonly middle aged or older, but HS has been reported in dogs as young as 3 years of age[1]. The clinical signs at time of presentation are often non-specific (weight loss, lethargy, anorexia) associated with lameness, pain and presence of soft tissue mass in the localized form. Anaemia is a common complication.[1,2,3,4,5]

The radiographic characteristics of musculoskeletal and periarticular lesions due to HS, including location, are similar to what would be anticipated in primary musculoskeletal neoplasms and joint-associated neoplasms respectively. The most often reported locations are stifles, elbows and proximal humeri, although involvement of vertebrae, ribs or other joints has been described. Bone lesions reported have an aggressive pattern, characterized predominantly by bone lysis, most often associated with a soft tissue mass, except in instances of involvement of the proximal aspect of the humerus or the hip joint, where a soft tissue mass is typically not present. Dogs with periarticular lesions may present with lytic lesions involving multiple bones of a joint, in addition to a periarticular soft tissue mass. A possible association between HS and cranial cruciate ligament rupture has also been suspected.[5,6] In the dogs with proximal humeral

involvement, the neoplasm was thought to arise from bone marrow and destroy the surrounding cortical and trabecular bone, whereas the neoplastic process was thought to arise from histiocytes near synovial tissues and destroy multiple surrounding bones in dogs with periarticular involvement.[5]

HS is a highly aggressive neoplasm with variable prognosis and reported metastatic rates of 70% to 91%, thereby local and distant staging by mean of thoracic radiographs and abdominal ultrasound are necessary. A more favourable outcome may be expected for dogs with localized HS than for dogs with the disseminated form, which has a grave prognosis. Particularly, dogs with the periarticular form of HS may have a more favourable outcome than dogs with HS of any other anatomic locations, independent of the metastatic status. However, the presence of distant metastasis in dogs with localized HS appears to be a negative prognostic indicator.[2] Treatment consisting of surgery, radiation, chemotherapy, or a combination of these appears to improve outcome in dogs with HS. A median survival of 17 months is reported when the localized form is treated aggressively with chemotherapy or multimodal therapy, while non-resectable or disseminated disease has 35% response rate and median survival of 4 months when treated with Lomustine.[4] In a study of HS in 37 Flat-Coated Retrievers, dogs receiving only palliative therapy survived a median of 17 versus 167 days in dogs receiving any kind of radiation, chemotherapy, surgery or combinations.[3] Haemophagocytic HS follows a rapidly progressive clinical course despite treatment and the reported median survival time is approximately 7 weeks, probably due to a more aggressive behaviour linked to the cellular ability to phagocytose material including host red blood cells.[2]

References

1-Clifford CA, Skorupski KA, Moore PF. Chapter 33, Part IV Specific Malignancies in the small animal patient, Section F: Histiocytic Diseases. In: Withrow SJ, Vail DM, Page RL. **Small Animal Clinical Oncology**, 5th ed., Elsevier Saunders, St Louis, Missouri, 2013; 706-715

2-Constantino-Casas F, Mayhew D, Hoather TM, Dobson JM. The clinical presentation and histopathologic-immunohistochemical classification of histiocytic sarcomas in the Flat Coated Retriever. **Vet Pathol.** 2011; 48(3): 764-771.

3-Fidel J, Schiller I, Hauser B, Jausi Y, Rohrer-Bley C, Roos M, Kaser-Hotz B. Histiocytic sarcomas in Flat-Coated Retriever: a summery of 37 cases (November 1998-March 2005). **Vet Comp Oncol.** 2006; 4(2): 63-74.

4-Klahn SL, Kitchell BE, Dervisis NG. Evaluation and comparison of outcomes in dogs with periarticular and nonperiarticular histiocytic sarcoma. **J Am Vet Med Assoc.** 2011; 239(1): 90-96.

5-Schultz RM, Puchalski SM, Kent M, Moore PF. Skeletal lesions of histiocytic sarcoma in nineteen dogs. **Vet Radiol Ultrasound.** 2007; 48(6): 539-543.

6-Castellanos VC, O'Neill S, Seiler GS. What is your diagnosis? Histiocytic sarcoma. **J Am Vet Med Assoc.** 2010; 236(12): 1293-1284.

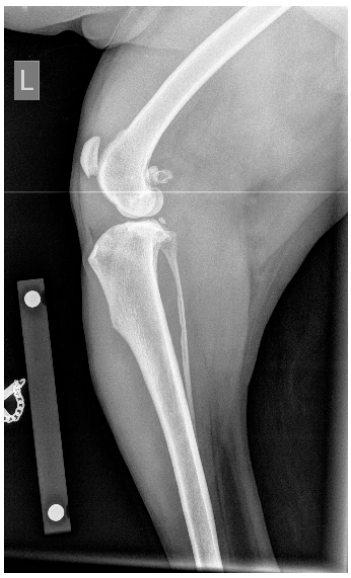

Figure 4.1 - Medio-lateral view of the L stifle

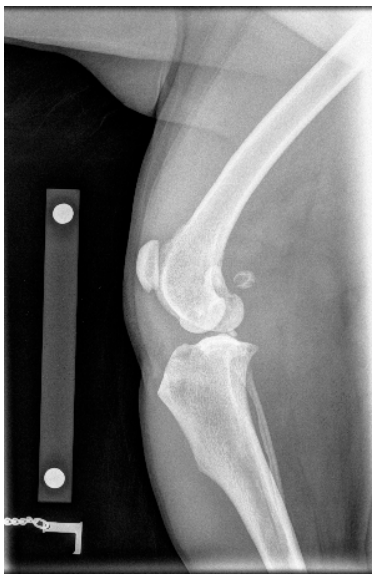

Figure 4.2 - Medio-lateral view of the L stifle

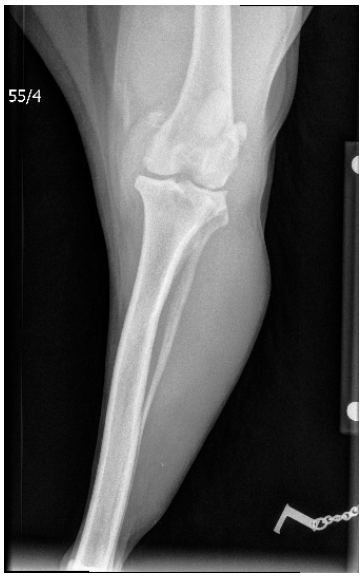

Figure 4.3 - Caudo-cranial view of the L stifle

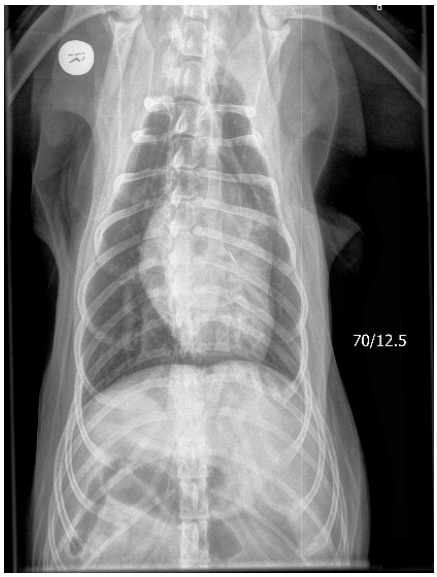

Figure 4.4 - Dorso-ventral thoracic radiograph

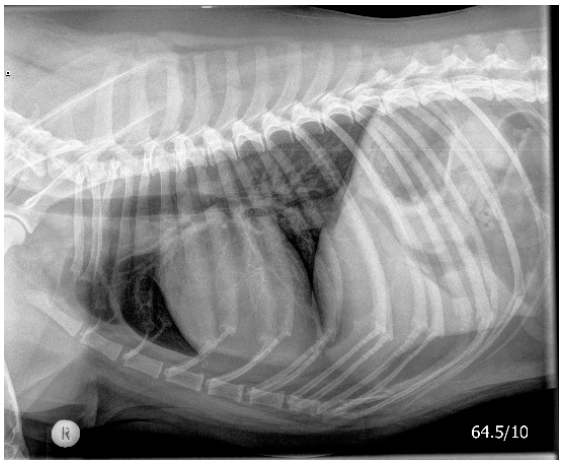

Figure 4.5 - Right lateral thoracic radiograph

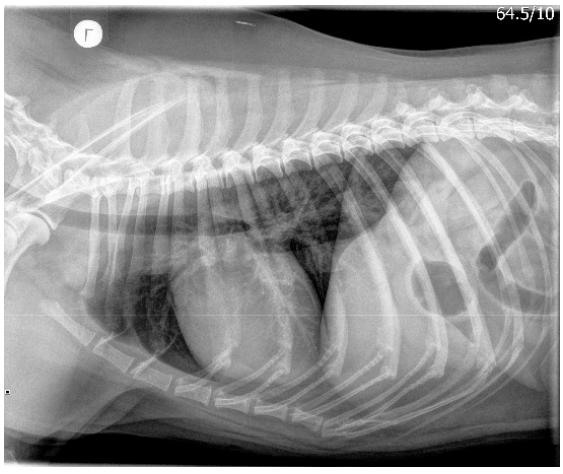

Figure 4.6 - Left lateral thoracic radiograph

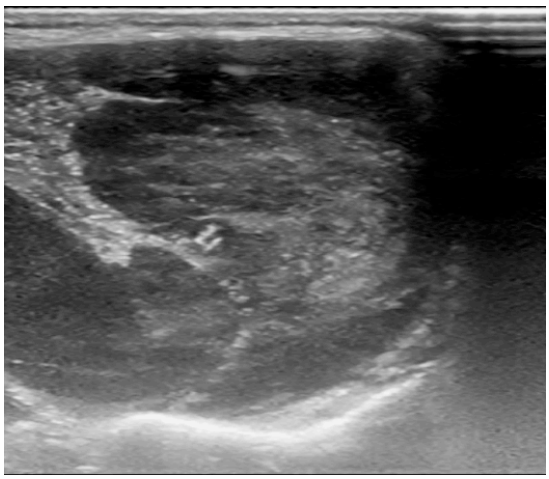

Figure 4.7 - Transverse ultrasound image of the left cranial tibial muscle

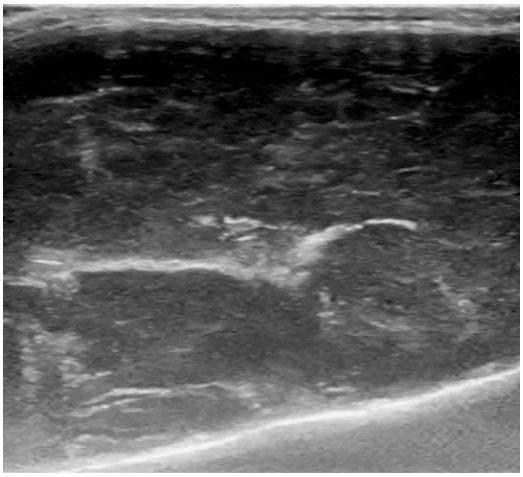

Figure 4.8 - Longitudinal ultrasound image of the left cranial tibial muscle

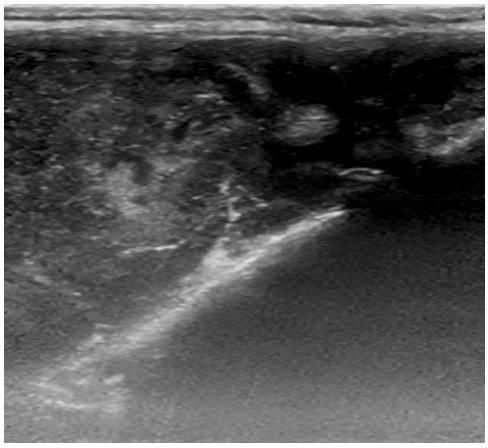

Figure 4.9 - Proximal ultrasound aspect of the left cranial tibial muscle

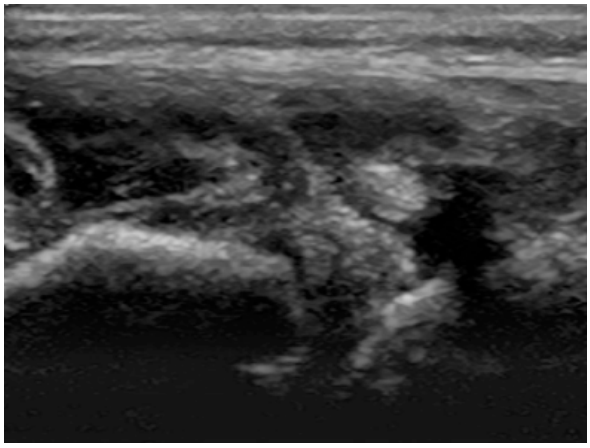

Figure 4.10 - Longitudinal ultrasound image of the left stifle (distal part on the left)

Case 5. Extra Hepatic Porto-Systemic Shunt

Signalment and History

An 8-month-old entire female Shih Tzu presented with a two months history of progressive periodic lethargy and altered mentation. The initial signs were of being sleepy, and then the dog seemed lifeless and weak, lying down and not wanting to get up. The owners noted the dog to be stiff in her front limbs and sometimes walking into objects. When the episodes started, she would bark a lot, not particularly at anything or anyone. The dog did not warn owner of the need to urinate. An initial treatment of a 2 weeks course of steroid and one injection of multivitamins was initiated. Throughout the dog maintained a good appetite and defecation was normal. The dog was fully vaccinated and wormed against ecto- and endoparasites.

Clinical Signs

Physical examination was unremarkable at time of presentation.

Ultrasonographic Examination

1. **Equipment** - See Appendix 1
2. **Restraint** - Poppy was placed in dorsal recumbency.

Abdominal Ultrasound Report

A large long abnormal supernumerary vessel seemed to arise from the portal vein at the level of the hepatic hilus. It coursed along the dorsal aspect of the pyloric antrum before curving dorsally to the right around the stomach and finally joined the vena cava on the left side (Figs.5.1 and 5.2). The size of the liver was moderately decreased, but the echogenicity and architecture were within normal limits. The size of both kidneys was at the upper end of normal (length approximately 4.4cm). A tiny amount of floating echoic material was visible in the lumen of the bladder consistent with sediment, cell debris or concentrated urine.

Diagnosis

Extra-hepatic porto-caval shunt.

Further Investigations

Biochemistry revealed moderate panhypoproteinaemia (TP = 49g/L, Alb = 26g/L, Glob = 23g/L), moderate increase of the liver enzymes (ALKP = 453 U/L, AST = 68 U/L)

and markedly raised pre- and post-prandial bile acid concentrations (Pre-prandial bile acids = 132.4μmol/L, post-prandial bile acids – result not included).

Coagulation tests revealed a mild increased of the Prothrombine Time (PT = 12.9s) and Kaolin Cephalin Clotting Time (KCCT = 84.5s).

These results were consistent with liver dysfunction that can explain hepatic encephalopathy linked to the porto-systemic shunt.

Outcome

The dog was medicated for a hepatic encephalopathy (Lactulose syrup, L-arginine, Ampicillin) and fed with a hepatic support diet for one month prior surgery. A moderate improvement in clinical signs was seen.

The dog underwent a porto-systemic shunt ligation one month later. At surgery microhepatica and an enlarged gallbladder were found. The extrahepatic shunt was identified running from the portal vein at the level of the coeliac artery, forming an U bend along the dorsal aspect of the stomach before joining the vena cava cranial to the phrenico-abdominal vein. The exploration also identified unusually enlarged lymphatic and blood vessels running through the mesentery and along the gastro-intestinal tract. Similarly, the mesenteric lymph nodes and some of the gut-associated lymphoid tissue were more prominent than normal. A foreign body was found in the stomach as an incidental finding, which was removed by gastrotomy. An ameroid constrictor was placed around the supernumerary shunting vessel. A liver biopsy was taken. The abdomen was lavaged and closed.

The histopathological appearance of the liver was consistent with the clinical diagnosis of porto-systemic shunt and no concurrent abnormality was detected in the sections examined.

The dog made a good recovery from anaesthesia and surgery, with no early complications, and was discharged few days later with continued medication (Synulox®, Pfizer –Amoxicillin/Clavulanic acid, Metacam®, Boehringer Ingelheim – Meloxicam, Keppra®, Ucb Pharma Sa – Levetiracetam, Zantac®, Boehringer Ingelheim – Ranitidine, and Lactulose) and a hepatic support diet.

Discussion

In congenital porto-systemic shunts (PSS), the portal blood, derived essentially from the gastrointestinal tract, the pancreas and the spleen, flows directly into the systemic circulation by abnormal vessel communication thus bypassing the liver parenchyma.[1,2] As a consequence the portal blood, which normally carries many substances to the liver

including trophic hormones, nutrients, bacterial products, and intestinal-derived toxins, is not subjected to hepatic metabolism, resulting in poor hepatic development, deficient protein production, reticuloendothelial dysfunction, altered fat and protein metabolism, hepatic atrophy, and eventually liver failure.[1]

Several types of congenital PSS are encountered in dogs and cats; including intrahepatic porto-caval shunts, extrahepatic porto-caval shunts, extrahepatic porto-azygos shunts, portal vein atresia with resultant multiple portal-caval anastomoses, hepatic arteriovenous malformations, and microintrahepatic PSS called microvascular dysplasia.[1] Congenital PSSs occur in 80% of cases as a single intrahepatic or extrahepatic communication. Rarely, some animals have two or more congenital communications. Congenital intrahepatic PSSs count for approximately 25% to 33% of congenital PSSs in dogs and cats and occur most often in larger-breed dogs, with prevalence in the Irish Wolfhounds, Retrievers, Australian Cattle Dogs, and Australian Shepherds. Single extrahepatic PSSs constitute 66% to 75% of congenital single PSS in both species, and they are most often encountered in smaller breeds and cats, with a breed predisposition in Yorkshire Terriers, Cairn Terriers, Jack Russel Terriers, Havaneses, Malteses, Dandie Dinmont Terriers, Pugs, Dachshunds, West Highland White Terriers and Miniature Schnauzers.[1,2,3] Porto-caval shunts, including all different types of communication, are reported to be more common (75%), compare to porto-azygos shunt (25%).[2] Both sexes are equally affected, although a significantly higher number of females compared to males was affected by porto-azygos shunt in one study[2].

Most dogs and cats with PSS have signs of chronic or acute illness before 1 to 2 years of age, though some have been older than 10 years of age. The age of first diagnosis is significantly higher in case of porto-azygos shunts compared to porto-caval ones. This may be explained by the fact that probably less blood bypasses the liver in porto-azygos shunt, the azygos vein being smaller in diameter compare to caudal vena cava and because respiration causes diaphragmatic compression during which the shunt may be intermittently closed.[2] Dogs with intrahepatic PSS generally have a largest volume of diverted portal blood, thus tend to develop more severe clinical signs at an earlier age than those with extrahepatic PSS.[1,3]

Clinical signs are associated with the volume and origin of blood bypassing the liver, resulting in impaired hepatic function, hepatic encephalopathy, chronic gastrointestinal signs, lower urinary tract signs, coagulopathies, and delayed growth. Small stature, weight loss or failure to gain weight, anaesthetic intolerance, dullness or lethargy at

times, polyuro-polydypsia, inappropriate behaviour and central nervous system signs, including stargazing, staring into walls or corners, random barking, intermittent blindness, pacing, circling, seizures or aggression, are often reported.[1] Gastrointestinal signs, such as vomiting, diarrhoea, anorexia, pica, and/or gastro-intestinal bleeding, occur in approximately 30% of dogs but are less frequent in cats. 20% to 50% of animals with congenital PSS present with signs of lower urinary tract disease, such haematuria, stranguria, pollakiuria, or urinary obstruction, due to formation of ammonium urate calculi, which can be associated with bacterial urinary tract infections.[1]

Mild to moderate, microcytic, normochromic, non-regenerative anaemia is a common haematological change. Leucocytosis, due to inadequate hepatic endotoxin and bacteria clearance from the portal circulation, has been associated with a poor prognosis. Low albumin, low urea, hypercholesterolemia and hypoglycaemia, due to decreased hepatic synthesis are common serum biochemical abnormalities as well as excess serum liver enzyme activities. 2-hour postprandial serum bile acid is almost always increased whereas increased fasting serum bile acid is less constant, although both may be normal in a few cases. Ammonia concentrations, increased in 62 to 88% of congenital PSS, are not as sensitive as the serum bile acid test, especially after prolonged fasting or with effective medical management of hepatic encephalopathy. Measurement of 6-hour postprandial blood ammonia concentrations increased detection sensitivity to 91% in dogs with PSS.[1] Prolonged aPTT is another finding in most dogs with PSS prior to correction, although spontaneous bleeding is rare. Urinalysis abnormalities include a low urine specific gravity, resulting from polydipsia and poor medullary concentration gradient, and ammonium biurate crystalluria, resulting from the deficient hepatic urea cycle. Proteinuria is often seen in dogs with PSSs, suspected to be secondary to glomerular sclerosis or another underlying glomerulopathy.[1]

Whereas history, clinical signs and laboratory results give high suspicion of congenital PSS, the definitive diagnosis of presence and type of congenital PSS may be determined by imaging. Abdominal ultrasound is highly sensitive (92%) and specific (98%) in identifying congenital PSS, with a sensitivity and specificity of 100% for intrahepatic PSS.[5] Left, central, and right divisional intrahepatic shunts can often be differentiated, whereas to fully define extrahepatic shunt morphology, additional examinations are often required. The combination of a small liver, large kidneys, and uroliths increases the predictability for congenital PSS. The portal vein/aorta and portal vein/caudal vena cava ratios are reported to be smaller in animals with extrahepatic PSS compared with

animals with microvascular dysplasia, intrahepatic PSS and those without portal venous anomalies. Ratios of ≥0.8 and ≥0.75 respectively, excluded the presence of extrahepatic PSS in one study[4]. Computed tomography (CT) angiography is the gold standard for evaluating the portal venous system.[1] All portal tributaries, branches and the fully defined morphology of intra- or extrahepatic shunts can be visualized with accuracy. Six general types of extrahepatic PSSs (spleno-caval, spleno-azygos, spleno-phrenic, right gastric-caval, right gastric-caval with a caudal shunt loop, and right gastric-azygos with a caudal shunt loop), identified in one study of 25 dogs that underwent CT angiography with 3-dimentional reconstruction, are likely to represent the most common extrahepatic porto-systemic shunt conformations.[5] Contrast-enhanced magnetic resonance angiography (CE-MRA) can also provide excellent assessment of portal vascular anatomy with short acquisition times (<10 min). However, it does not allow accurate identification of renoliths or cystoliths, which are readily identified with CT or ultrasonography.[6] CT angiography and CE-MRA are accurate, fast and non-invasive procedures for assessment of shunt morphology that are very helpful in surgical planning, however drawbacks such as requirement of general anesthesia, higher expense and potential for adverse reactions to contrast media have to be considered.[1,5,6]
Medical management, based on a readily digestible diet with a moderate amount of high biologic value proteins, antimicrobials, and lactulose, may be required prior to surgical management of PSS or when surgery is not possible or declined, to control clinical signs associated with shunting.[1,3] Several types of surgical interventions have been used, based on the location of the shunting vessel and the preference of surgeon, including ameroid constrictor, cellophane bands, and ligatures.[3] The mortality rate in dogs with congenital extrahepatic PSS during the perioperative period was 4% in a recent study[3] and the overall mortality rate was 10% in dogs treated surgically and 29% for dogs receiving medical management only. Furthermore surgical treatment, in association with medical management, is associated with longer survival time than is medical management alone.[3]

References

1-Berent AC, Weisse C. Chapter 279-Hepatic vascular Anomalies. In: Ettinger SJ, Feldman EC, **Textbook of Veterinary Internal Medicine**, 7th Ed, Vol 2, St. Louis, Missouri 2010; 1201-1254.

2-Van den Bossche L, Van Steenbeek FG, Favier RP, Kummeling A, Leegwater PA, Rothuizen J. Distribution of extrahepatic congenital portosystemic shunt morphology in predisposed dog breeds. **BMC Vet Res** 2012; 8: 112.

3-Greenhalgh SN, Dunning MD, McKinley TJ, Goodfellow MR, Kelman KR, Freitag T, O'Neill EJ, Hall EJ, Watson PJ, Jeffery ND. Comparison of survival after surgical or medical treatment in dogs with a congenital portosystemic shunt. **J Am Vet Med Assoc** 2010; 236(11): 1215-1220.

4-D'Anjou MA, Penninck D, Cornejo L, Pibarot P. Ultrasonographic diagnosis of portosystemic shunting in dogs and cats. **Vet Radiol Ultrasound** 2004; 45(5): 424-437.

5-Nelson NC, Nelson LL. Anatomy of extrahepatic portosystemic shunts in dogs as determined by computed tomography angiography. **Vet Radiol Ultrasound** 2011; 52(5): 498-506.

6-Mai W, Weisse C. Contrast-enhanced portal magnetic resonance angiography in dogs with suspected congenital portal vascular anomalies. **Vet Radiol Ultrasound** 2011; 52(3): 284-288.

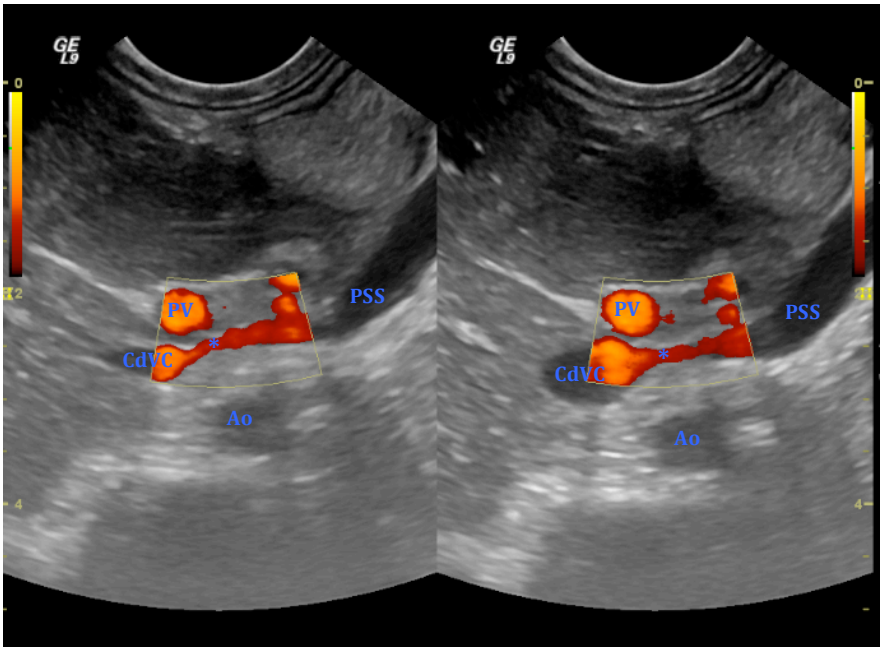

Figure 5.1 - Ultrasound images with Power Doppler examination of the portosystemic shunt joining the left side of the caudal vena cava

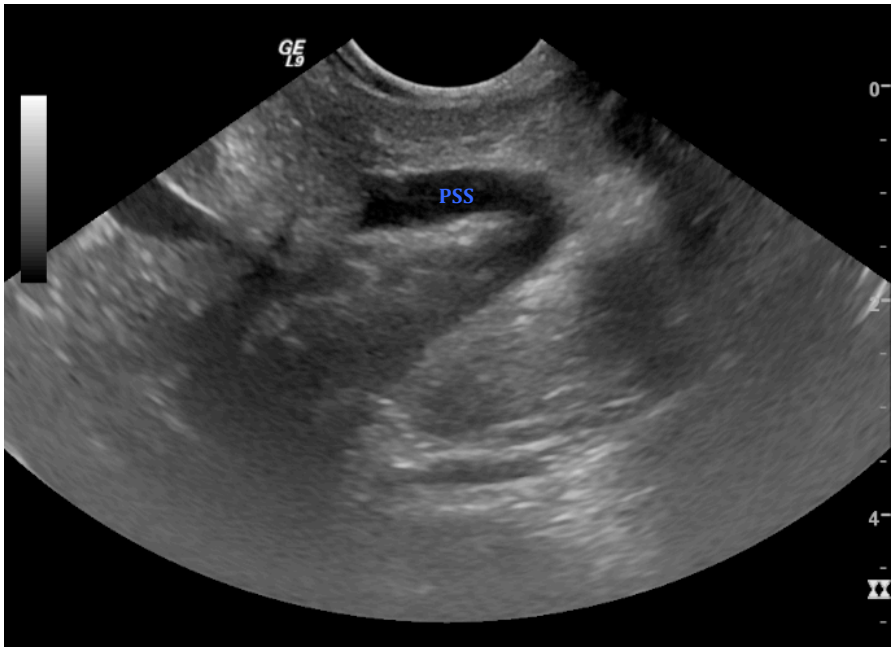

Figure 5.2 - Ultrasound image of the portosystemic shunt

Ao: Aorta; CdCV: Caudal Vena Cava; PSS: Portosystemic shunt; PV: Portal Vein; *: junction between PSS and CdCV

Case 6. Thoracic Mass causing Budd-Chiari-like Syndrome

Signalment and History

A nine-year-old female neutered West Highland White Terrier was presented with a fortnight history of coughing and abdominal enlargement, but no signs of lethargy, anorexia, weight loss or behaviour change. Abdominal effusion consistent with transudate was found at the referral veterinary clinic. The bitch was referred to the Small Animal Hospital, University of Glasgow for further investigations.

Clinical Signs

a) Abdominal distension
b) Occasional cough during consultation.

Ultrasonographic Examination

1. **Equipment** - See Appendix 1
2. **Restraint** - No sedation used. The dog was placed in lateral and dorsal recumbency for an abdominal ultrasound scan.

Abdominal Ultrasound Report

A moderate to marked amount of free fluid was found, largely in the cranial abdomen (Fig.6.1). A prominent caudal vena cava and hepatics veins were visible, associated with a slightly heterogeneous hepatic parenchyma. A heterogeneous mass, of at least 6 centimeters in diameter, associated with some acoustic shadowing and reverberating foci was found in the caudal thorax adjacent to the diaphragm, while scanning the liver (Fig.6.2). This mass appeared to be compressing the caudal vena cava and was surrounded by pleural effusion (Fig.6.3). Otherwise no significant abnormality was visible in the remaining abdomen.

Diagnosis

Budd-Chiari-like syndrome linked to a large caudal pulmonary mass compressing the intra-thoracic caudal vena cava and causing hepatic congestion and ascites.

Radiographic Appraisal

Thoracic radiographs (Figs.6.4 to 6.6) were performed to assess the pulmonary mass seen on ultrasound. All thoracic radiographs are well positioned and centred. The images are well processed. The right lateral radiograph (Fig.6.5) is slightly overexposed. Primary markers and exposure settings are present, although the right (R)

marker on the right lateral radiograph is outside the primary beam, and a secondary R marker has been added. The radiographs are of diagnostic quality.

Radiological Report

A large heterogeneous and cavitary mass involving the right caudal lung lobe is visible, which has slightly displaced the cardiac silhouette to the left side. A diffuse bronchial pattern, more marked in the middle and caudal lung lobes, associated with a marked diffuse bronchiectasis is noted. A slightly prominent pulmonary trunk on the dorso-ventral view is noted, which may be due to the slight displacement of the cardiac silhouette, although a pulmonary hypertension linked to the pulmonary changes cannot be excluded. A markedly decreased abdominal contrast associated with an enlargement of the liver and a distended abdominal cavity is consistent with the significant amount of abdominal free fluid and the hepatic congestion seen on ultrasonographic examination.

Advanced imaging – Thoracic Computed Tomography

Thoracic CT (Figs.6.7 to 6.10) was performed to assess if there was more extensive local invasion by the intrathoracic mass and rule out pulmonary metastatic disease.

A very large cavitary and heterogeneous mass with fluid line delineation within is seen in the right caudal lung lobe surrounding the right caudal and accessory main bronchi (Fig.6.7). Some small mineralized foci are seen within the mass, and a larger round mineralized structure is also visible in the middle of the mass consistent with a dystrophic mineralization or a foreign body given its symmetric shape (Figs.6.8 and 6.9). A very slight peripheral enhancement is visible on post-contrast images with a focal marked enhancement around the bifurcation of the right caudal and accessory main bronchi, most likely consistent with compressed main pulmonary vessels. The mass has displaced the dorsal mediastinum to the left; however an encroachment of the mediastinum could not be ruled out. A mild diffuse interstitial pattern, more marked surrounding the mass, is also noted. No obvious bronchiectasis and bronchial wall thickening is visible otherwise. The sternal lymph node is mildly enlarged. A moderate to marked amount of abdominal effusion and a moderate enlargement of the liver associated with a dilation of hepatic veins and a dorsal compression of the thoracic caudal vena cava (Fig.6.10) are evident, consistent with Budd-Chiari-like syndrome. The azygos vein is subjectively slightly prominent, likely secondary to the caudal vena cava compression and redistribution of venous return to the heart. Diagnostic differential included a neoplastic process (e.g. bronchio-alveolar carcinoma, pulmonary

adenocarcinoma), an abscess with or without foreign body or less likely a pulmonary cyst.

Outcome

Ultrasound-guided fine needle aspiration of the mass was not performed regarding its cavitated aspect and the potential risk to spread infection. Surgical lung lobe removal was elected as treatment and diagnostic tool allowing histopathology to be performed. The bitch underwent a median sternotomy to remove the mass. The mass was located in the caudal right lung lobe and well circumscribed in the lung parenchyma, no involvement of the surrounding tissues was noted. A lobectomy was performed using a stapling device with a reinforcing suture placed to ensure the stump was airtight. The thoracic lymph nodes were unremarkable in appearance. A drain was placed before closing the sternotomy. Recovery was uneventful, and the dog was discharged four days later.

Macroscopically, the mass lesion contained a large pus-filled cavity, in which were numerous small hard spherical mineralisations. No bacteria were isolated after culture. A pulmonary adenocarcinoma with secondary pneumonia and abscess formation was diagnosed histopathologically. The tumour had a mixed acinar and papillary appearance with some small areas of squamous differentiation.

Discussion

Primary pulmonary neoplasia is a rare condition in dog, with an overall frequency of 1 to 1.25% of cases[1,2], however it is encountered with increasing frequency in older dogs and cats. As in cats, adenocarcinomas are the most frequent type of primary lung tumour in dogs (≈80-88%)[1,2], whereas squamous cell carcinomas, also called epidermoid carcinomas, are uncommon (≈7%)[1] and anaplastic carcinomas are rare (≈3%)[1,2]. This is in contrast to humans, where pulmonary squamous cell carcinomas and anaplastic carcinomas predominate. Sarcomas and benign primary lung tumours, such as adenomas, have also been rarely reported in dogs and cats. The mean age of dogs with primary lung tumours varies between 9 and 11 years[1,2] and the condition is rarely seen less than 6 years of age.[1] No sex predisposition has been found, and even if a breed predisposition has been reported in the Boxer in one study, this has not been confirmed in more recent studies.[1,2,3]

Duration of clinical signs range from few days to years, with a mean time of several months.[1] The major presenting sign is coughing, often harsh and non productive, which may be accompanied by decrease in exercise tolerance, tachypnea or dyspnoea.

However a majority of dogs has no clinical sign referable to the respiratory system in the early stage of disease. Non-specific clinical signs of general debility are also commonly noted such as lethargy, anorexia or weight loss. A small number of dogs with primary lung tumours may be presented for lameness, due to bone metastasis or hypertrophic pulmonary osteoarthropathy.[1,2] Weight gain and progressive abdominal distension associated with the presence of peritoneal effusion, due to thoracic caudal vena cava compression by a pulmonary mass, are not commonly encountered clinical signs, and are referred to as Budd-Chiari-like syndrome.

This syndrome corresponds to a mechanical obstruction of hepatic venous outflow somewhere between the level of the hepatic sinusoids and the entry of the caudal vena cava into the right atrium, which excludes cardiac or pericardial diseases such as right heart failure, pericardial effusion or restrictive pericarditis. This obstruction results in clinical signs of apparent right-sided heart failure, with hepatomegaly secondary to passive hepatic venous congestion, formation of peritoneal effusion, with high protein and low cellular levels characteristic of modified transudate, and possible pitting oedema of the limb.[4,5,6] Tachycardia, tachypnea, lethargy, abdominal pain and collapse are other clinical signs associated with Budd-Chiari-like syndrome.[4,5,6] The original condition described by Budd and Chiari was primarily obstruction of the hepatic veins in humans; however, most of their patients also had some degree of obstruction of the caudal vena cava.[6] Causes reported in dogs include dirofilariosis, cor triatrium dexter, extra- and intraluminal neoplasia of the caudal vena cava, kinking of the thoracic caudal vena cava (e.g. by oesophageal or thoracic neoplastic process), caudal vena cava fibrosis or thrombosis, congenital vascular abnormalities, congenital diaphragmatic hernia, and intrahepatic post-sinusoidal obstructions.[4,5,6] Diagnostic tools vary depending upon the location of the post-sinusoidal obstruction. Echocardiography, cardiac catheterization and angiography or venography, ultrasonography, thoracic radiography, contrast-enhanced computed tomography, nuclear scintigraphy, hepatic biopsy, measurement of wedged hepatic vein pressure, and necropsy may be used for diagnosis. Treatment and prognosis for animals with Budd-Chiari-like syndrome depends on whether the underlying cause can be identified and corrected.[5]

Routine radiographic examination of the thorax is the first and most common diagnostic tool used in veterinary medicine to assess pulmonary condition. The radiographic finding most frequently encountered in primary pulmonary neoplasia in dogs is a single circumscribed mass, most commonly seen at the periphery of the lung lobes, in contrast to humans, where perihilar masses are more common.[1,2,3] Pulmonary masses are

generally well-circumscribed, and may be cavitated where necrosis has occurred. Diffuse mixed peribronchial or broncho-interstitial to alveolar patterns, homogeneous lobar consolidation or multiple circumscribed masses have also been described with less frequency in cases of primary neoplasms in dogs. Various patterns may also occur together, however, the radiographic pattern of primary lung neoplasia appears to be less variable in dogs than in cats.[1,2,3] In dogs, the anatomically larger right lung has been reported as a more frequent site for primary lung neoplasms than the left lung.[1,2,3] No significant correlation between histological diagnosis and radiographic pattern of the lesion has been found, however tendencies have been observered.[1,2] Adenocarcinomas are observed primarily in the lung periphery, as a well-circumscribed mass, frequently cavitary, and less commonly as lobar alveolar infiltrates, which may or may not be calcified. Bronchiolo-alveolar carcinomas, a specific histological subtype of pulmonary adenocarcinoma, are commonly described as solitary nodules in the middle and peripheral lung regions. Generalized, mixed alveolar to interstitial pattern or, more rarely, homogeneous alveolar consolidation involving one or more lung lobes may also be seen, however more common in cats. In contrast to cats in where they are more commonly seen in the middle and peripheral portions of the lung, squamous cell carcinomas in dogs typically arise from larger bronchi and are therefore located in the perihilar region and may cause displacement and/or compression of the trachea or mainstem bronchi.[2] Pleural effusion and regional lymphadenopathy, related to local neoplastic extension and/or metastasis, are the most common other radiographic findings seen. However, pleural effusion is relatively uncommon in dogs compared to cats[1,2] and radiographic evidence of tracheo-bronchial or mediastinal lymph nodes enlargement may be unclear, because of superimposed masses and lung patterns.

Computed tomography of the thorax may help to fully assess involvement of the lungs, as a planning tool for surgical resection of pulmonary mass, lymph node involvement, local invasion of the primary neoplasia and presence of pulmonary metastasis.[3] Most common CT findings of primary lung tumours in dogs, described in one study, were essentially well-circumscribed solitary pulmonary masses located in the central to periphery of the lung, bronchocentric in origin with internal air bronchograms, associated with narrowing, displacement or obstruction of the involved bronchi. Most primary lung tumours had mild to moderate heterogeneous contrast enhancement, whereas homogeneous enhancement was less common. Rare internal mineralisations were also noted.[3]

Local metastasis or direct extension to adjacent organs (e.g. pleura, mediastinum, oesophagus) is common but extra-thoracic metastasis within the kidneys, liver, spleen, adrenal, and brain and/or appendicular or axial skeleton may occur. More than 90% of squamous cell and anaplastic carcinomas have been reported to metastasize, whereas only 50% of adenocarcinomas.[1,2,3]

As radiographic and CT findings are not associated with histology subtype and not pathognomonic of primary lung neoplasm, other differential diagnoses have to be considered, especially in case of cavitary masses, such as abscesses, fungal or bacterial granulomas, eosinophilic pulmonary granulomatosis, pulmonary thromboembolism or congenital malformation and further diagnostic tests, such as biopsy or fine needle aspiration, are necessary to establish the final diagnosis.[2,7] Moreover secondary pneumonia or abscesses may be encountered in cases of primary lung tumour. Most often, a definitive diagnosis can be made only following thoracotomy with removal or biopsy of the neoplastic tissue.[2]

Lobectomy is the treatment of choice in dogs with a solitary pulmonary lung tumour. The neoplastic cell type and presence or absence of metastatic disease have been found to be of value as prognostic indicators. Dogs with pulmonary adenocarcinomas are reported to have a longer mean survival time (19 months) than animals with other types of primary lung carcinomas (8 month for squamous cells carcinomas), following surgical resection of the pulmonary mass, with mean survival time ranged from 10 to 13 months.[2] Dogs exhibiting regional lymph node involvement at time of diagnosis have a much poorer prognosis, therefore examination and biopsy study of the tracheobronchial lymph nodes should be performed at the time of surgery, as well as evaluation of other accessible lung lobes for signs of metastatic lesions or additional primary tumour sites. Surgical resection is not usually indicated in case of distant metastasis or extrapleural involvement. Chemotherapy may be considered in animals with non-resectable or recurrent lesions or in whom surgery is contraindicated due to concurrent disease.[2]

References

1-Barr FJ, Gibbs C, Brown PJ. The radiological features of primary lung tumours in the dog: a review of thirty-six cases. **J Small Anim Pract** 1986; 27(8): 493-505**.**

2-Miles KG. Review of primary lung tumors in the dog and cat. **Vet Radiol Ultrasound** 1988; 29(3): 122-128.

3-Marolf AJ, Gibbons DS, Podell BK, Park RD. Computed tomographic appearance of primary lung tumors in dogs. **Vet Radiol Ultrasound** 2011; 52(2): 168-72.

4-Baig MA, Gemmill T, Hammond G, Patterson C, Ramsey IK. Budd-Chiari-like syndrome caused by a congenital hiatal hernia in a Shar-Pei dog. **Vet Rec** 2006; 159(10): 322-323.

5-Langs LL. Budd-Chiari-like syndrome in a dog due to liver lobe entrapment within the falciform ligament. **J Am Anim Hosp Assoc** 2009; 45(5): 253-256.

6-Schlicksup MD, Weisse CW, Berent AC, Solomon JA. Use of endovascular stents in three dogs with Budd-Chiari syndrome. **J Am Vet Med Assoc** 2009; 235(5): 544-550.

7-Robinson DA, DeNardo GA, Burnside DM. What is your diagnosis? Pulmonary abscess. **J Am Vet Med Assoc** 2003; 223(9): 1259-1260.

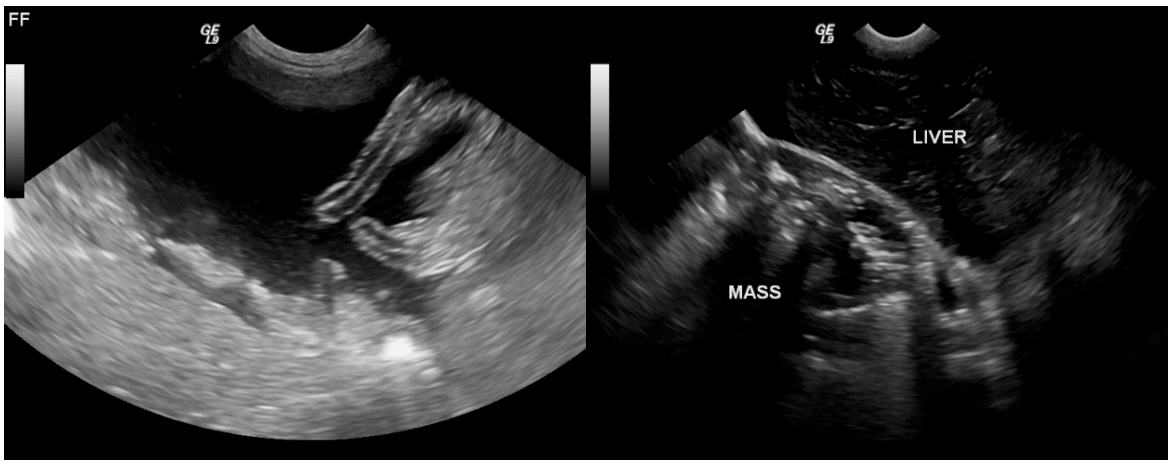

Figure 6.1 - Ultrasound image demonstrating abdominal effusion

Figure 6.2 - Ultrasound image showing the pulmonary mass pushing the diaphragm

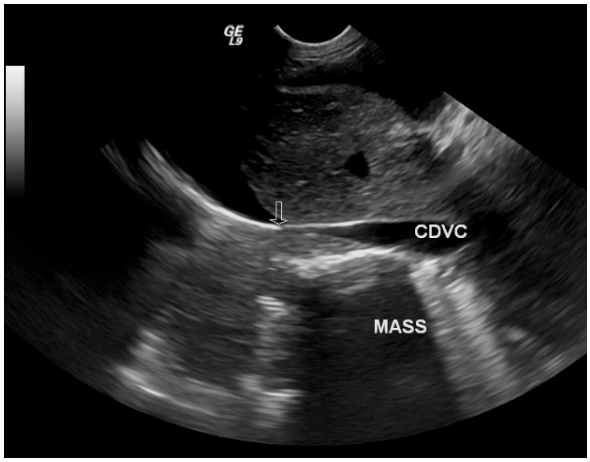

Figure 6.3 - Ultrasound image showing the compression of the caudal vena cava by the pulmonary mass

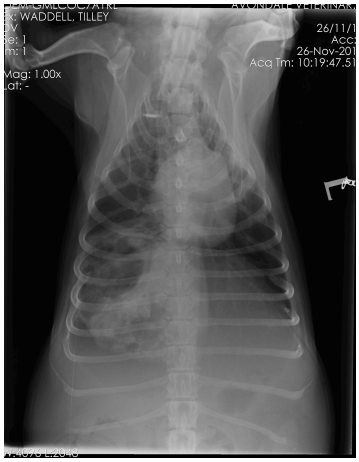

Figure 6.4 - Dorso-ventral thoracic radiograph

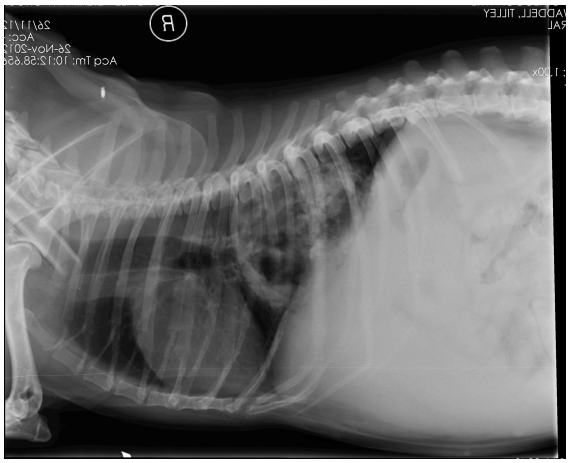

Figure 6.5 - Right lateral thoracic radiograph

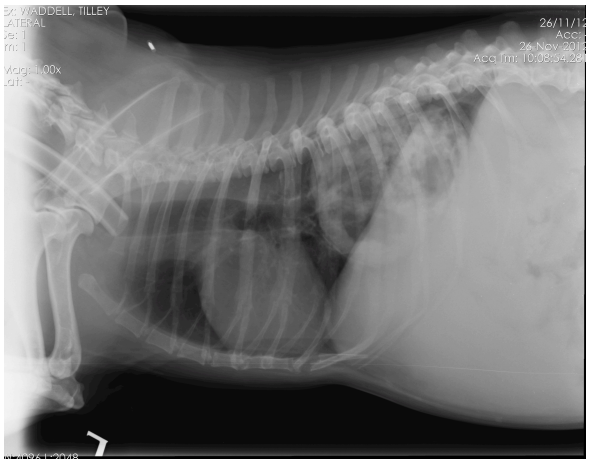

Figure 6.6 - Left lateral thoracic radiograph

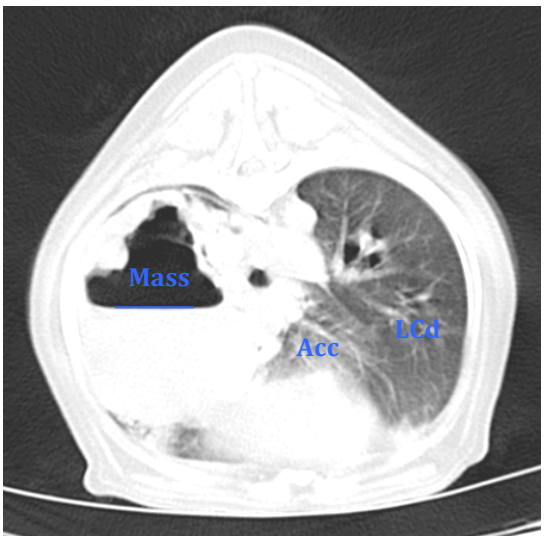

Figure 6.7 - Transverse CT image of the right-sided cavitary pulmonary mass (Lung window)

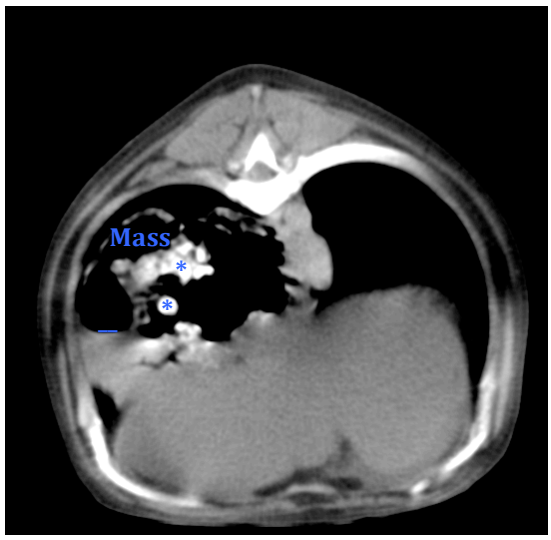

Figure 6.8 - Transverse CT image showing mineralisations of the pulmonary mass (Soft tissue window)

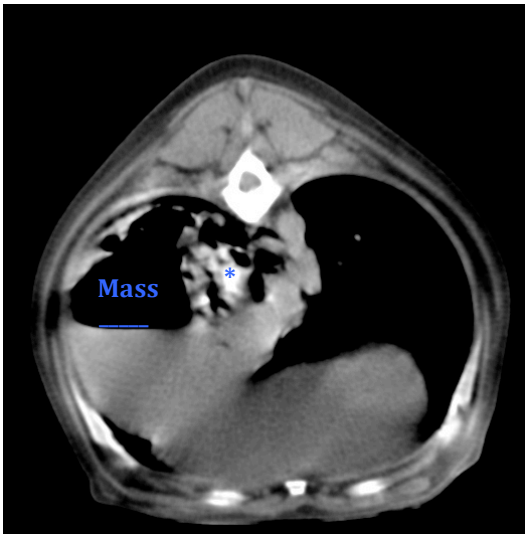

Figure 6.9 - Transverse CT image showing mineralisations of the pulmonary mass and fluid line delineation (Soft tissue window)

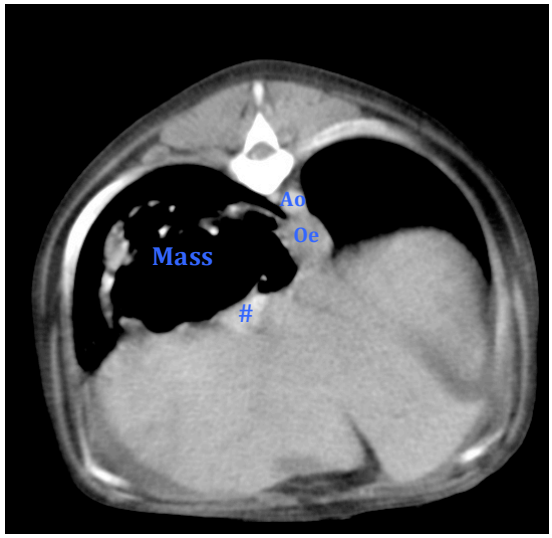

Figure 6.10 - Delay post contrast transverse CT image showing compression of the caudal vena cava (Soft tissue window)

Ao: Aorta; Acc: Accessory lung lobe; LCd: Left caudal lung lobe; Mass: Pulmonary mass; Oe: oesophagus; *: mineralisations within the pulmonary mass; #: Caudal Vena Cava; ---: fluid line delineating the limit between gaz dorsally, and fluid ventrally, within the pulmonary mass

Case 7. Sub-lumbar Foreign Body

Signalment and History

A 4-year-old male neutered crossbreed dog had been presented with a right inguinal swelling and subsequent cellulitis and pyrexia. The dog had been administrated meloxicam followed by marbofloxacin with the owners noting an improvement once marbofloxacin was started, but no complete resolution. The dog was referred to the Small Animal Hospital, University of Glasgow, for further investigations.

Clinical Signs

a) Swelling involving the right inguinal region and the prepuce, extending to the right hind limb, just distal to the hock
b) Oedematous lesion on the cranial ventral abdominal wall
c) Pyrexia at 40.4^{o}C
d) Tachycardia at 120 beats per minute, with synchronous femoral pulse.

Radiographic Examination

1. **Equipment** - See Appendix 1
2. **Restraint** - The dog was sedated. Positioning was achieved using wedges of dressing material and rope ties.

Area	View	kV	mAs	Grid
Caudal Abdomen	Right Lateral (Fig.7.1)	68	10	O

Radiographic Appraisal

Only one lateral view of the caudal abdomen was made and the radiograph is well positioned and centred (Fig.7.1). The image is well processed. A thin radio-opaque line parallel to the length of the film is visible at the level of the spinous processes, consistent with a dusty detector – processing default. Exposure setting and an R marker have been added to the radiograph. The radiograph is of diagnostic quality.

Radiological Report

Small bubbles of gas opacity are visible in the soft tissue cranial to one femur and the pelvis in the caudal sub-lumbar area. The more ventral bubbles seem to be in the soft tissue of the limb, however the presence of air bubbles in the abdominal cavity and the caudal sub-lumbar space cannot be excluded. An increase in soft tissue opacity with blurred margins is noted in the caudal sub-lumbar space ventral to the vertebral bodies of L5 to L7. There is a subjective slight ventral displacement of the descending colon at

the level of the pelvic inlet. These features are consistent with medial iliac lymphadenopathy or the presence of a sub-lumbar mass (e.g. neoplastic process), abscess or granuloma, although superimposition of the hind limb emphysema cannot be ruled out. Very mild new bone production is present at the ventral aspect of L2 consistent with mild spondylosis. Normal gas-filled small intestinal loops and colon are visible.

Differential Diagnosis

Diffuse subcutaneous emphysema of the cranial part of a hind limb linked to an infectious and/or necrotic process (e.g. cellulilitis, open wound, gas forming bacteria, foreign body). A neoplastic process is less likely. Suspected iliac medial lymphadenopathy, caudal sub-lumbar abscess, granuloma or mass.

Ultrasound Report

Ultrasonography of the inguinal area, the right thigh and the abdomen was performed (Figs.7.2 and 7.3).

A large amount of hypoechoic fluid about 2cm deep, containing echoic particles associated with bright linear structures within was visible in the subcutaneous soft tissue of the inguinal area, consistent with cellulitis and the presence of a pocket of pus, inflammatory fluid accumulation or haematoma. Anechoic infiltrating linear areas were seen in the sub-cutaneous soft tissue of the right ventral abdominal wall, consistent with oedema and/or cellulitis. An enlargement of the right hypogastric lymph node – thickness about 9mm – associated with a moderately hypoechoic and heterogeneous parenchyma and well defined but slightly uneven margins was noted, consistent with reactive lymphadenopathy, though a neoplastic infiltration cannot be excluded. Because of the underlying sub-cutaneous oedema of the right ventral abdominal wall, ultrasonography of the right side of the abdomen was incomplete.

Advanced Imaging – Computed Tomography Report

Computed tomography of the caudal abdomen, pelvis and thighs was performed (Figs.7.4 to 7.6). It reveals a swelling of the right sub-lumbar muscles at the level of L4-L5 associated with a mild hypoattenuated centre surrounded by a mild hyperattenuating peripheral rim (Fig.7.4). These features are most likely consistent with an abscess, a necrotic area or a granuloma possibly associated with a migrating foreign body; a neoplastic process is considered less likely. The swelling of the right sub-lumbar muscles extended cranially to L2 and caudally to L7-S1, therefore accurate delineation

of the medial iliac lymph nodes is not possible. Some small bubbles of gas attenuation are visible at the lateral aspect of the right sub-lumbar muscles at the level of L6-L7. A large soft tissue attenuating mass with irregular margins associated with a moderate to marked internal accumulation of small gas attenuating areas is visible at the medial aspect of the right thigh, extending cranially into the subcutaneous tissue of the right inguinal area and ventro-lateral abdominal wall. Surrounding soft tissue swelling is noted. A mild enlargement of the right popliteal lymph node is visible – about 10mm thick.

These features are consistent with an extensive cellulitis from the medial aspect of the right thigh to the right inguinal area and ventro-lateral abdominal wall, with mild right popliteal lymphadenopathy, associated with right sub-lumbar muscle swelling and an abscess formation, necrotic area or granuloma at L4-L5, probably linked to a migrating foreign body

A mild spondylosis at the level of L2 and a distended bladder are also noted.

Further Investigations

Fine needle aspiration of the fluid accumulated in the inguinal area was performed. Macroscopically, it was thick and yellow, consistent with pus. Cytology of the aspirate revealed a high number of neutrophils with moderate degenerative changes and intracellular bacteria. No bacteria were isolated from the sample after culture; this may be due to the previous course of antibiotics.

Haematology revealed a leukocytocis (29.03 x 10^9 leukocytes/L), with a left shift and evidence of toxic neutrophils.

Biochemistry revealed hypoalbuminaemia (22g/L), hypoglobulinaemia (55g/L) and increased AST (58U/L) and ALKP (389U/L).

A mildly prolonged KCCT was noticed likely due to the underlying inflammatory response.

Outcome

The dog underwent exploratory laparotomy with abscess debridement and lavage. Abdominal evaluation showed evidence of chronic low-grade inflammation with yellowish-brown patchy discoloration across the omental surface and fibrin tags visible throughout the abdomen adherent to serosal surfaces. An oval nodular mass lesion could be palpated in the right sub-lumbar region measuring approximately 3x6cm, identified after dissection as an abscess cavity with a fibrous tract, 5mm in diameter, running cranially towards the diaphragm and caudally to the inguinal ring. All necrotic and

devitalized tissues were debrided, retrieving several pieces of grass seed in the process. The large abscess cavity of the right thigh was debrided. All sites of abscesses and the abdominal cavity were copiously lavaged and flushed with sterile saline. Omentalisation of the sub-lumbar abscess and foreign body track was performed. A closed suction drain with a 100ml reservoir was placed in the abscess cavity on the right medial thigh before suturing.

The dog recovered well from surgery and was discharged four days later. At follow up examination 1 month later, the dog was doing well and was back to its normal self. The dog seemed to be sneezing 2 or 3 times a week but without nasal discharge, coughing or ill health associated. A little lump was noticed at the top of the scar, most likely consistent with a mild skin reaction around suture material, otherwise the wound had healed nicely.

Discussion

Migrating foreign bodies are a relatively common problem encountered in veterinary medicine, particularly in dogs. The most common migrating foreign bodies reported are grass awns of different species, depending on region,[1,2,3] although other types can be found such as porcupine quills[4] or other plant sticks[5]. The sharp point of the floret of the awn, as with porcupine quills[4], with backward pointing barbs allows for skin penetration and prevents retrograde movement.[1] Consequently, foreign bodies migrate and progress through the body in different areas, depending of the entrance site, causing a wide range of clinical signs associated with the site of implantation. Common routes of entrance include interdigital spaces, external ear canal, conjunctival sac, nasal cavity and oral cavity, with secondary involvement of ears, eyes, nose, subcutaneous soft tissue, lumbar area, costal region, and thoracic cavity.[1,2,3] Clinical signs are typically chronic, intermittent and recurrent, resulting from local inflammation and infection, and previous history of fur or migrating foreign body removal is common. Young (< 5 years)[1] hunting and working dog breeds with long coats, which can retain potential foreign bodies, such as Springer Spaniel or Golden Retriever[1] have an increased prevalence of migrating foreign bodies, because of increased exposure.[1,2,3] However in one study of 35 dogs[1], English Pointers (17%) and Labrador Retrievers (28%) were the most common breeds affected by migrating grass awn. Migrating foreign bodies are also reported in cats.[1] Relapse following conservative medical management (or recurrence following unsuccessful surgical exploration) and the migratory nature of the,

often, small sized foreign bodies makes localisation difficult even when advanced imaging is used.

Localisation of foreign bodies of plant origin is difficult with plain radiography, as the foreign material has the same radiopacity as surrounding soft tissue. Radiographs can be useful in case of intrathoracic foreign bodies to detect the diseased region of lung. Abnormalities include most commonly focal pulmonary interstitial to alveolar pattern in the caudal or accessory lung lobes, as after inhalation foreign bodies progress along the trachea and caudal bronchi, before migrating through the lung parenchyma and the pleural space. Additional finding such as pneumothorax, pleural effusion or pleural thickening may be found.[1,2] Soft tissue swelling or mass, in sub-lumbar or subcutaneous areas, as well as bony changes consistent with osteomyelitis, discospondylitis[4] or secondary periosteal reaction to surrounding soft tissue inflammation/infection[1,2] may also be visualized on plain radiographs. However in number of cases radiographs may be normal or not give enough information to localise migrating foreign bodies.

Advanced imaging, such as CT and MRI, can be a valuable tool for further investigating the exact site of damage and localising foreign bodies.[1,2,3,4,6,7] Presence of fluid-dense, rim enhancing pockets within muscles or subcutaneous areas may indicate presence of abscesses and/or granulomas on computed tomography images.[1,6] Better location of the diseased lung associated with identification of additional lesions, such as soft tissue tracking with surrounding contrast enhancement, mediastinal lesions, lymphadenopathy, body wall masses, bone destruction or reaction and extension of the lesion, can be assessed with CT in cases of intrathoracic migrating foreign bodies.[1] In a few animals, foreign bodies may be visualised as linear hyperdense structures.[1,6] MRI is the most sensitive technique for early diagnosis and characterization of the severity and extent of spinal and paraspinal infection.[3,7] Visualisation of T2-hyperintense areas or pockets within the hypaxial and epaxial musculature or the subcutaneous soft tissue, consistent with myositis, cellulitis, abscess or necrosis, T2-hyperintense tubular sinus tracts with peripheral contrast enhancement, signs of epidural empyema, spinal cord compression, neuritis, discospondylitis or periostitis, allows a valuable guide for surgical planning.[7] Focal T2-hypointense linear structures may be indicative of the presence of migrating foreign bodies.[3,7] STIR and fat-suppressed sequences should be added to conventional T2-weighted and pre- and post-contrast T1-weighted sequences to improve detection of paravertebral sinus tracts and perineural, epidural and vertebral lesions.[7]

As CT and MRI are valuable and accurate tools for determination of the correct site of abnormality and tracing the path, but not the foreign body itself, the use of

ultrasonography has been recommended to visualise and localise foreign bodies within sub-lumbar areas, abdominal and thoracic walls, orbits, joints or other subcutaneous or muscular locations. The use of a high frequency (10-15MHz) linear probe is recommended.[2] Grass awns appear as a linear spindle-shaped shadow of variable length, with two to three parallel reflecting interfaces corresponding to the seed and husk. Acoustic shadowing is inconsistent and more easily seen on transverse images because of the almost curvilinear interface of plant foreign bodies. Accumulation of inflammatory fluid around foreign bodies may be helpful in identification by creating an anechoic halo and enhancing interfaces. Additional findings including abscess/granuloma, soft tissue inflammatory/ infectious reactions, and presence of fistulous tracts or lymphadenopathy may also be identified by ultrasonography. Furthermore ultrasound guided removal of a migrating foreign body, by introducing forceps through a fistulous tract, should be considered if possible. A planned echo-guided surgical approach may be a timesaving procedure to localize and remove the grass awn before conventional surgical treatment of the soft tissue involved is considered.[2]

Prognosis for recovery is generally good after surgery, if correct location of affected areas is achieved.

References

1-Schultz RM, Zwingenberger A. Radiographic, computed tomographic, and ultrasonographic findings with migrating intrathoracic grass awns in dogs and cats. **Vet Radiol Ultrasound** 2008; 49(3): 249-255.

2-Gnudi G, Volta A, Bonazzi M, Gazzola M, Bertoni G. Ultrasonographic features of grass awn migration in the dog. **Vet Radiol Ultrasound** 2005; 46(5): 423-426.

3-Whitty CC, Milner HR, Oram B. Use of magnetic resonance imaging in the diagnosis of spinal empyema caused by a migrating grass awn in a dog. **New Zealand Vet J** 2013; 61(2): 115-118.

4-Sauvé CP, Sereda NC, Sereda CW. Identification of an intra-cranial intra-axial porcupine quill foreign body with computed tomography in a canine patient. **Can Vet J** 2012; 53(2): 187-189.

5-Sutton A, May C, CoughlanA. Spinal osteomyelitis and epidural empyema in a dog due to migrating conifer material. **Vet Rec** 2010; 166(22): 693-694.

6-Laksito MA, Chambers BA, Hodge PJ, Milne ME, Yates GD. Fibrotic myopathy of the iliopsoas muscle in a dog. **Aust Vet J** 2011; 89(4): 117-121.

7-Holloway A, Dennis R, McConnell F, Herrtage M. Magnetic resonance imaging features of paraspinal infection in the dog and cat. **Vet Radiol Ultrasound** 2009; 50(3): 285-291.

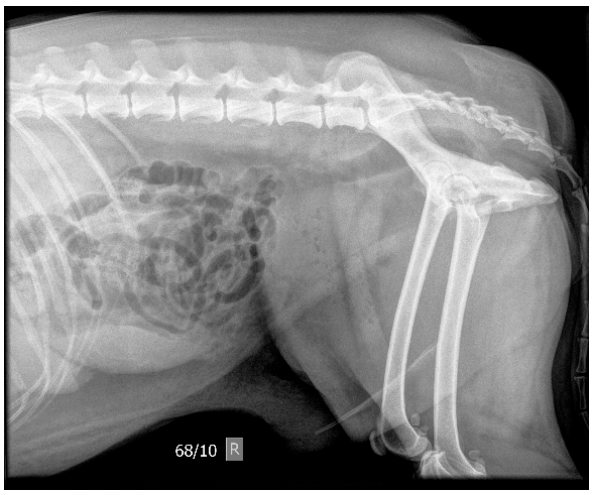

Figure 7.1 - Right lateral caudal abdominal radiograph

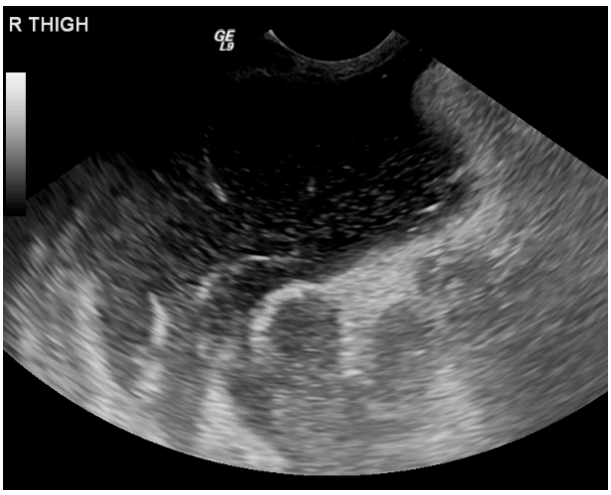

Figure 7.2 - Ultrasound image of the right inguinal area showing fluid accumulation (Microconvex transducer)

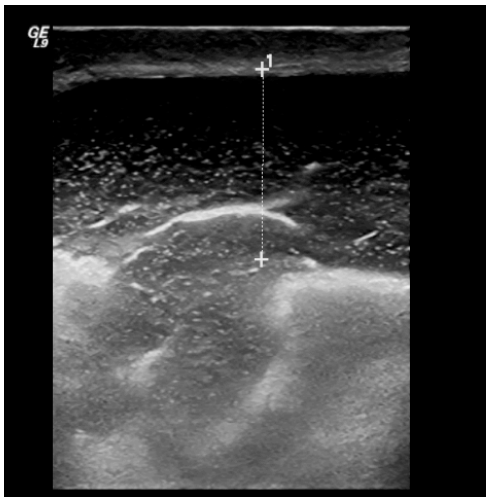

Figure 7.3 - Ultrasound image of the right inguinal area showing fluid accumulation (Linear transducer)

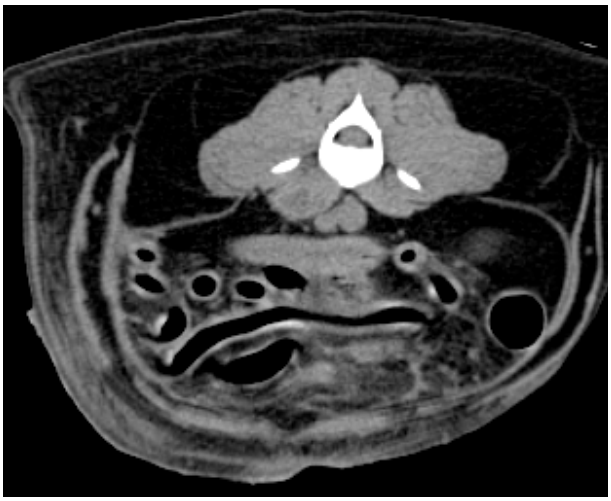

Figure 7.4 - Transverse CT image of the right sublumbar hypoattenuating lesion and subcutaneous cellulitis (Soft tissue window)

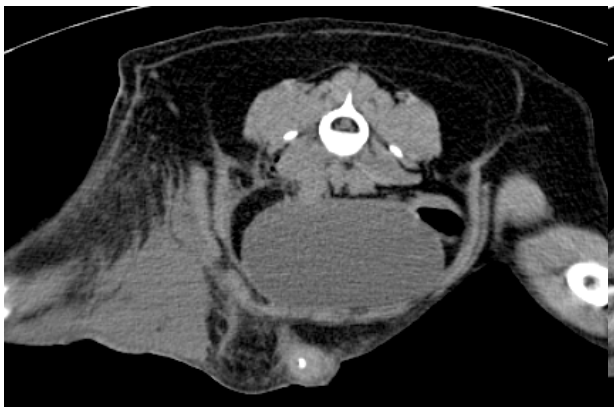

Figure 7.5 - Transverse CT image of right sublumbar emphysema and thigh cellulitis (Soft tissue window)

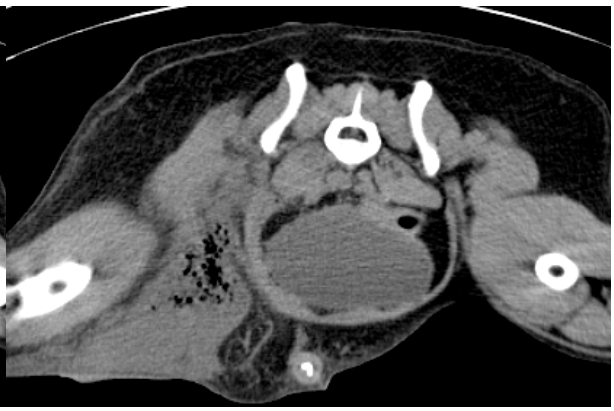

Figure 7.6 - Transverse CT image of right thigh cellulitis (Soft tissue window)

Case 8. Feline Conn's Syndrome

Signalment and History

A 12-year-old male neutered Domestic Short Hair was presented with a 2-week history of muscle weakness and ataxia. The cat could not lift its head at that time, was walking into things and his appetite was poor. The referring veterinary surgeon found a low serum potassium concentration. The cat responded to potassium supplemented fluid therapy well and recovered a good appetite. He relapsed with a second episode of weakness and ventroflexion of the neck, the day before presentation at the Small Animal Hospital, University of Glasgow. He was fully vaccinated and recently dewormed and was kept indoors due to his FIV status.

Clinical Signs

Physical examination was unremarkable.

Ultrasound Examination

1. **Equipment** - See Appendix 1.
2. **Restraint** - The cat was sedated and put in dorsal recumbency for the abdominal ultrasound scan.

Abdominal Ultrasound Report

A marked diffuse enlargement of the left adrenal gland (height x length approximately 15 x 18mm) was found. The gland was rounded in shape with a slightly heterogeneous parenchyma (Fig.8.1). Power Doppler examination was used to evaluate the integrity of the vasculature adjacent to the left adrenal mass. The adrenal was adjacent to the aorta but did not seem to invade it or the caudal vena cava (Fig.8.2). The right adrenal gland was within normal limits in size and echogenicity (Fig.8.3). A mild to moderate diffuse thickening of the muscular layer of the small intestinal wall, more marked in the ileum (wall thickness about 4.6mm), but without loss of the wall layering was noted. A supernumerary hyperechoic longitudinal line was visible in the mucosa of some small intestinal loops. These features were most likely consistent with a chronic inflammatory process or age related changes. An early stage of lymphoma was considered less likely. The size of the kidneys was at the upper normal limit (length about 4.8cm). A moderate hyperechogenicity of both cortices associated with a mild decrease in corticomedullary definition was noted consistent with age related change or an underlying nephropathy. Some small mineralized elements associated with acoustic shadowing were visible at

the level of the pelvis of the left kidney consistent with pelvic mineralisation - most likely - or very small non-obstructive renal stones (Fig.8.4). A mild bilateral renal pelvic dilation was noted consistent with an increased glomerular filtration (e.g. fluid therapy). The spleen was moderately enlarged associated with a mildly mottled parenchyma consistent with a reactive splenitis, congestion or extramedullary haematopoiesis; a neoplastic process was less likely. A marked distension of the bladder was also noted.

Diagnosis

Left adrenal mass consistent with a neoplastic process, benign or malignant, most likely secreting, as the origin of the hypokalaemia. (primary hyperaldosteronism – Conn's Syndrome)

Radiographic Examination

1. **Equipment** - See Appendix 1
2. **Restraint** - As per ultrasound examination, the cat was sedated. Positioning was achieved using wedges of dressing material and rope ties.

Area	View	kV	mAs	Grid
Whole body	Right Lateral (Fig.8.5)	50	6.3	N
	Left Lateral (Fig.8.6)	50	6.3	N

Radiographic Appraisal

Both radiographs are not well centred and include the thorax and the abdomen. On the left lateral view (Fig.8.6), the cranial part of the thorax and the caudal part of the abdomen are missing. The images are well processed. Markers and exposure setting have been added post-exposure on both radiographs. The radiographs are of diagnostic quality for the abdomen.

Radiological Report

A rounded well-defined soft-tissue structure of approximately 18mm in diameter is seen in the dorso-cranial aspect of the abdomen, cranial to the left kidney and superimposed on the right kidney shadow, consistent with the adrenal mass seen on ultrasound. A rounded fairly well defined soft-tissue lesion of approximately 20mm in diameter is seen in the ventro-caudal aspect of the abdomen on the right lateral view, superimposed over the bladder, but slightly displaced over the caudo-ventral abdominal wall on the left lateral view. This is most likely consistent with a subcutaneous or cutaneous mass, differential diagnosis including granuloma, benign or malignant neoplastic process, less likely abscess or haematoma. Small mineralised elements are visible at the level of the

pelvis of the left kidney consistent with pelvic mineralization or very small renal stones. A mild diffuse broncho-interstitial pattern is noted most likely consistent with the age, the expiratory status and the exposure setting of the radiographs. Mild to moderate vertebral spondylosis and mild costo-chondral and sternal degenerative changes are noted.

Further Investigations

Haematology revealed no significant abnormality.

Blood pressure was within upper normal limits (160mmHg)

Biochemistry revealed a very mild increase in liver enzymes (ALT = 50U/L, AST = 72U/L) and low-end normal potassium. The plasma aldosterone concentration was high (979pmol/L - reference range: 190-390pmol/L), which confirms, in association with the left adrenal mass and the history of hypokalaemia, a primary hyperaldosteronism.

Urinalysis was within normal limits.

Fundoscopic examination was unremarkable.

Outcome

A course of potassium gluconate and spironolactone was started and the cat was discharged. A follow-up examination was done 2 weeks later. The cat had improved well at home and the owners reported that he had returned to normal. Appetite and thirst were stable and no further episodes of neck ventroflexion had been noted. Clinically, the cat was bright and alert and physical examination was unremarkable. Blood pressure was within normal limits. A mild elevation in ALT was still present but improved from previous measurement. Potassium and sodium were within normal limits.

An abdominal CT angiogram was performed 1 month later (Figs.8.7 to 8.9), to assess the vasculature surrounding the mass with more accuracy and for surgical planning. The left adrenal mass appeared to be close to the caudal vena cava, but no obvious vascular invasion was identified. The peritoneum had a mild hazy appearance cranial to the mass, which may have suggested a mild focal reactive steatitis.

A left adrenalectomy was performed following CT. No vascular invasion of the caudal vena cava, aorta or renal vessels was seen. The mass was fully excised, biopsy samples from local lymph nodes and liver were performed and the abdominal cavity was lavaged before closure. Recovery from anaesthesia was uneventful and potassium concentration remained stable.

Histology of the adrenal mass confirmed a benign adrenocortical adenoma, with no clear evidence of local infiltrative behaviour. The lymph node sample showed

enlargement due to an increase in marginal zone cell numbers, and the liver biopsy showed chronic diffuse and moderate portal hepatitis.

One week after surgery, the cat presented with inappetance and vomiting without decline in condition or abnormal blood results. Gastritis secondary to meloxicam was suspected, which resolved with fluid therapy and gastro-protectant.

A further follow-up one month after surgery was unremarkable.

Discussion

Aldosterone is the major mineralocorticoid secreted by the zona glomerulosa of the adrenal gland in response to stimulation of the renin-angiotensin-aldosterone system and extracellular potassium concentrations. Its principal function is regulation of systemic blood pressure and homeostasis of extracellular fluid volume in response to changes in haemodynamics and electrolytes. Aldosterone acts by increasing secretion of potassium and hydrogen and resorption of sodium and chloride in the distal nephrons of the kidneys, and sodium retention results in an expansion of the extracellular fluid volume.[1,2]

Primary hyperaldosteronism, or Conn's syndrome, described in humans, dogs and cats, is due to an abnormal increased secretion of aldosterone by the adrenals. The most common causes in humans are unilateral adenoma and bilateral adrenal hyperplasia, whereas the most common reported cases in cats are unilateral adenomas or carcinomas, with a small minority of adrenal hyperplasia[1,3]. Although unilateral adrenal disease is much more common in cats, a few cases of bilateral disease have also been reported[1,2].

Feline primary hyperaldosteronism has also been diagnosed in association with other endocrine diseases such as hyperthyroidism, hyperparathyroidism, hyperadrenocorticism or hyperprogesteronism.[1,3,4] Secondary hyperaldosteronism is also described, in which the increased secretion of aldosterone is linked to another condition, such as cardiovascular disease, renal disease and hepatic failure, in normal response to the activation of the renin-angiotensin-aldosterone system.[1,2]

Cats diagnosed with primary hyperaldosteronism are usually older cats and there is no apparent sex or breed predilection.[1] Clinical signs typically result from hypokalaemic polymyopathy due to increased urinary loss of potassium and/or systemic hypertension caused by blood volume expansion. Weakness is the most common presenting sign, followed by cervical ventroflexion. Vision loss and acute blindness, secondary to retinal detachment and intraocular haemorrhage, are the most common reported clinical signs due to systemic hypertension. On physical examination, evidence of cardiovascular

disease secondary to the systemic hypertension, including cardiac murmurs or tachycardia, may be found. Possible additional presenting signs include lethargy, episodic forelimb stiffness, dysphagia, polyuria-polydypsia, polyphagia, nocturia, weight loss or diarrhoea.

A moderate-to-severe degree of hypokalaemia associated with increased kaliuresis is typically seen, whereas serum sodium concentration may be normal or mildly increased because of the increased water resorption accompanying the sodium resorption. An elevated plasma aldosterone concentration is characteristic, associated with a low plasma renin activity related to the renin-aldosterone dissociation (in contrary to secondary hyperaldosteronism). However the latter being not widely available, the diagnosis of primary hyperaldosteronism in cat is often made by the clinical signs associated with hypokalaemia, systemic hypertension, increased plasma aldosterone concentration in association with adrenal changes (mass, hyperplasia) on imaging modalities. Serum creatinine kinase concentration is also usually markedly elevated, secondary to hypokalaemic polymyopathy. Evidence of renal disease may be found, including increased serum creatinine and urea concentration, isosthenuria and proteinuria, linked to the secondary hyaline renal parenchymal sclerosis and fibrosis.[1,2]

Imaging of the adrenal glands is usually done to identify adrenal changes. Ultrasound findings include adrenal mass and/or hyperplasia, adrenal calcification, changes in echogenicity and vascular invasion of the caudal vena cava, phrenico-abdominal veins, or renal veins. Mineralisations of adrenal parenchyma are common in adult cats, and if this only change is present it does not necessarily indicate neoplastic process. CT and MRI are also used to improve imaging of the adrenal glands and to evaluate arterial and venous invasion by the tumour (angiogram), which is useful in planning a surgical removal. However in skinny cat, where adrenals and adjacent vessels are readily imaged on ultrasound, CT and MRI may be less useful than in large, fat dog, when advanced imaging is perhaps more likely to influence surgical decision making.[1,2,4]

In cases of unilateral disease, surgical removal of the affected adrenal gland remains the preferred treatment. Surgery seems to be curative for both adenomas and carcinomas, with signs of hypokalaemia and hypertension resolving without further treatment.[1,2,3,5]

The immediate postoperative period is the most critical and cats who survive this often have survival times of many years. Invasion of the caudal vena cava from an adrenal tumour, or associated thrombosis is usually considered a contraindication for surgery, but successful outcome has been reported even with vena cava thrombosis[5]. Medical management may also be considered in case of bilateral disease, vascular thrombus or if

surgery cannot be performed (e.g. financial reason). It consists of spironolactone therapy – an aldosterone antagonist, potassium supplementation, and antihypertensive drugs as needed. Clinical signs of polymyopathy appear to respond well to medical treatment with potassium supplementation and spironolactone, although serum potassium concentrations often remain below the reference range. Treatment with amlodipine can be used to manage hypertension but in some cases the hypertension is refractory to treatment.[2] Reported survival times for cats treated medically often range from many months to years, however chronic renal failure continue to develop and may be a cause of euthanasia.[1,2]

References

1-Schulman RL. Feline primary hyperaldosteronism. **Vet Clin North Am Small Anim Pract** 2010; 40(2): 353-359.

2-Ash RA, Harvey AM, Tasker S. Primary hyperaldosteronism in the cat: a series of 13 cases. **J Feline Med Surg** 2005; 7(3): 173-182.

3-Smith RR, Mayhew PD, Berent AC. Laparoscopic adrenalectomy for management of a functional adrenal tumor in a cat. **J Am Vet Med Assoc** 2012; 241(3): 368-372.

4-Moore LE, Biller DS, Smith TA. Use of abdominal ultrasonography in the diagnosis of primary hyperaldosteronism in a cat. **J Am Vet Med Assoc** 2000; 217(2): 213-215.

5-Rose SA, Kyles AE, Labelle P, Pypendop BH, Mattu JS, Foreman O, Rodriguez CO Jr, Nelson RW. Adrenalectomy and caval thrombectomy in a cat with primary hyperaldosteronism. **J Am Anim Hosp Assoc** 2007; 43(4): 209-214.

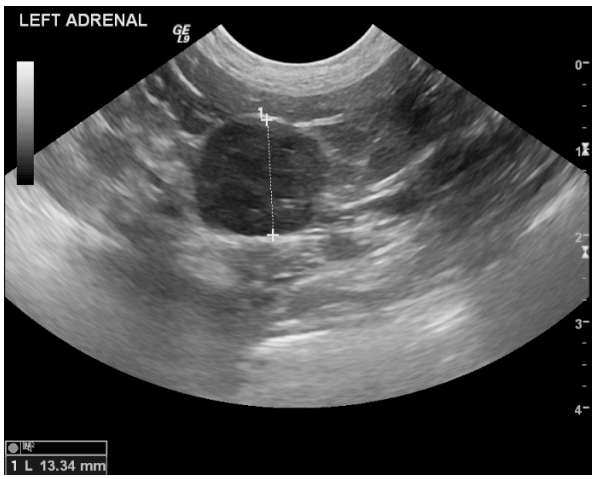

Figure 8.1 - Ultrasound image demonstrating marked left adrenomegaly with heterogeneous parenchyma

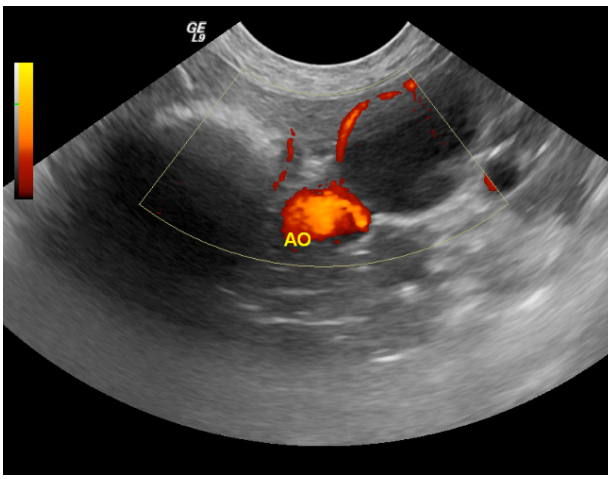

Figure 8.2 - Power Doppler ultrasound image of the left enlarged adrenal gland and adjacent aorta (Ao)

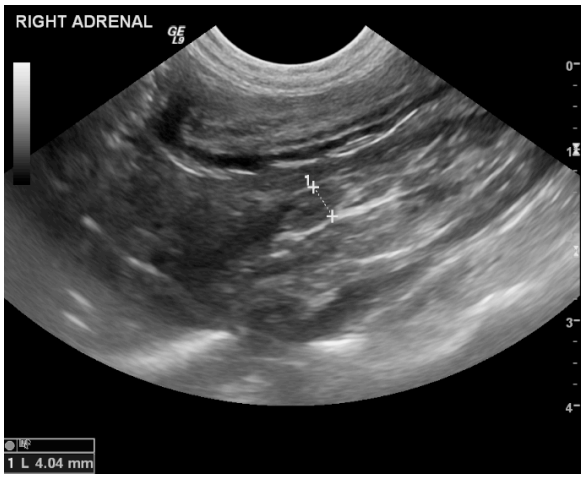

Figure 8.3 - Ultrasound image of the normal right adrenal gland

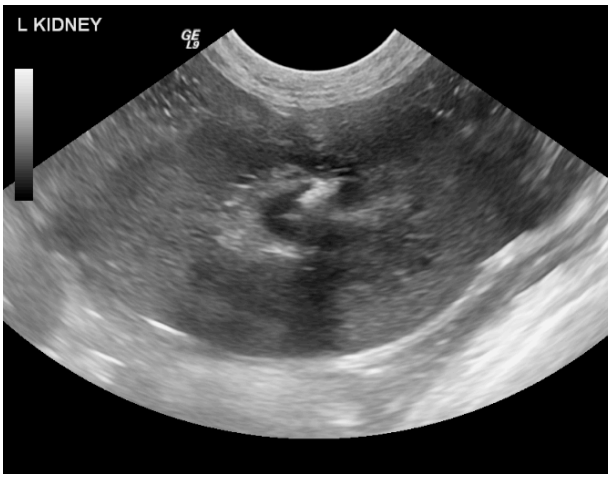

Figure 8.4 - Ultrasound image of the left renal pelvic mineralisations, with acoustic shadowing

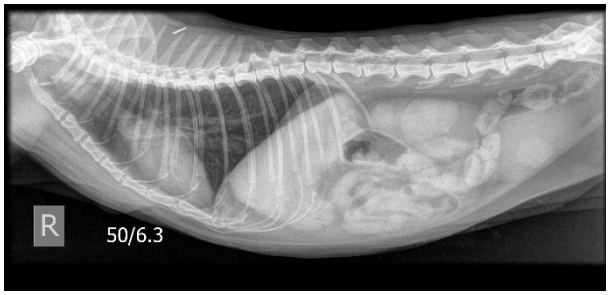

Figure 8.5 - Right lateral radiograph of the body

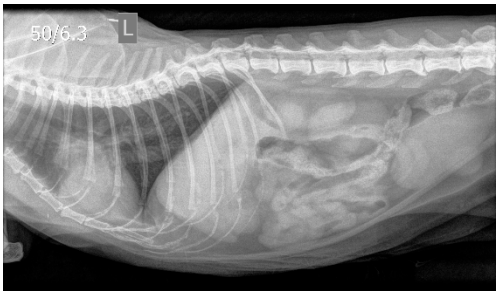

Figure 8.6 - Left lateral radiograph of the body

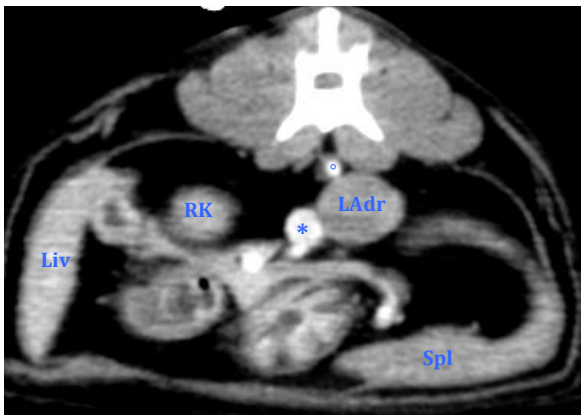

Figure 8.7 - Transverse post-contrast CT image showing the left adrenal mass adjacent to but not invading the caudal vena cava and aorta (Soft tissue window)

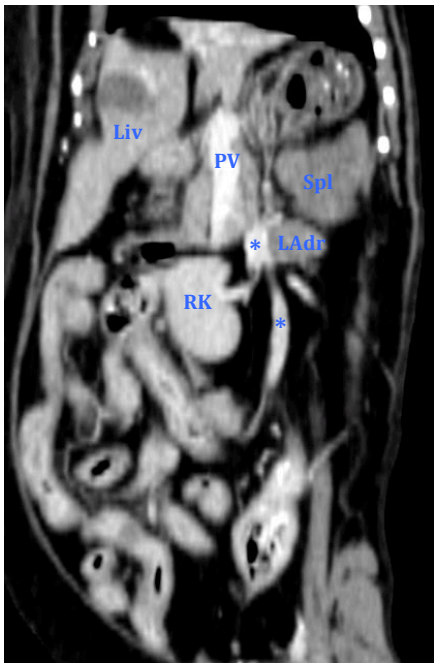

Figure 8.8 - Dorsal oblique MPR post-contrast CT image of the left adrenal mass adjacent to the caudal vena cava (Soft tissue window)

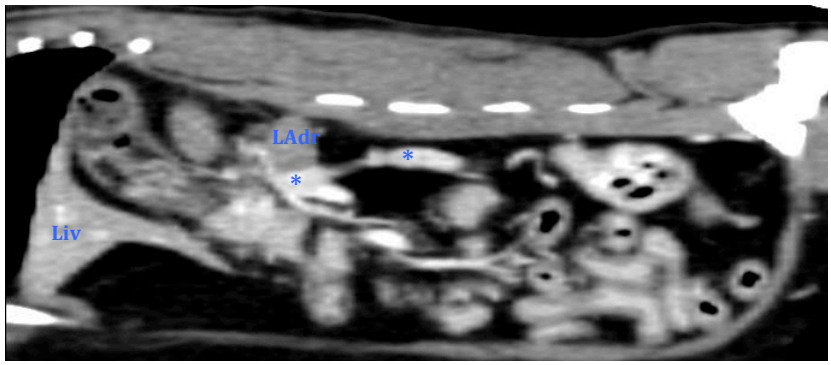

Figure 8.9 - Sagittal MPR post-constrast CT image of the left adrenal mass adjacent to the caudal vena cava (Soft tissue window)

Ladr: Left adrenal mass; Liv: Liver; PV: Portal vein; RK: Right Kidney; Spl:Spleen; *: Caudal vena cava; °: Aorta

Case 9. Mechanical ileus

Signalment and History

Two weeks prior to presentation, a 2-year-old male neutered Weimaraner had an episode of presumed gastric dilation. A stomach tube was passed, gas was evacuated from the stomach and the dog returned to normal. Two days prior to presentation, the dog vomited several piles of frothy fluid overnight and the abdomen started to distend again, which worsened over the day. Gastric dilation was suspected and a stomach tube was passed again. Foul smelling dark brown liquid material was evacuated from the stomach. The dog had 2 further episodes of vomiting and had not passed any faeces. A progressive intermittent ataxia motivated an emergency consultation at the Small Animal Hospital, University of Glasgow. The dog was a known scavenger, living on a farm with horses and chickens. The dog was fully vaccinated and dewormed on a regular basis.

Clinical Signs

a) Very quiet
b) Brick red buccal mucosa, increased capillary refill time
c) Hypothermia, cold extremities
d) Tachycardia (heart rate = 200 beat per minute)
e) Reduced femoral pulse quality, absent metatarsal and metacarpal pulses
f) Distension of multiple intestinal loops on abdominal palpation
g) Intermittent ataxia and reduced proprioception on all four limbs, intermittent hyperextension of the hind limbs and wide based stance.

Radiographic Examination

1. **Equipment** - See Appendix 1
2. **Restraint** - No sedation was used. Positioning was achieved using wedges of dressing material and rope ties.

Area	View	kV	mAs	Grid
Abdomen	Right Lateral (Fig.9.1)	66	7.1	O
	Left Lateral (Fig.9.2)	66	7.1	O
	Dorso-ventral (Fig.9.3)	73	12.5	O
Thorax	Left Lateral (Fig.9.4)	64,5	10	O

Radiographic Appraisal

A small amount of the diaphragm is missing on all abdominal views (Figs.9.1 to 9.3). Only the left lateral view of the thorax (Fig.9.4) was available. The radiograph of the

thorax is well positioned and centred. The images are well processed. Primary markers are present on all radiographs except the dorso-ventral abdominal view (Fig.9.3), although the left marker is outside the primary beam on the left lateral abdominal view, and a secondary L marker has been added. Exposure settings have been added on all radiographs, except the right lateral abdominal view. The radiographs are of diagnostic quality.

Radiological Report

A marked gas and/or fluid dilation of several small intestinal loops, which are stacked on top of each other, is visible, with the diameter of the small intestinal loops being 2 to 2.8 times the height of the vertebral body of L5. These changes are consistent with a mechanical ileus indicating small intestinal obstruction. In the mid ventral abdomen, on the left lateral view (Fig.9.2), there is a moderately heterogeneous soft tissue opacity mass, of about 4x4.5cm, with very small mineralized elements within. This could be consistent with faeces in the ascending colon displaced ventrally by the dilated loops, although an ill-defined foreign body or accumulation of ingesta upstream of the obstruction cannot be excluded. Small areas of mineral opacity are visible in the caudal descending colon. A moderate decrease in abdominal contrast is noted consistent with peritonitis, a mild amount of abdominal free fluid and/or the thin body condition of the animal.

The size of the cardiac silhouette is at the lower end of the normal limits, which may suggest hypovolaemia (Fig.9.4). A moderate diffuse bronchial pattern is noted consistent with a moderate chronic bronchitis.

Differential Diagnosis

Small intestinal mechanical ileus, consistent with small intestinal obstruction, caused by foreign body most likely, intussusception, volvulus, less likely intestinal neoplastic mass or granuloma.

Ultrasound Examination

1. **Equipment** - See Appendix 1.
2. **Restraint** - The dog was not sedated; he was put in lateral and dorsal recumbency for the abdominal ultrasound scan.

Abdominal Ultrasound Report

An abdominal ultrasound (Figs.9.5 to 9.10) was performed to assess the cause and site of intestinal obstruction. The stomach was severely dilated with large amount of food

and fluid contents (Fig.9.5). In the lumen many small linear hyperechoic particles with acoustic shadowing were seen in suspension. The small intestinal loops were generally severely dilated by fluid swirling, with serosal-to-seraosal diameter up to 2.6 cm, although mild peristaltic waves were still evident (Figs.9.6 and 9.7). Small intestinal wall layering was within normal limits. In the right caudal abdomen a transition between dilated loop and non-dilated was seen associated with the presence of a hyperechoic structure, of at least 3.5 cm of length, causing clean acoustic shadowing, consistent with a foreign body, most likely in the distal jejunum (Figs.9.8 and 9.9). The mesenteric lymph nodes were prominent (thickness about 6.5mm), however the echogenicity and shape were within normal limits (Fig.9.10). The abdominal fat was moderately hyperechoic, but no free fluid was identified.

Further Investigations

A mild hypokalaemia was revealed on blood samples, otherwise unremarkable.

Outcome

The dog underwent exploratory abdominal surgery where very red, hyperaemic distended small intestine with very little movement was found. An area of mild bruising was present about 20cm proximal to the site of intestinal obstruction, likely secondary to the passage of foreign material. A very small amount of clear straw-coloured fluid was present in the abdomen. The stomach was grossly distended and flaccid. A foreign body of about 4cm long and 2cm in diameter was identified in the distal jejunum. An enterotomy was performed and a corncob was removed. A gastrotomy was performed and about 2 litres of dark brown thick liquid was suctioned. Full wall jejunal and gastric biopsies were taken and incisional gastropexy was performed due to the dog's signalment and history. Lavage of the abdominal cavity was done prior to closure.

The dog recovered well from surgery and was discharged four days later. Histopathological results of biopsy samples were consistent with mild chronic gastritis associated with mild mucosal fibrosis and acute enteritis with moderate villous stunting.

At follow up examination 2 weeks later, the dog was back to normal and the wound had healed well.

Discussion

Gastrointestinal obstruction is common condition in small animals. Clinical signs are nonspecific and may be acute or more chronic depending on location, degree and duration of obstruction.[1] The most common clinical signs include vomiting,

inappetance, anorexia and lethargy, although diarrhoea or weight loss may be seen.[1,2,3,4,5] On physical examination small animals often present with abdominal pain and dehydration, in some cases an abdominal mass may be palpable. Fever is also noted in few cases. Foreign bodies are the most common cause of gastrointestinal obstruction in small animals (78%[2]) although numerous other causes such as intussusception, neoplasia, adhesions and strictures may generate gastrointestinal obstruction.[2,3,5]

As gastrointestinal obstructions may lead to hypovolaemic shock, systemic inflammatory response syndrome and sepsis, secondary to dehydration, electrolyte imbalances and intestinal ischemia and necrosis, a prompt and accurate diagnosis providing possible cause, location and severity of obstruction is recommended to reduce the time to surgery and perioperative morbidity. Imaging diagnostic modalities are indicated when intestinal obstruction is suspected on the basis of history, clinical signs and physical examination to determine the presence or absence of obstruction.[2,3,4,5]

Radiography is frequently used to assess small animals suspected of having gastrointestinal obstructions. On abdominal radiographs, a diagnosis of obstruction is based on detection of gastric or segmental small-intestinal dilatation by gas and/or fluid, abnormal shape or position of small intestine, such as stacked loops or plication, gravel sign or detection of a foreign body or a mass.[2,3,4] Radiopaque foreign bodies may be easily identified, although many foreign bodies retrieved, included fruit pits, corncobs, trichobezoars, rubber toy, socks or ear plug, can easily be missed on plain radiographs.[1,2,3,4] Linear foreign bodies, more often seen in cats than in dogs[1], are also challenging to be identify on radiographs. Plication and stacked dilated intestinal loops may be visible, although in numerous cases no obvious sign of obstruction is visible. In one recent study[3], abdominal radiography produced a definitive result of obstructed or not obstructed small intestine in 70% of dogs presented for vomiting. About 30% of obstructed dogs did not have radiographic signs of segmental small intestinal dilatation, of which 50% were due to linear foreign bodies. The small intestinal diameter to height of the body of the fifth vertebra (SI/L5) ratio is often used to assess dilation of the small intestinal loops on radiographs in dogs, as the probability of small intestinal obstruction increases with increasing SI/L5 ratio.[2] However, severe small-intestinal dilatation, (SI/L5 ratio > 2), especially segmental dilatation, was detected in about 50% of the dogs with small-intestinal mechanical obstruction, but also in about 10% of dogs without obstruction, in the same study[3]. Furthermore in another recent report[2], sensitivity and specificity for diagnosis of small intestinal obstruction were only 66% using an SI/L5 ratio of 1.7, and the use of the SI/L5 ratio was not associated with increased accuracy of

diagnosis. Small-intestinal dilatation is supportive of a diagnosis of small-intestinal obstruction, but the lack of small-intestinal dilatation does not exclude small-intestinal mechanical obstruction. This observation may be explained by duration of disease, vomiting that may empty small-intestinal lumen, or linear foreign bodies with plication that prevented luminal distention.[2] Additional findings, such as decreased or loss of serosal details, consistent with the presence of free fluid and/or peritonitis, or presence of free bubbles of gas within the abdominal cavity, suggestive of gastro-intestinal perforation, may be seen on abdominal radiographs, although non-specific for gastrointestinal obstruction.[2,3,4]

Ultrasonography has been shown to be more sensitive (85 to 100%), specific (94 to 96%) and accurate than radiography in the diagnosis of small intestinal obstruction.[3,5] A definitive result of obstructed vs. non-obstructed small intestine was observed in 97% of vomiting dogs, compared to the 70% in radiography.[3] Signs in favour of mechanical obstruction observed by ultrasonography include segmental gastrointestinal fluid and/or gas dilatation or plication, visualisation of the cause of obstruction (e.g. foreign bodies, intussusception, intestinal mass), and abnormal motility (e.g. hypermotility without contents progression, hypomotility or both), although the latter does not appear to be a distinguishing feature of obstruction.[3,4,5] Foreign bodies appear as hyperechoic interface with strong distal acoustic shadowing whereas intussusception is seen as a series of multi-layered concentric rings and may be due to foreign body or intestinal mass. In cases of linear foreign body, a stationary linear hyperechoic structure with surrounding plicated intestinal loops is visible.[5] Animals with intestinal obstruction present a larger overall small intestinal diameter than non-obstructed ones, due to fluid accumulation within the lumen proximal to the obstruction. One recent study[3] indicates that a jejunal serosal-to-serosal diameter of at least 1.5cm is a very good test for diagnosis of small-intestinal mechanical obstruction. Furthermore, ultrasonographic examination of the gastrointestinal tract allows measurement of intestinal wall thickness, assessment of wall stratification and integrity, localisation of the level of obstruction and the length of gastro-intestinal tract affected, presence of peritoneal free fluid, echogenicity of the mesentery and evaluation of adjacent structures such as lymph nodes and pancreas.[3,4,5] However, these additional findings are not specific for gastrointestinal obstruction, but can give more information regarding optional treatment and prognosis. One of the major limitations of ultrasonography of the gastro-intestinal tract is the presence of intraluminal gas, which can impair recognition of foreign body or mass. This is more often the case in assessment of the gastric lumen, for which abdominal radiographs may

be more accurate. Operator experience may also impact on the ability to recognize small intestinal mechanical obstruction and cause of obstruction.[3,5]

To conclude, both abdominal radiography and ultrasonography are accurate for diagnosing small-intestinal obstruction, however abdominal ultrasonography yields greater accuracy, fewer equivocal results and provides greater diagnostic confidence compared with radiography.[3] The choice between both diagnostic imaging tools may be influenced by multiple factors, such as tentative diagnosis, patient size, co-morbidities, clinician preference, experience, cost and availabity.[3,4,5] Gastrointestinal contrast studies may also be performed; nevertheless some limitations may be taken into account. Gastrointestinal barium contrast studies may be non-diagnostic if the contrast is not retained due to vomiting, are time and money consuming, and may delay surgical exploration. Furthermore, a gastrointestinal barium contrast study is contraindicated if gastro-intestinal perforation is suspected or immediate surgery is contemplated and may increase patient stress.

References

1-Hayes G. Gastrointestinal foreign bodies in dogs and cats: a retrospective study of 208 cases. **J Small Anim Pract** 2009; 50(11): 576-583

2-Ciasca TC, David FH, Lamb CR. Does measurement of small intestinal diameter increase diagnostic accuracy of radiography in dogs with suspected intestinal obstruction? **Vet Radiol Ultrasound** 2013; 54(3): 207-211.

3-Sharma A, Thompson MS, Scrivani PV, Dykes NL, Yeager AE, Freer SR, Erb HN. Comparison of radiography and ultrasonography for diagnosing small-intestinal mechanical obstruction in vomiting dogs. **Vet Radiol Ultrasound** 2011; 52(3): 248-255.

4-Tyrrell D, Beck C. Survey of the use of radiography vs. ultrasonography in the investigation of gastrointestinal foreign bodies in small animals. **Vet Radiol Ultrasound** 2006; 47(4): 404-408.

5-Garcia DA, Froes TR, Vilani RG, Guérios SD, Obladen A. Ultrasonography of small intestinal obstructions: a contemporary approach. **J Small Anim Pract** 2011; 52(9): 484-490.

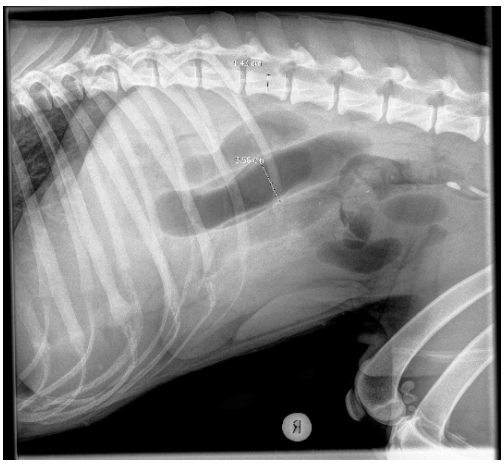

Figure 9.1 - Right lateral abdominal radiograph

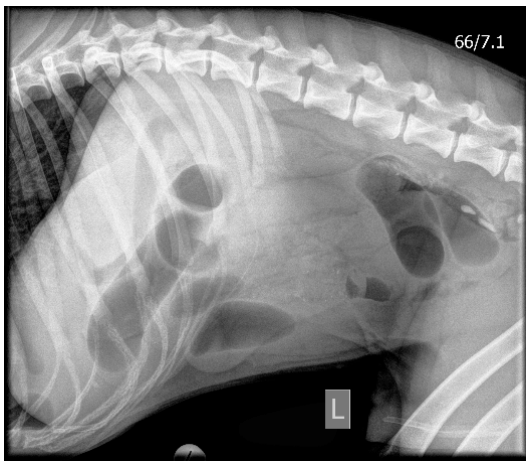

Figure 9.2 - Left lateral abdominal radiograph

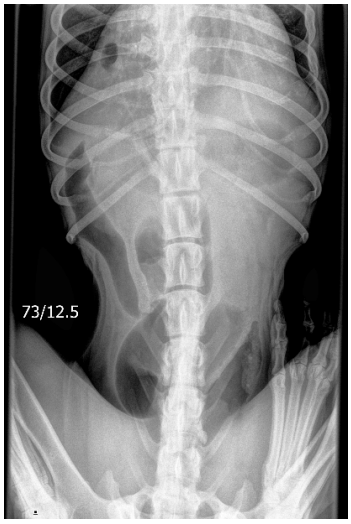

Figure 9.3 - Dorso-ventral abdominal radiograph

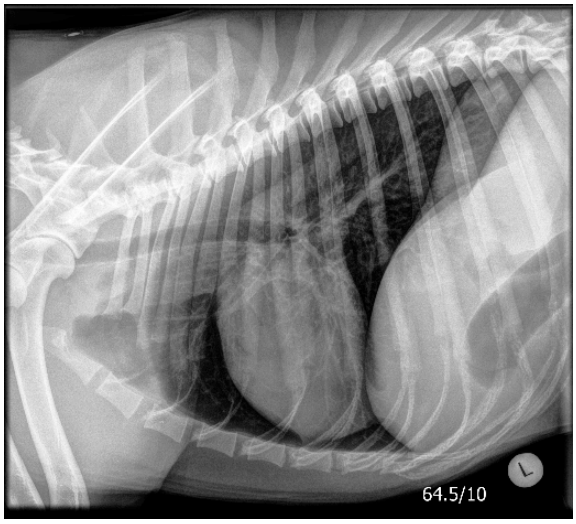

Figure 9.4 - Right lateral thoracic radiograph

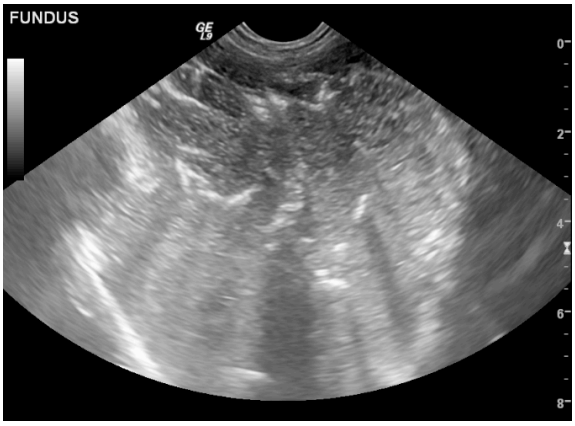

Figure 9.5 - Ultrasound image showing gastric fluid dilation, with small hyperechoic structures floating within the lumen

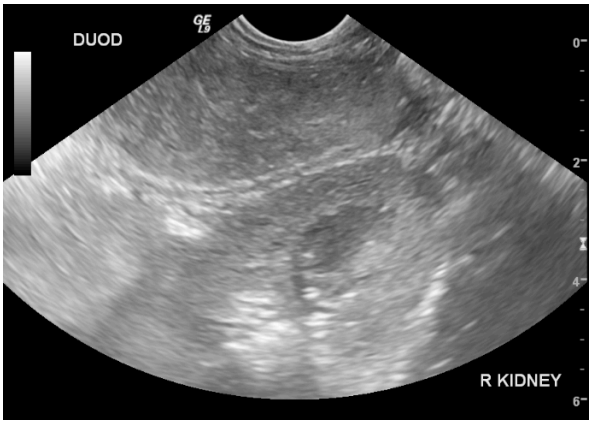

Figure 9.6 - Ultrasound image showing marked duodenal fluid dilation

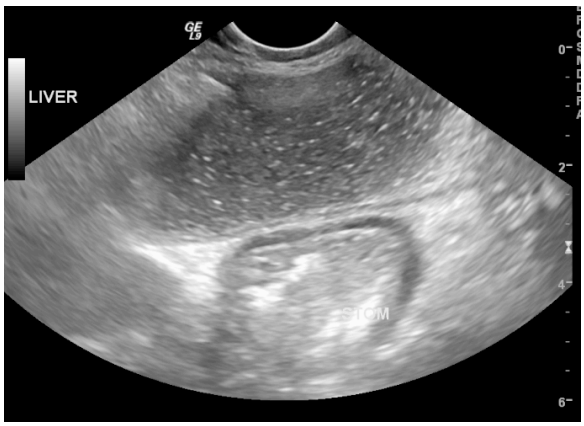

Figure 9.7 - Ultrasound image showing marked small intestinal fluid dilation

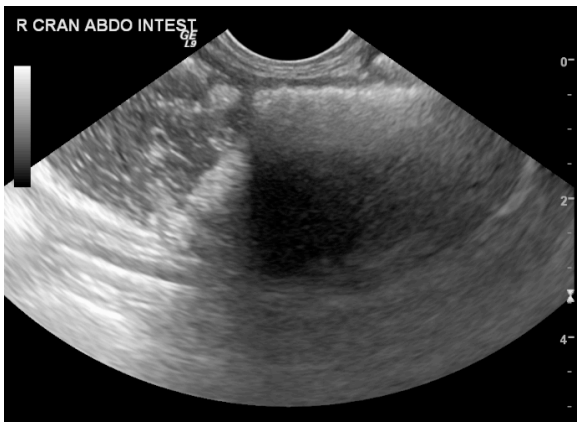

Figure 9.8 - Ultrasound image demonstrating small intestinal dilation proximally to the foreign body

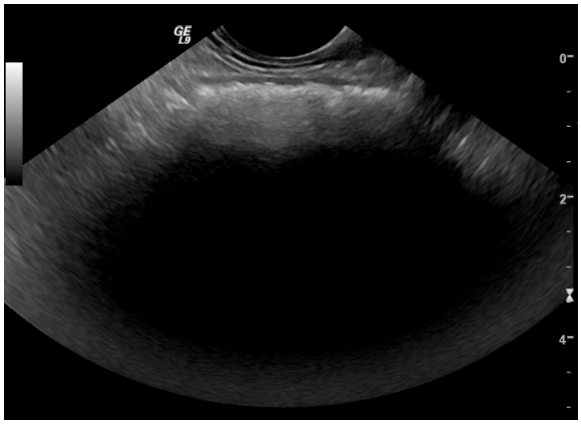

Figure 9.9 - Ultrasound image of the small intestinal foreign body, with strong distal acoustic shadowing

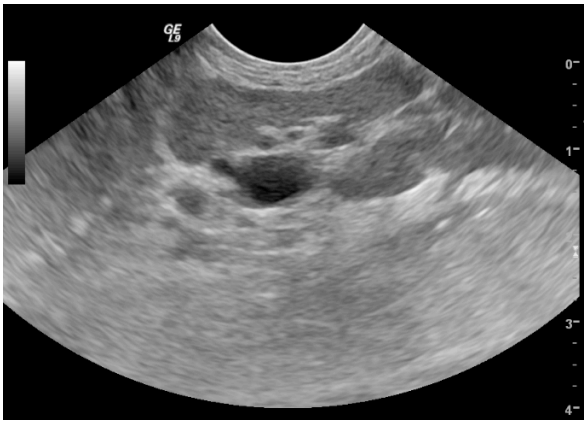

Figure 9.10 - Ultrasound image demonstrating moderate mesenteric lymphadenomegaly.

Case 10. Parasitic pneumonia

Signalment and History

An 8-year-old female neutered Golden Retriever, had a history of cutaneous mast cell tumour of grade II removed from the 5th digit of the left front foot with an associated infiltration of the left pre-scapular lymph node, which was removed in 3 month previously. At that time, the dog underwent further investigations for a general staging and no other significant abnormality was detected. The dog was treated with chemotherapy (vinblastine, prednisolone). No sign of illness or metastatic process was recognised during this time. Seven days after his last chemotherapy treatment, a retching non-productive cough, associated with variable appetite and hyperthermia developed, which was unresponsive to antibiotics.

Clinical Signs

a) Very nervous, too excited for a correct assessment of chest auscultation
b) Hyperthermia (39.6°C)
c) Retching cough during consultation.

Radiographic Examination

1. **Equipment** - See Appendix 1
2. **Restraint** – The dog was sedated. Positioning was achieved using wedges of dressing material and rope ties.

Area	View	kV	mAs	Grid
Thorax	Right Lateral (Fig.10.1)	64.5	10	O
	Left Lateral (Fig.10.3)	64.5	10	O
	Dorso-ventral (Fig.10.5)	70	12.5	O

Radiographic Appraisal

The images are well processed. The right lateral (Fig.10.1) and dorso-ventral (Fig.10.5) views are well positioned and centred. The caudo-dorsal part of the lung field is missing on the left lateral view (Fig.10.3). The dorso-ventral view is expiratory. Primary markers are present on the right lateral and dorso-ventral views; an L marker has been added to the left lateral view. Exposure settings have been added on right lateral and dorso-ventral radiographs. The radiographs are of diagnostic quality.

Radiological Report

A moderate to marked diffuse broncho-interstitial pattern, more marked on the ventral and caudal aspect of the lung field, is visible associated with moderately ill-defined

patchy areas of alveolar pattern diffusely spread within the lung field. Particularly, larger areas of alveolar pattern associated with air bronchograms are visible in the ventral part of the cranial lung field, more visible on the right lateral view suggesting they are more probably located in the ventral aspect of the cranial part of the left cranial lung lobe, and of the accessory lung lobe.

Mildly irregular costo-chondral junctions are visible, most likely consistent with age related changes.

Differential Diagnosis

Diffuse pulmonary broncho-interstitial pattern associated with patchy moderately ill-defined alveolar areas consistent with pneumonia (infectious, parasitic, inflammatory, less likely fungal), haemorrhage or less likely a neoplastic process; metastatic (although the appearance was unusual for metastatic spread of mast cell tumour) or primary.

Advanced Imaging – Thoracic Computed Tomography

A thoracic CT (Figs.10.7 to 10.12) was performed for a better assessment of the location, extension and type of the pulmonary infiltrates. A moderate diffuse broncho-interstitial pattern is noted associated with a moderate dilation of the bronchial tree consistent with bronchiectasis (Fig.10.10). Multiple well defined nodular (Figs.10.11 and 10.12) to moderately ill-defined patchy areas of alveolar patterns (Figs.10.7 to 10.9) are seen diffusely spread through the peripheral aspect of the lung field, associated with air bronchograms. Several adjacent ill-defined ground-glass opacity (Figs.10.8 and 10.9) areas are also visible, mostly in the caudo-dorsal lung field. Additional mildly thickened pleural fissure lines are noted.

A few small areas of gas attenuation are visible in the soft tissue of the right axillary area, most likely consistent with vein punction (e.g. catheter placement, intravenous injection) although an injury or early infectious process cannot be completely ruled out.

A very mild thoracic spondylosis is noted.

The pulmonary changes were indicated of parasitic pneumonia regarding the peripheral ground glass and nodular changes, although pneumonia of other origin (infectious, fungal) with or without pulmonary hemorrhages or less likely atypical neoplastic process could not be completely ruled out.

Further Investigations

Biochemistry showed a mild hyperglobulinaemia.

Coagulation profile was within normal limits.

Bronchoscopy and broncho-alveolar lavage were performed. One lungworm was seen in the trachea. A diffuse, chronic and severe tracheobronchial inflammation was evident on visual inspection. Lavage cytology showed severe neutrophilic and eosinophilic inflammation. No organism was seen. A few Gram-negative colonies were isolated from lavage culture, but were not thought to be significant. No primary bacterial respiratory pathogen was isolated.

An abdominal ultrasound was performed and no significant abnormality was detected. Ultrasound guided percutaneous aspirations of consolidated lung were performed and cytologic examination was consistent with mixed cell inflammation as seen in the broncho-alveolar lavage. No neoplastic cell was seen.

Direct faecal microscopy failed to identify larvae. *Crenosoma vulpis* and *Angiostrongylus vasorum* were found on faecal Baermann analysis.

Outcome

The dog was treated with Advocate®, Bayer (imidacloprid/moxidectin) and a single subcutaneous administration of dexamethasone at anti-inflammatory dose and was discharged with a course of antibiotics (Synulox®, Pfizer - Amoxicillin/Clavulanic Acid - 500mg PO BID) in case of secondary pulmonary infection.

A follow up examination was performed 3 weeks later. The cough had mostly resolved and the dog had returned to normal exercise. Marked improvement in pulmonary changes was seen on repeat thoracic radiographs (Figs.10.2, 10.4 and 10.6, page 93), although some peripheral alveolar change remained, particularly in the right middle lung lobe and in the cranial aspect of the cranial lung lobes, associated with a mild diffuse bronchial pattern. These changes may be due to the persistence of lungworm infection, secondary bacterial infection, pulmonary haemorrhages and/or focal areas of atelectasis associated with bronchial occlusion by debris/parasites. Repeat faecal Baermann analysis was negative. A course on monthly Advocate® was continued.

Discussion

Angiostrongylus vasorum (A. vasorum) is a nematode heartworm infecting dogs and related canids, belonging to the superfamily *Metastrongyloidea*. First reported in south west France, hence its nickname French Heartworm, its distribution has since been recognised in many other countries worldwide including south east England and Wales, Ireland, Germany, Denmark, Italy, Canada, south America and Africa. Isolated endemic foci are generally observed throughout these regions.[1,2,3,4] *A. vasorum* has an indirect life cycle with gastropods (slugs and snails) acting as the intermediate host. Paratenic

hosts, such as the common frog (*Rana temporaria*) have been described in the life cycle and they can also act as intermediate hosts.[3] Wild and domestic dogs, the primary hosts, become infected as a result of ingesting an intermediate host containing the L3 larvae. The larvae are liberated in the small intestine and migrate through the intestinal wall to the mesenteric lymph nodes, where two further moults occur. Immature L5 larvae then migrate via the hepatic portal vein, liver and caudal vena cava to the right side of the heart and pulmonary arteries. Here they reach maturity approximately 33 to 35 days after infection. After a prepatent period of around 38 to 60 days, deposition of eggs starts in the terminal pulmonary arteries, thence mature into L1 larvae that emerge in the alveoli. L1 larvae enter the gastrointestinal tract after they are expelled from the trachea by coughing, they are swallowed and later excreted in the faeces.[1,2,3] Infected dogs develop severe pulmonary parenchymal lesions at the time of patency because of intense immune responses to egg and larval antigens, including eosinophilic inflammation, haemorrhages, arterial thrombosis, periarteritis, and coalescing granulomata. In the chronic stage, fibrosis of the pleura and the lung parenchyma develops.[1,3,4,5] *Angiostrongylus vasorum* infection is associated with high morbidity and mortality (2 to 13%)[3] in dogs, with a reported mortality about 24% from data collated from referral centres.[3]

Affected dogs are generally young (< 2 years) and infection in older dogs could reflect a degree of immune-compromise predisposing to infection.[3] Clinical signs can be highly variable or absent depending on parasitic burden. Respiratory compromise (e.g. coughing, dyspnoea, tachypnea) and bleeding diatheses (e.g. epistaxis, petechial or ecchymotic haemorrhages, haemarthrosis, brain haemorrhages, haematuria, etc.) as a result of coagulopathy, are the most common clinical signs encountered (reported in 50 to 65% and 35% of cases respectively).[2,3] The mechanism of coagulopathy is not well understood; it is thought that antigenic factors secreted by the parasites may lead to disseminated intravascular coagulation and consumptive coagulopathy. Associated anaemia, thrombocytopenia, prolonged prothombin time (PT), activated partial thromboplastin time (aPTT) and buccal mucosal bleeding time, elevated D-dimer concentration and decreased fibrinogen levels may be found.[2,5,6] Exercise intolerance, lethargy, weakness, decreased appetite with loss of body weight, collapse, gastro-intestinal, ocular and neurologic signs are also reported and may be not associated with respiratory compromise.[1,2,3,4,5,6] Indeed, despite marked pulmonary pathology, evidence of respiratory signs may be mild in numerous cases. Thoracic auscultation may reveal increased or harsh lung sounds and crackles. Pulmonary vessel thrombosis, vascular

inflammation and vascular smooth muscle hypertrophy, due to the presence of adult worms in the pulmonary arterial vasculature, may lead to pulmonary hypertension and, eventually, right-sided cardiac dysfunction (cor pulmonale).[5] However, in one series of experimentally infected Beagles[4], pulmonary and vascular changes induced by *A. vasorum* were reflected by marked radiographic changes and arterial hypoxemia, but did not result in pulmonary hypertension and echocardiographic changes in cardiac size and function, regardless of inoculation dose. Pyrexia may be found on physical examination, and neutrophilia is another common finding.[3,4]

Various degrees of radiographic and CT changes are seen, accompanying the pathological changes. In experimentally infected dogs, abnormalities have been described as developing 5 to 7 weeks post-inoculation[2] and being most pronounced at 7 to 9 weeks post-inoculation on radiographs[1,2,4] and 9 to 13 weeks on CT[1]. Radiographic changes may range from mild to severe mixed and patchy broncho-interstitial to alveolar pattern, and are very typically multifocal and most pronounced at the lung periphery.[1,2,3,4,5] The severity and onset of pulmonary lesions is dependant on the inoculated dose, in experimentally infected dogs.[1,4] Pulmonary arteries may rarely appear tortuous, slightly enlarged or truncated. Furthermore, pleural fissure lines, consistent with pleural effusion, and enlargement of the tracheobronchial lymph nodes may be visible. These changes have been described in experimentally and naturally affected dogs and may be seen in dogs even without respiratory signs. The presence of pneumothorax and subcutaneous emphysema has also been described.[1,2,3,5] In experimentally infected dogs, clinical signs tend to resolve in low-grade infected dogs and improve in high-grade infected dogs 13 weeks post-inoculation, and the radiographic signs tend to improve.

On CT, multiple large nodules merging to areas of consolidation, containing air bronchograms of varying extent, and multicentric ground-glass opacities are visible. Well-delineated wedge-shaped consolidated areas, with the broad base toward the periphery, are also seen. The nodular and consolidated lesions show marked contrast enhancement, and several suspicious intraluminal filling defects suggestive of thrombosis (e.g. parasites within the pulmonary arteries, vascular thrombi) may be found on post-contrast images. The nodular changes correspond to histopathologic granulomata, consisting mainly of macrophages, multinucleated giant cells and lymphocytes, accumulated around larvae and eggs. Parts of the consolidation are due to haemorrhage, inflammatory response and/or infarction. A mild to moderate amount of pleural effusion may be found. Bronchial thickening associated with possible peripheral

bronchiectasis may develop with advanced disease. As for the radiographic signs, the severity of the pulmonary lesions on CT is dose dependent in experimentally infected dogs, and pleural fissure lines are noticed with high inoculation doses. Regional lymph nodes are enlarged after infection.[1]

Even if radiographic and CT findings and distribution of the lesions are highly suggestive of parasitic pneumonia in association with history and clinical signs, the diagnosis of angiostrongylosis is based on either positive Baermann faecal analysis or finding *A. vasorum* larvae on broncho-alveolar lavage (BAL).[2,3,5] Ultrasound-guided fine needle aspirate of the peripheral pulmonary lesions may be done to exclude other pulmonary condition such as neoplasia if suspected, however it would not give a definitive diagnosis. Baermann faecal analysis is considered the most sensitive currently available method for diagnosis of L1 larvae in dogs infected with angiostrongylosis. However, negative results occur prior to patency or in animals that intermittently shed. Repeated Baermann faecal analysis and/or BAL might be necessary to obtain positive results, and negative result does not preclude disease.[3] Serological and faecal polymerase chain reaction (PCR) tests have been also developed, but are not yet fully validated.[3,5] Post-mortem examination can also confirmed the diagnosis.

Fenbendazole (Panacur®, Intervet), at 20 mg/kg to 50 mg/kg per os (PO) q 24 h for 5 to 21 days, is generally used as treatment and reported to be successful in 95% of cases. Authorised therapies include imidacloprid/moxidectin (Advocate®, Bayer) for treatment and prevention and milbemycin oxime (Milbemax®, Novartis Animal Healthy) for reducing the level of infection.[3]

After treatment, resolution of clinical signs is generally noted as well as negative faecal sample for *A. vasorum* within the following 2 or 3 weeks.[3,4] However, pulmonary changes are still visible on radiographs and CT. Nine weeks after treatment in experimentally studies, a marked improvement of the pulmonary lesions, particularly the alveolar pattern, is noted on radiographs and fissure lines are no longer visible. However, a generalized slight to moderate broncho-interstitial pattern remains present and a complete resolution of the pulmonary changes is generally not seen.[1,2,4] Similar changes are visible in naturally infected dogs re-examined radiographically 2 to 15 weeks post-treatement.[2] On CT, the pulmonary consolidations and large nodules generally disappear almost completely after treatment. Remaining mild scattered ground-glass opacities, subpleural interstitial thickening, mild pleural thickening, and in some cases small nodular changes, are visible 9 weeks post-treatment, regardless of infection grade in experimentally infected dogs. These changes are consistent with

residual interstitial fibrosis, focal inflammatory and thrombotic changes, and mild pleural fibrosis as documented histopathologically.[1,4] The tracheobronchial lymph nodes are generally decreased in size compared to pre-treatment.[1]

The routinely used parasitological tests can be repeatedly negative. While the outcome is favourable in the majority of animals, a more guarded prognosis is advised for those animals, which present with severe dyspnoea, or in which a diagnosis is challenging or the response to therapy is incomplete. [3,5]

Crenosoma vulpis (C. vulpis), also called the fox lungworm, is a metastrongylid infecting domestic canids in the temperate regions of North America and Europe that has been recently recognised as an important cause of chronic respiratory disease in dogs. The life cycle is similar to *A. vasorum*. Animals acquire infection by the ingestion of infective third-stage larvae contained in the tissues of the intermediate hosts (various species of terrestrial gastropods). The prepatent period is 19 to 21 days. Adults worm live in the trachea, bronchi and bronchioles, with a life span of about 10 months, and first-stage larvae are passed in the faeces. Crenosomosis is usually characterized by bronchitis with a dry, non-productive cough that can be elicited by tracheal palpation and may be accompanied by gagging. High parasitic burdens may induce mucoid or mucopurulent discharge in the airways, with a chronic and productive cough. In most cases, a mild to moderate bronchial pattern, possibly associated with a diffuse interstitial component, most evident in the diaphragmatic lobes, is observed on radiographs.[7] Affected dogs are relatively young (median 4 years reported in one study[8]), although all ages may be encountered. Broncho-alveolar lavage cytology generally reveals inflammation with predominance of eosinophils and *C. vulpis* larvae may be identified in BAL. As for *A. vasorum*, faecal examination with Baermann technique is the most sensitive method for a definitive diagnosis. *C. vulpis* infection has to be considered in the differential diagnosis in dogs of all ages presenting with acute or chronic cough. Although cough may be severe, fatal infections in dogs have never been reported.[8]

References

1-Dennler M, Makara M, Kranjc A, Schnyder M, Ossent P, Deplazes P, Ohlerth S, Glaus TM. Thoracic computed tomography findings in dogs experimentally infected with *Angiostrongylus vasorum*. **Vet Radiol Ultrasound** 2011; 52(3): 289–294.

2-Boag AK, Lamb CR, Chapman PS, Boswood A. Radiographic findings in 16 dogs infected with *Angiostrongylus vasorum*. **Vet Rec** 2004; 154(14): 426-430.

3-Gallagher B, Brennan SF, Zarelli M, Mooney CT. Geographical, clinical, clinicopathological and radiographic features of canine angiostrongylosis in Irish dogs: a retrospective study. **Irish Vet J** 2012; 65(1): 5.

4-Kranjc A, Schnyder M, Dennler M, Fahrion A, Makara M, Ossent P, Morgan J, Deplazes P, Glaus TM. Pulmonary artery thrombosis in experimental *Angiostrongylus vasorum* infection does not result in pulmonary hypertension and echocardiographic right ventricular changes. **J Vet Intern Med** 2010; 24(4): 855-862.

5-Traversa D, Guglielmini C. Feline aelurostrongylosis and canine angiostrongylosis: a challenging diagnosis for two emerging verminous pneumonia infections. **Vet Parasitol** 2008; 157(3-4): 163-174.

6-Zarelli M, Shiel R, Gallagher B, Skelly C, Callanan S, McAllister H. Imaging diagnosis: CT findings in a dog with intracranial hemorrhage secondary to angiostrongylosis. **Vet Radiol Ultrasound** 2012; 53(4): 420-423.

7-Traversa D, Di Cesare A, Conboy G. Canine and feline cardiopulmonary parasitic nematodes in Europe: emerging and underestimated. **Parasit Vectors** 2010; 3: 62.

8-Unterer S, Deplazes P, Arnold P, Flückiger M, Reusch CE, Glaus TM. Spontaneous Crenosoma vulpis infection in 10 dogs: laboratory, radiographic and endoscopic findings. **Schweiz Arch Tierheilkd** 2002; 144(4): 174-179.

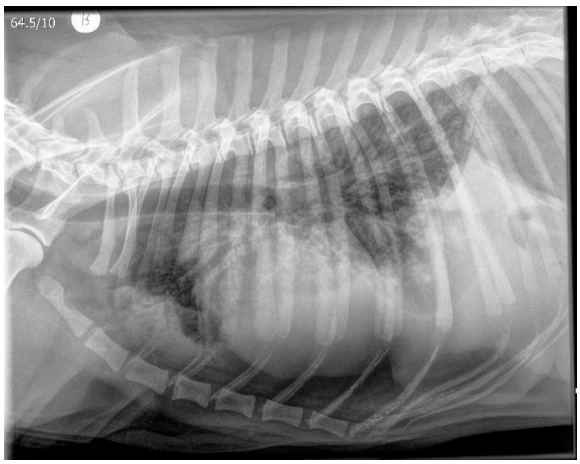

Figure 10.1 - Right lateral thoracic radiograph

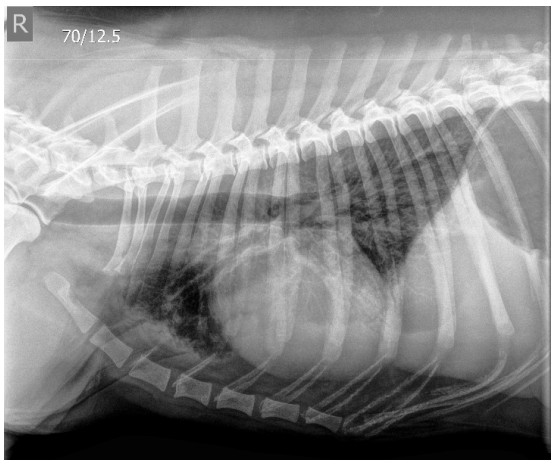

Figure 10.2 - Right lateral thoracic radiograph, follow up 3 weeks later

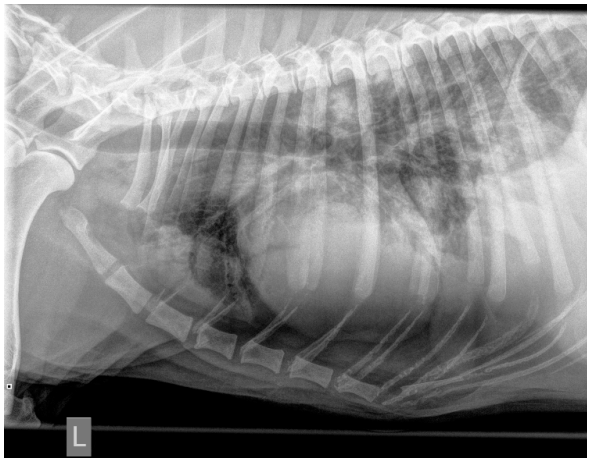

Figure 10.3 - Left lateral thoracic radiograph

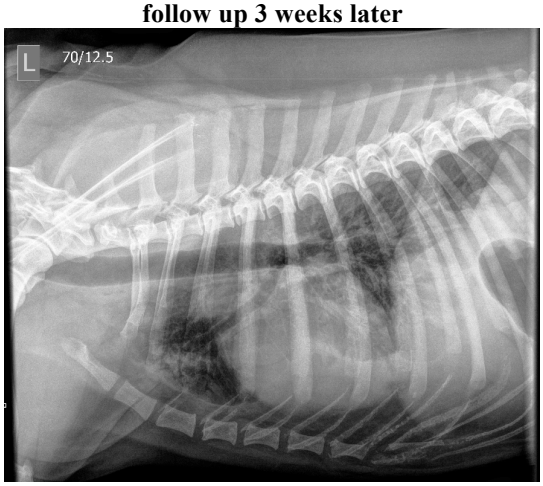

Figure 10.4 - Left lateral thoracic radiograph, follow up 3 weeks later

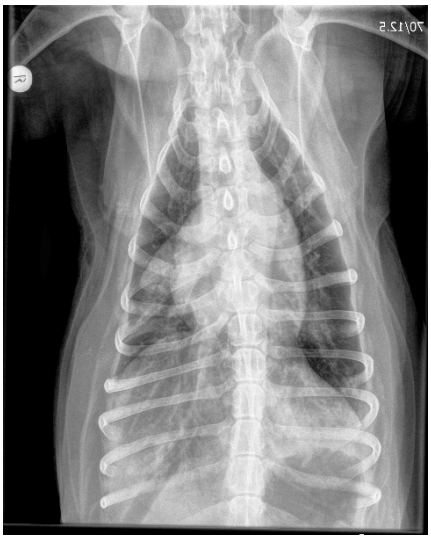

Figure 10.5 - Dorso-ventral thoracic radiograph

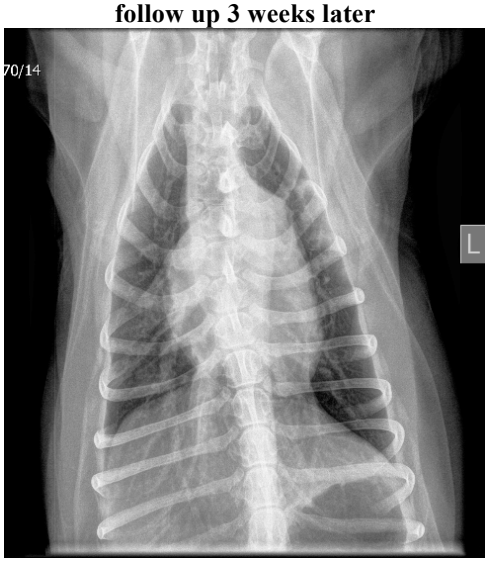

Figure 10.6 - Dorso-ventral thoracic radiograph, follow up 3 weeks later

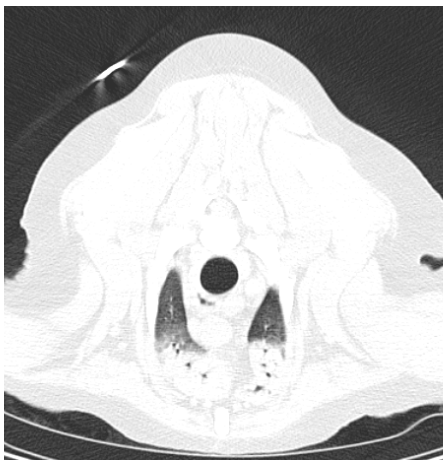

Figure 10.7 - Transverse CT image demonstrating consolidation of the ventral cranial lung lobes (Lung window)

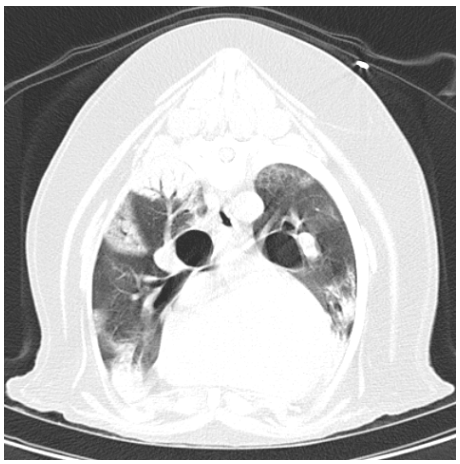

Figure 10.8 - Transverse CT image showing alveolar pattern and ground glass opacities at the periphery of the cranial lung lobes (Lung window)

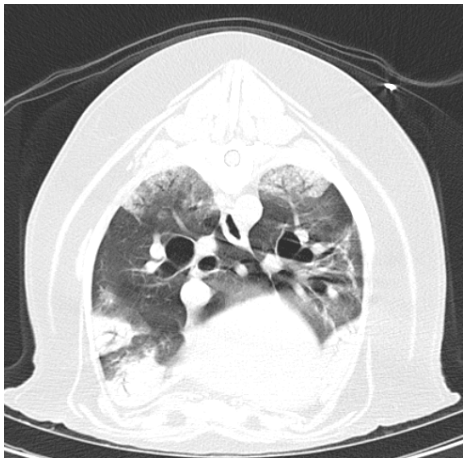

Figure 10.9 - Transverse CT images showing A alveolar pattern and ground glass opacities at the periphery of caudal lung lobes (Lung window)

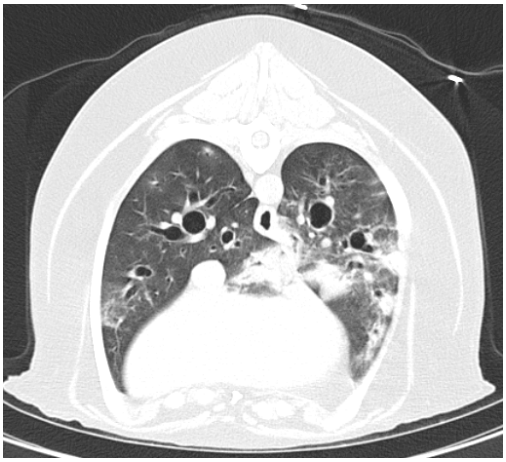

Figure 10.10 - Transverse CT image demonstrating bronchial wall thickening and bronchiectasis (Lung window)

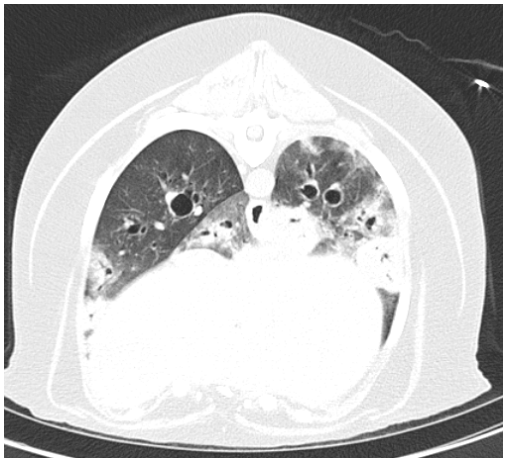

Figure 10.11 - Transverse CT image showing alveolar pattern within the caudal lung lobes (Lung window)

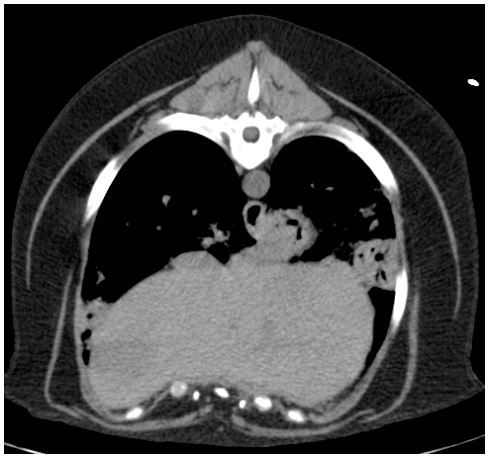

Figure 10.12 - Transverse CT image demonstrating nodular alveolar pattern within the caudal lung lobe (Soft tissue window)

Case 11. Gallbladder Rupture secondary to Biliary Mucocoele

Signalment and History

A 4-year-old neutered male Border Terrier presented with lethargy, and investigations at the time included abdominal ultrasonography, which showed a gallbladder mucocoele. The dog was administrated a course of antibiotics. By the start of the following week it had improved clinically and was back to normal. However, a repeat abdominal scan suggested a progression of the mucocoele, and a blood sample showed a significant elevation in ALT and particularly in ALKP. The dog was referred to the Small Animal Hospital, University of Glasgow, for management of suspected obstruction. The dog was fed on a sensitivity diet.

Clinical Signs

On presentation the dog was bright, alert and in good clinical health. Physical examination was unremarkable.

Ultrasound Examination

1. **Equipment** - See Appendix 1
2. **Restraint** - The dog was sedated and put in dorsal recumbency for the abdominal ultrasound scan.

Abdominal Ultrasonographic Report

The gallbladder was enlarged, filled by immobile hyperechoic material giving a stellate pattern surrounded by immobile hypoechoic material, consistent with biliary mucocoele (Fig.11.1). A thickening of the gallbladder wall associated with the hypoechoic peripheral rim was noted. A large markedly heterogeneous well-circumscribed cavitary mass (approximately 63 x 25 x 25 mm) adjacent to the gallbladder and the ventral aspect of the pylorus, in the area of the quadrate hepatic lobe, was visible associated with a marked hyperechogenicity of the surrounding fat (Figs.11.2 to 11.4). The gastric wall adjacent to the mass and the reactive fat was mildly thickened, without loss of layering. These features were consistent with a haematoma, abscess, hepatic necrosis, or neoplastic process most likely of hepatic origin (e.g. haemangiosarcoma, hepatocellular carcinoma, cystic adenoma or adenocarcinoma). Taking into account the close proximity of the mass and the gallbladder, the gallbladder wall and contents, and the history, a leakage of the mucocoele with perforation of the biliary tract was also considered. An anechoic nodule was present in the hyperechoic reactive fat, consistent

with a reactive or infiltrated lymph node, fat necrosis, small abscess, metastatic process or piece of mucocoele. The splenic parenchyma was mildly mottled consistent with a reactive splenitis, congestion, extramedullary haematopoiesis or lymphoid hyperplasia, although a neoplastic infiltration could not be completely excluded. The rest of the abdomen was unremarkable.

Diagnosis

Large well-defined heterogeneous and cavitary mass in the area of the quadrate hepatic lobe, adjacent to the gallbladder, associated with marked surrounding steatitis, and focal reactive gastritis.

Further Investigations

Haematology showed a mild lymphopenia.

Biochemistry showed slightly low urea (2mmol/L) and albumin (28g/L), elevated cholesterol (7.95mmol/L) and triglycerides (0.74mmol/L), increased ALT (244U/L) and AST (47U/L) and a further large increase in ALKP (6796U/L) and GGT (72U/L). These results were consistent with progressive biliary obstruction and hepatopathy.

Outcome

The dog underwent exploratory surgery with a view to cholecystectomy and liver lobectomy if the lesion identified was within the quadrate lobe. At surgery, there was debris from the biliary mucocoele scattered throughout the abdomen, with patches of chronic low-grade inflammation in the cranial abdomen. The gallbladder was massively distended and solid on palpation, typical of biliary mucocoele. The gallbladder had previously ruptured shedding mucocoele contents into the abdomen, then walled-off with fibrous tissue and adhesions to stomach and liver. This lesion was resected and a cholecystectomy and duodenotomy were performed to confirm patency of the remainder of the biliary tree between liver and duodenum.

The dog recovered well after surgery and was discharged 2 days later. However, 10 days later, it was re-examined, being quieter than normal, inappetant, with abdomen distension. A repeat ultrasonographic examination showed a marked volume of slightly echogenic abdominal effusion (Fig.11.5). The site of gallbladder was difficult to image due to gas and surrounding inflammation. A brownish fluid sample from the abdomen had high bilirubin concentration, indicating bile peritonitis.

The dog underwent a 2nd exploratory surgery. Around 1 litre of bile stained fluid was removed. A leaking bile duct was identified distal to the cholecystectomy site, which

may have resulted from weakening of the bile duct wall as a result of inflammation from the previous biliary pathology. The hole was closed with mattress suture and no further bile leakage was seen. The abdomen was lavage and an abdominal drain was placed before closure. No bacteria were isolated on culture from the abdominal fluid. The dog recovered well from the second surgery and was discharged 5 days later.

A follow up examination was performed 2 weeks after. The dog was doing well, the wound had healed well and skin staples were removed.

Histopathological diagnosis of the mucocoele-like lesion was consistent with a haematoma associated with chronic inflammation, fibrotic changes and maturing granular tissue.

Discussion

Gallbladder mucocoeles are characterized histologically by hyperplasia of mucus-secreting glands within the gallbladder mucosa and abnormal intraluminal accumulation of mucus and inspissated bile. Although the exact pathogenesis of the disease is unknown, gallbladder mucocoeles may result from dysfunction of these mucus-secreting cells, which undergo cystic hyperplasia. Cysts and individual glands become dilated by mucus with a similar histologic appearance to that within the gallbladder lumen. The inciting cause of mucus hypersecretion is probably multifactorial. Factors that promote biliary stasis, such as decreased gallbladder motility, or increased concentration of bile salts within the gallbladder lumen due to increased water absorption across the gallbladder mucosa could cause formation of gallbladder mucocoele. Nutritional factors may also play a role and the fact that it appears to be more prevalent in certain medium-sized breeds, particularly Cocker Spaniels[1,2], may suggest a genetic factor.[1] Inspissated bile and mucus often extend through the biliary tree causing various degrees of extrahepatic biliary obstruction and marked gallbladder distension. Gallbladder rupture secondary to distension and wall necrosis is reported in 43 to 47% of dogs with biliary mucocoele.[1,2,3]

Clinical signs of dogs with gallbladder mucocoele are nonspecific, including most commonly vomiting, anorexia and lethargy, as well as polyuria-polydipsia, diarrhoea or abdominal distension.[1,2,4] However this condition can occasionally be an incidental finding.[1] Physical examination findings may include signs of abdominal pain, icterus, fever, tachypnea and tachycardia.[1,2,4] Most often, dogs have high serum liver enzyme activities, high serum total bilirubin concentration, leucocytosis and neutrophilia, which are particularly high in case of biliary rupture.[1,2]

Abdominal ultrasonography is the gold standard imaging modality for diagnosis of gallbladder mucocoele.[1,2,5] Immobile, echogenic bile with a finely striated, stellate or kiwi fruit-like pattern within the lumen of the gallbladder is seen on ultrasound, often associated with distension of the intrahepatic and/or extrahepatic biliary system.[1,5] A surrounding hypoechoic rim, attributed to mucin between the gallbladder wall and the mucocoele with a thickening of the gallbladder wall can also be noted.[2] Ultrasonography is a highly reliable modality for the identification of gallbladder rupture, with reported sensitivity of 85.7% and specificity of 100% in one study of 30 dogs with biliary mucocoele.[1] Loss of gallbladder wall continuity, hyperechoic fat in the cranial portion of the abdomen, echogenic peritoneal fluid in the gallbladder fossa, free abdominal fluid, and striated or stellate echogenic material outside the gallbladder lumen are highly suggestive of biliary rupture.

Surgical treatment (cholecystectomy) is recommended in cases of gallbladder mucocoele. Although dogs without clinical signs and evidence of biliary rupture may undergo surgery on an elective basis, presence of signs of gallbladder rupture is considered a surgical emergency. Gallbladder rupture appears to result from physical distension of the gallbladder secondary to mucocoele formation and biliary obstruction, resultant in ischaemic necrosis of the gallbladder wall. Early surgical intervention may prevent secondary bacterial infection. For the same reason, the use of prophylactic antimicrobials in dogs with suspected ruptured gallbladder is also recommended. In dogs with gallbladder rupture, care should be taken to remove all mucinous bile from the abdominal cavity and to lavage the abdomen thoroughly.

Cholecystectomy for dogs with gallbladder mucocoele is associated with relatively high perioperative mortality rate, most often secondary to septic biliary peritonitis linked to gallbladder rupture and/or postoperatively leakage of bile. However positive bacteriologic cultures of samples from gallbladder wall, luminal contents or abdominal free fluid, is relatively rare (<10%[1,2]) in dogs with gallbladder mucocoele.[1,3] Postoperative biliary leakage is reported in 4.7-8.7% of dogs that undergo extrahepatic biliary surgery. In one study of 23 dogs with biliary mucocoele that underwent cholecystectomy, overall perioperative mortality rate was 21.7%, although mortality rate was not significantly higher for dogs with gallbladder rupture.[1] This result is consistent with another study[2] in which the survival rate for dog with gallbladder mucocoele was 81%. Nevertheless, the prognosis for dogs with gallbladder mucocoele that undergo cholecystectomy and survive the perioperative period is excellent. A complete resolution of clinical signs associated with bilirubin concentration that returns

to reference range is generally observed in these cases. However, high serum activity of liver enzymes may still be present, possibly caused by concurrent hepatocellular diseases that were unrelated to the gallbladder mucocoele or by extension of the pathologic process underlying the development of gallbladder mucocoele into the intrahepatic biliary tree or hepatic parenchyma. For instance hyperadrenocorticism or exogenous corticosteroid administration may account for or contribute to high serum liver enzyme activities.[1,3] Persistent ultrasonographic abnormalities in hepatic echogenicity may also indicate concurrent or persistent hepatic disease.

References

1-Pike FS, Berg J, King NW, Penninck DG, Webster CR. Gallbladder mucocoele in dogs: 30 cases (2000-2002). **J Am Vet Med Assoc** 2004; 224(10): 1615-1622.

2-Crews LJ, Feeney DA, Jessen CR, Rose ND, Matise I. Clinical, ultrasonographic, and laboratory findings associated with gallbladder disease and rupture in dogs: 45 cases (1997-2007). **J Am Vet Med Assoc** 2009; 234(3): 359-366.

3-Mesich MLL, Mayhew PD, Paek M, Holt DE, Brown DC. Gall bladder mucocoeles and their association with endocrinopathies in dogs: a retrospective case-control study. **J Small Anim Pract** 2009; 50(12): 630–635

4-Mehler SJ, Mayhew PD, Drobatz KJ, Holt DE. Variables associated with outcome in dogs undergoing extrahepatic biliary surgery: 60 cases (1988-2002). **Vet Surg** 2004; 33(6): 644-649.

5-Besso JG, Wrigley RH, Gliatto JM, Webster CR. Ultrasonographic appearance and clinical findings in 14 dogs with gallbladder mucocoele. **Vet Radiol Ultrasound** 2000; 41(3): 261-271.

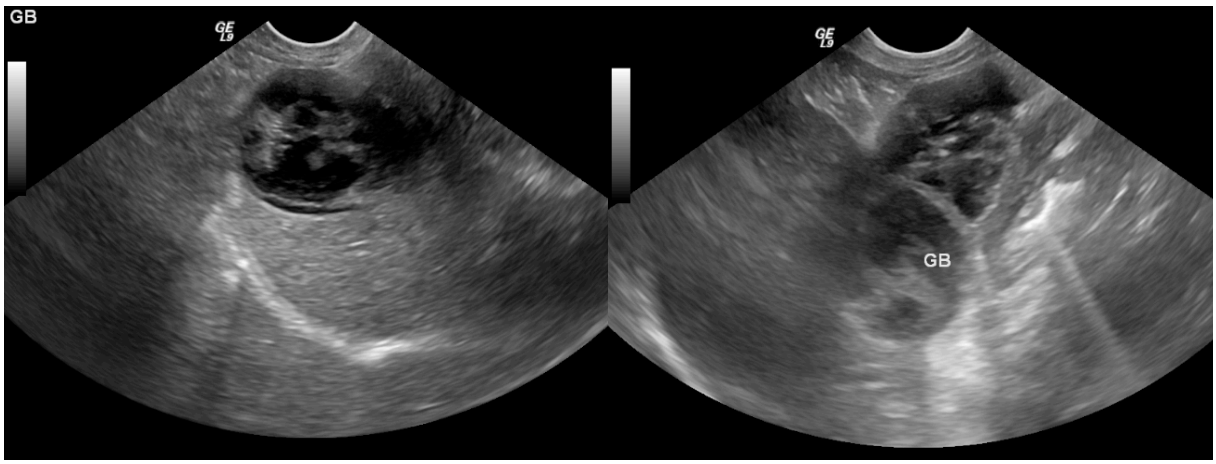

Figure 11.1 - Ultrasound image demonstrating biliary mucocoele

Figure 11.2 - Ultrasound image of the irregular heterogeneous mass adjacent to the gallbladder

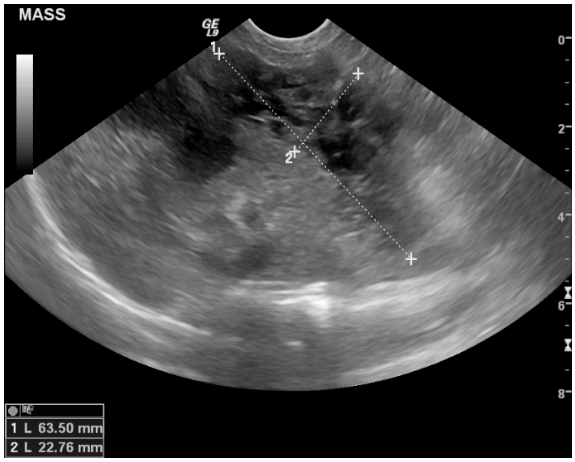

Figure 11.3 - Ultrasound image of the irregular heterogeneous mass adjacent to the gallbladder

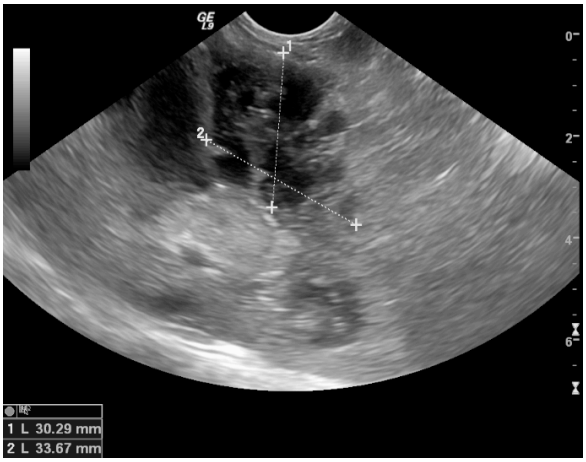

Figure 11.4 - Ultrasound image of the irregular heterogeneous mass adjacent to gallbladder

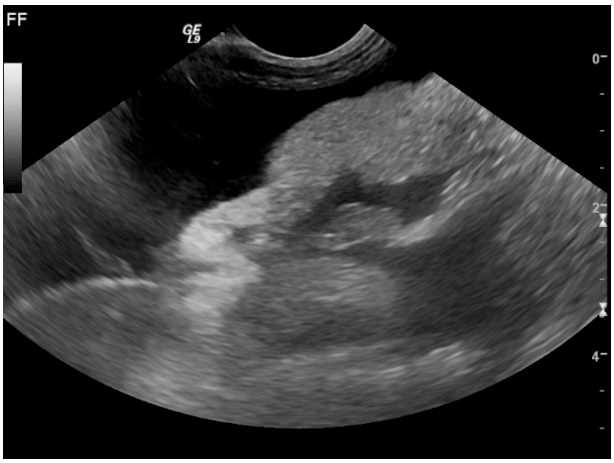

Figure 11.5 - Ultrasound image demonstrating the marked amount of abdominal free fluid (Post-operative)

Case 12. Bronchial Carcinoma

Signalment and History

A 12-year-old male neutered indoor Oriental Shorthair cat was presented with weight loss. The owners had initially ascribed this to increased exercise due to the presence of 3 new kittens chasing him. No change in behaviour was noticed. The cat was still eating well, being fed separately from the other 3 cats. *Ad libitum* water was shared between the 4 cats. The animal had a history of asthma but it was not really considered an issue. He had had a short course of steroids, and since was generally breathing faster. Thyroid levels had been tested twice and were within normal limits.

Clinical Signs

a) Dry cough when being examined
b) Low body condition

Radiographic Examination

1. **Equipment** - See Appendix 1
2. **Restraint** - The cat was sedated. Positioning was achieved using wedges of dressing material and rope ties.

Area	View	kV	mAs	Grid
Thorax	Right Lateral (Fig.12.1)	47	3.2	O
	Dorso-ventral (Fig.12.2)	47	3.2	O
Abdomen	Right Lateral (Fig.12.3)	48	2.5	O
	Ventro-dorsal (Fig.12.4)	48	2.5	O

Radiographic Appraisal

The thoracic inlet is missing on the dorso-ventral view of the thorax (Fig.12.2) and the cranial abdomen is missing on both abdominal radiographs (Figs.12.3 and 12.4). Otherwise all the radiographs are well positioned. The images are well processed. Primary markers are present on all but the right lateral view of the abdomen on which a secondary R marker has been added. Radiographic settings have been added on all views. The radiographs are of diagnostic quality.

Radiological Report

A diffuse severe broncho-interstitial and peri-bronchial pattern is visible, moderately more marked in the ventral lung field and the accessory lung lobe on the lateral thoracic view (Fig.12.1). On the dorso-ventral view, an area of alveolar pattern is noticed in the region of the accessory, right caudal and right middle lung lobes. A moderate shift to

the right of the cardiac silhouette with an effacement of its contours is noted on the dorso-ventral view, suggesting collapse of the accessory lung lobe. Otherwise the size of the cardiac silhouette is within normal limits on the lateral view. The pulmonary vessels cannot be clearly assessed due to the overlying alveolar pattern. An increased opacity is noticed at the level of the tracheal bifurcation, and slightly dorsally. This feature may be due to a superimposition of the pulmonary pattern, although the presence of a moderate tracheo-bronchial lymphadenopathy is suspected.

Very mild new bone production is visible at the ventral aspect of C7 and T1 consistent with mild spondylosis. Mild degenerative changes are visible at the sterno-chondro-costal junctions, most likely related to age.

Moderate gas distension of the stomach is noticed, most likely related to air swallowing. The colon is mildly distended at the inlet of the pelvis by a moderate amount of faecal material, which does not appear to be very dry. However, the diameter of the colon remains within normal limits.

Differential Diagnosis

Diffuse severe broncho-interstitial and peri-bronchial pattern associated with suspected collapse of the accessory lung lobe consistent with a marked chronic bronchopneumopathy (e.g. allergic (feline asthma), infectious, parasitic) with or without fibrotic changes, or a neoplastic infiltration (e.g. broncho-alveolar carcinoma, adenocarcinoma, lymphoma), less likely non-cardiogenic oedema or haemorrhage. Alveolar pattern seen in the accessory lung lobe associated with a shift of the cardiac silhouette is consistent with atelectasis due to a prolonged decubitus, although could be due to primary pulmonary disease, as described previously.

Advanced Imaging – Thoracic Computed Tomography

A thoracic CT (Figs.12.5 to 12.10) was performed to further assess the pulmonary changes. A severe diffuse broncho-interstitial pattern, more marked ventrally and on the left side is visible, associated with diffusely moderately enlarged bronchi at the periphery of the lung field, consistent with bronchiectasis. The right caudal lung lobe appears to be less affected than the others. The thickening of bronchial walls varies from mild to very marked, with a more severe area in the dorsal part of the left caudal lung lobe (Fig.12.8). The accessory and right middle lung lobes appear to be consolidated, with air bronchograms, and moderately decreased in size, causing a mild right shift of the cardiac silhouette (Figs.12.5 and 12.6). A few small areas of mineralization are evident in the soft tissue window (Fig.12.7). The bronchi are clearly

visible along their entire length within these lung lobes, and their distal aspects are markedly enlarged, consistent with a severe bronchiectasis (Figs.12.5 and 12.6). A soft tissue attenuating mass-like lesion (approximately 10mm in diameter) is present at the base of the right cranial lung lobe, ventrally to the bifurcation of the right cranial and middle main bronchi (Fig.12.9). At the periphery of the dorsal aspect of the very caudal left lung lobe, there is a moderate amount of broad based soft tissue attenuating material, fairly smoothly delineated, consistent with a pleural thickening or sub-pleural mass (Fig.12.10). Similar, much smaller smooth broad-based nodular lesions are seen at the periphery of the ventral and lateral aspects of the right cranial lung lobe. At the cranial aspect of the left cranial lung lobe, there are some small soft tissue attenuating, rounded fairly well delineated lesions. In the left caudal lung lobe, there is an area associated with a small rounded soft tissue attenuating mass-like lesion just adjacent to the distal aspect of the main left caudal bronchus.

These features are most likely consistent with a diffuse neoplastic infiltration (e.g. broncho-alveolar carcinoma, lymphoma, adenocarcinoma), although a very marked chronic bronchopneumopathy (e.g. asthma regarding the history) associated with fibrotic changes and/or secondary infectious process cannot be excluded. Infectious (e.g. mycobacteria, other bacterial) or parasitic processes (e.g. *Aelurostrongylus abstrusus*, fungal less likely) are considered less likely.

A moderate splenomegaly is noted associated with undulated margins, most likely consistent with congestion linked to anaesthesia, extramedullary haematopoiesis, reactive splenitis, although a neoplastic infiltration cannot be excluded. Mild thoracic spondylosis is visible. The transverse colon is moderately distended with gas and faecal material. These findings are not demonstrated in figures presented.

Further Investigations

Abdominal ultrasonography was performed to ruled out any other condition and potential metastatic spread. The colon was moderately distended by faecal content, especially the descending colon. The stomach was moderately distended with gas, without any obvious obstruction, most likely consistent with gas swallowing. The size of both kidneys was at the lower normal limit (approximately 3.3cm bilaterally). A thickening and marked hyperechogenicity of both cortices associated with a decreased cortico-medullary definition and a slight hypoechoic peripheral rim was noted, most likely consistent with a chronic nephropathy. A hypoechogenicity, mild heterogeneity and moderate thickening of the pancreatic parenchyma were noted associated with an

irregularity of the margins, consistent with age related changes or chronic inflammatory changes. No hyperechogenicity of the surrounding fat was visible and the size of the pancreatic duct was within normal limits. A mild amount of sludge was visible in the gallbladder as well as within the pancreatico-duodenal papilla, without signs of obstruction. The spleen was markedly enlarged associated with a mildly mottled parenchyma, consistent most likely with congestion, possibly linked to sedation, extramedullary haematopoiesis or reactive splenitis.

Haematology revealed a mild poorly regenerative anaemia. Microscopic slide agglutination was mildly positive.

Biochemistry revealed hyperglobulinaemia and hypoalbuminaemia. The fPLI was elevated at 5.1µmol/l (reference range 0.1–3.5µmol/l) consistent with pancreatitis.

Urinalysis revealed hypersthenuria and was otherwise unremarkable.

The feline virus panel (FIV, FeLV, FCoV) was unremarkable.

A bronchoscopy was performed and severe inflammation of the main bronchi was detected with presence of muco-purulent material. A broncho-alveolar lavage was performed and cytology revealed degenerate neutrophils, extracellular cocci, mucus and red cells. Several groups of epithelial cells with criteria of malignancy were detected, consistent with a high suspicion of bronchial carcinoma. A sparse mixed bacterial culture was recovered but nothing of any significance.

Outcome

The cat improved with prednisolone and doxycycline therapy. However, it was presented a few days later with seizure, and regarding the poor prognosis and limited treatment options available, a decision to euthanasia was made.

Discussion

Feline primary lung tumours are rare, with a reported incidence of less than 0.4%, accounting for only 1 to 2% of all feline tumors.[1,2] Different histologic types of primary lung tumour have been described in cats and dogs, such as adenocarcinomas, with broncho-alveolar carcinomas being a subtype of well-defined adenocarcinomas, squamous cell carcinomas, anaplastic cell carcinomas, sarcomas or benign tumours. Adenocarcinomas are the most common histological type of lung tumour in all domestic animals. Squamous cell carcinoma and anaplastic cell carcinoma occur much less frequently, and benign tumours or sarcomas are extremely rare.[1,2,3]

Affected cats are generally old, with reported mean ages between 11 to 13 years.[1,2,3] No breed predisposition has been reported. Clinically, respiratory signs are evident in more

than 50% of the cases, such as tachypnea, dyspnoea and/or coughing, with a mean of 1 to 2 months of duration. Non-specific clinical signs, such as inappetance, weight loss and lethargy, are also common, encountered in 50% of the cases. Other clinical signs may include lameness and neurological signs, attributable to musculo-skeletal metastases or pulmonary hypertrophic osteopathy, and vomiting, regurgitation or gagging, which may be secondary to local invasion of the tumor.[1,2,3,4,5] On physical examination increased pulmonary sounds, wheezes, crackles, dull lung sounds, and increased upper airway sounds may be found. Cardiac arrhythmias might also be encountered secondary to cardiac metastasis.[2,4] Breed, age, sex, weight, clinical signs, duration of clinical signs, and radiographic findings are not associated with histologic type or morphology of primary lung tumours.[5,6]

Despite the lack of specificity, thoracic radiographs are the most effective screening tool for the assessment of pulmonary conditions in dogs and cats. A wide range of different patterns has been described in cases of primary pulmonary neoplasia in cats. The most common radiographic patterns seen are focal patterns (45[3] to 67%[5]), being either most commonly solitary soft tissue masses, generally well circumscribed with or without cavitation, or more ill-defined multiple masses. Localised patterns (20%)[1] such as lobar consolidation or segmental alveolar consolidation, or diffuse patterns (24%)[1], which are generally mixed broncho-interstitial to alveolar, have also been described and were the most common finding in contrast to focal patterns in one study[3]. More than one radiographic pattern is commonly encountered and caudal lung lobes are more frequently affected than cranial lung lobes.[1,5] In rare cases a normal radiographic pattern might be seen.[1] Although no obvious correlation between tumour type and radiographic appearance has been found[1,3,5,6], tendencies have been described in one review of 41 primary lung tumours in cats[1]. Adenocarcinomas tend to occur as a well-circumscribed and usually cavitated mass, as localized (lobar) alveolar pulmonary infiltrates, which may be calcified, or as multiple, poorly circumscribed masses. Bronchiolo-alveolar carcinomas are more pleomorphic, located in the middle to peripheral portion of affected lobes and evidence of bronchial involvement (e.g. broncho-interstitial pattern, peribronchial cuffing, or bronchiectasis) is generally seen, associated with a primary pattern (e.g. focal or multifocal masses, diffuse patterns).[1,2] Radiographic patterns associated with squamous cell carcinomas in the cat are extremely variable and do not occur in the hilar region as described in man and dogs, but more in the middle and peripheral portions of affected lobes.[1]

Extra-pulmonary metastases are reported in 71%[1] to 80%[5] of the cats with primary lung tumour on which general autopsies are performed. Regional lymph nodes are reported to be the most common sites of metastasis for primary pulmonary neoplasia, following by pleural metastasis. Skeletal muscles, myocardium, pericardium, axial or appendicular skeleton and abdominal organs, such as kidney, spleen or adrenals, are other reported sites for metastasis.[1,2,3] Common radiographic findings include evidence of pleural involvement, such as effusion or thickening, in nearly 50% of the cases[1,2], especially in broncho-alveolar carcinoma, and may indicate pleural metastasis. Thoracocentesis may be necessary to allow radiographic pulmonary detail to be assessed accurately, however malignant cells are not commonly found on pleural effusion cytology and no correlation between the presence or type of fluid and the histological type of tumour has been found.[3] Radiographic evidence of regional lymph node enlargement (e.g. mediastinal and/or tracheobronchial lymph nodes) may also be found in about one third of the cases, more commonly associated with adenocarcinomas.[1] Radiographic diagnosis of pleural metastasis has been reported with a sensitivity of 71% and a specificity of 69% for an overall accuracy of 70%, in one study[1], whereas radiographic diagnosis of lymph node involvement has a sensitivity of 50%, specificity 79%, and accuracy of 62% in the same study[1]. Cardiomegaly associated with pericardial effusion, cardiac and pericardial metastasis has also been described. In those cases differentiation from congestive heart failure associated with pleural effusion and pulmonary oedema may be difficult.[2] Partial oesophageal obstruction due to local invasion of primary lung tumour, highlighted by barium swallow, has also been described.[3] Skeletal abnormalities may be visible in case of bony metastasis or hypertrophic pulmonary osteopathy. Pneumothorax, pneumomediastinum, and subcutaneous emphysema have also been described.[3]

Even if radiology remains the most effective method to screen patients for pulmonary neoplasia, broad differential diagnoses result due lack of specificity. Differential diagnoses for solitary or multiple pulmonary masses include granulomas (e.g. eosinophilic pulmonary granulomatosis, parasitic pneumonia, infectious process), abscesses, haematomas, pneumonia, infarcts, cysts, bulla and primary or secondary neoplastic process.[1,2,4] Disseminated pulmonary patterns may be associated with pneumonia, haemorrhage, oedema, granulomas, feline asthma, fibrosis, and primary or secondary neoplasia.[1,4,7,8] In one study[4] comparing dyspnoeic cats with diffuse pulmonary primary conditions, no statistical difference was found between the inflammatory (including viral, bacterial, inflammatory, parasitic pneumonia and feline asthma) and neoplastic groups, with regard to age, body weight, clinical signs, duration

of clinical signs, physical examination findings, thoracic radiographic findings, duration of hospitalization, treatment, and outcome. Cats with bacterial or viral pulmonary disease had a significantly shorter duration of illness than all other cats (including inflammatory and neoplastic group). However, neoplasia could not be distinguished from inflammatory disease with certainty based on plain radiographs. The most likely radiographic diagnosis was accurate in only 6 out of 15 cases, 3 in each group (inflammatory vs. neoplasia).[4] Because of the suppression of the superimposition of the thoracic structures, CT improves the assessment of lung lobes involvement and extent of lesions, the different types of pattern, the visualisation of pulmonary metastasis and lymph node enlargement, that may help to better distinguish different pulmonary conditions.

However further tests (bronchoscopy, percutaneous biopsy, ultrasound guided fine needle aspiration or biopsy, thoracocentesis, lobectomy) are required to confirm the diagnosis. The limitations of tracheal wash and broncho-alveolar lavage cytology in cats have been reported to be in part affected by the nature and location of the disease, as well as by sample collection and processing techniques. Poor correlation between broncho-alveolar cytology and histology has been previously documented in feline patients. In dogs, broncho-alveolar lavage cytopathology yielded a definitive diagnosis in only 25% of cases in one report. The positive bacterial cultures in cats on broncho-alveolar lavage are also difficult to interpret, as 44-77% of healthy cats have been shown to have positive tracheobronchial cultures. A positive bacterial culture can be found in both inflammatory and neoplastic processes.[4] Cytology of pleural effusion after thoracocentesis does not appear to give an accurate diagnosis, as neoplastic cells are not commonly seen within. Ultrasound guided pulmonary fine-needle aspiration generally provides an accurate diagnosis in dogs and cats with focal pulmonary disease (84%), disseminated interstitial disease (83%), and mixed pulmonary pathology (77 and 82%).[4] In feline primary pulmonary neoplasia, the cytologic diagnosis is reported to be accurate in 80 and 85.7% of cases when ultrasound-guided aspiration is performed. The incidence of pneumothorax following ultrasound guided fine needle aspiration in dogs and cats has been reported to range from 0 to 31%. From a metadata analysis grouping 125 dogs and cats from 4 retrospective studies, the average occurrence of pneumothorax was 14.4%, haemorrhage 3.2%, and death as a consequence of the procedure 2.4%.[4] Surgical resection may be indicated in cats with a solitary primary lung tumor.[6] The median survival time is reported to be 115 days after surgical resection of primary lung tumour in cats in one study[6], with histological morphology of the primary lung tumour

being significantly association with survival time. Indeed, cats with moderately differentiated tumours had a significantly longer survival time (median of 698 days) than cats with poorly differentiated tumours (median of 75 days). However clinical findings (breed, age, gender, body weight, clinical signs, duration of clinical signs, and radiographic findings) were not significantly associated with survival time after surgery.

References

1-Koblikd P. Radiographic appearance of primary lung tumors in cats – A review of 41 cases. **Vet Radiol Ultrasound** 1986; 27(3): 66-73.

2-Ballegeer EA, Forrest LJ, Stepien RL. Radiographic appearance of bronchoalveolar carcinoma in nine cats. **Vet Radiol Ultrasound** 2002; 43(3): 267-271.

3-Barr F, Gruffydd-Jones TJ, Brown PJ, Gibbs C. Primary lung tumours in the cat. **J Small Anim Pract** 1987; 28(12): 1115-1125.

4-Sauve V, Drobatz KJ, Shokek AB, McKnight AL and King LG. Clinical course, diagnostic findings and necropsy diagnosis in dyspneic cats with primary pulmonary parenchymal disease: 15 cats (1996-2002). **J Vet Emerg Crit Care** 2005; 15(1): 38-47.

5-Hahn KA, McEntee MF. Primary lung tumors in cats: 86 cases (1979-1994). **J Am Vet Med Assoc** 1997; 211(10): 1257-1260.

6-Hahn KA, McEntee MF. Prognosis factors for survival in cats after removal of a primary lung tumor: 21 cases (1979-1994). **Vet Surg** 1998; 27(4): 307-311.

7-Gadbois J, D'Anjou MA, Dunn M, Alexander K, Beauregard G, D'Astous J, De Carufel M, Breton L, Beauchamp G. Radiographic abnormalities in cats with feline bronchial disease and intra- and interobserver variability in radiographic interpretation: 40 cases (1999-2006). **J Am Vet Med Assoc** 2009; 234(3): 367-375

8-Corcoran BM, Foster DJ, Fuentes VL. Feline asthma syndrome: a retrospective study of the clinical presentation in 29 cats. **J Small Anim Pract** 1995; 36(11): 481-488.

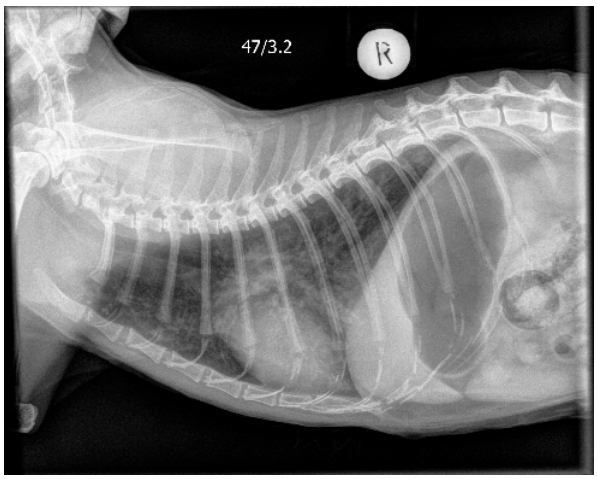

Figure 12.1 - Right lateral thoracic radiograph

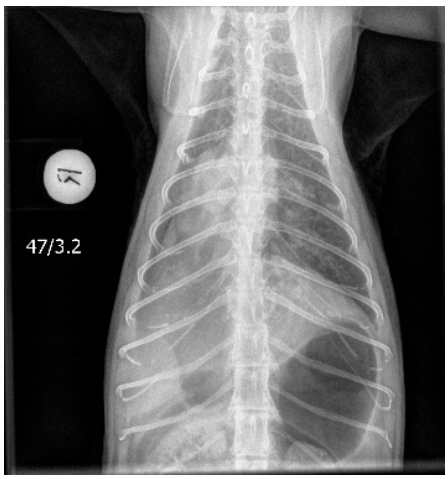

Figure 12.2 - Dorso-ventral thoracic radiograph

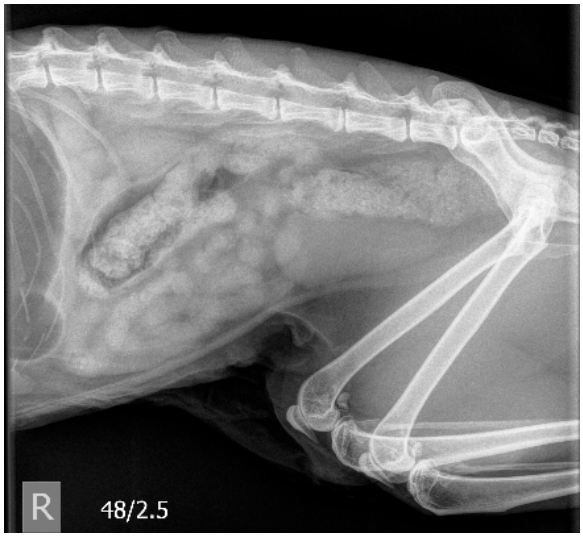

Figure 12.3 - Right lateral view of the caudal abdomen

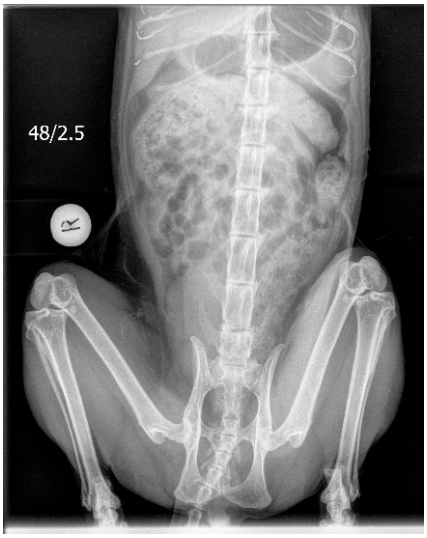

Figure 12.4 - Ventro-lateral view of the abdomen

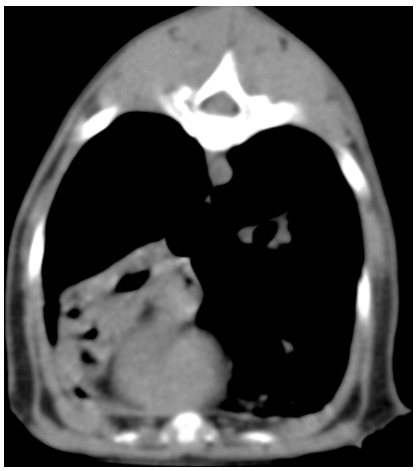

Figure 12.5 - Transverse CT image showing consolidation of the R middle and accessory lung lobes and associated bronchiectasis (Soft tissue window)

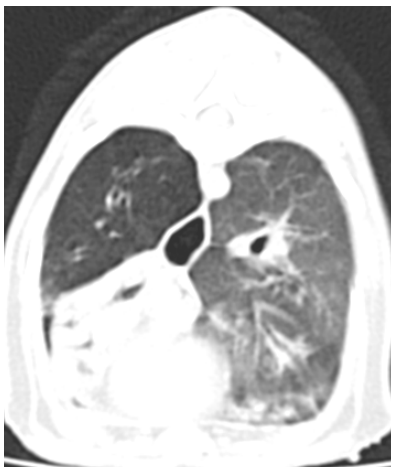

Figure 12.6 - Transverse CT image showing consolidation of the R middle and accessory lung lobes and associated bronchiectasis (Lung window)

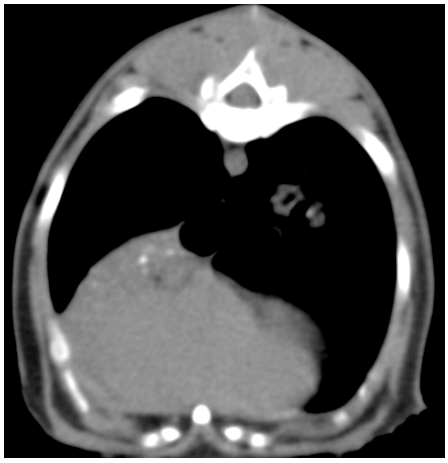

Figure 12.7 - Transverse CT image showing pulmonary consolidation and mineralisations (Soft tissue window)

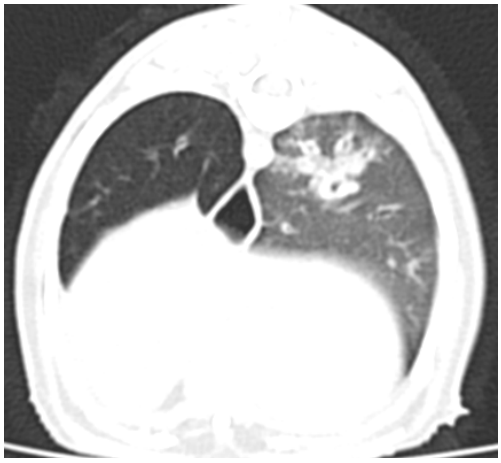

Figure 12.8 - Transverse CT image demonstrating bronchial wall thickening and bronchiectasis (Lung window)

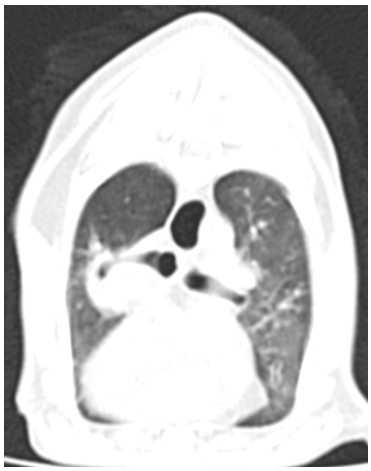

Figure 12.9 - Transverse CT image of the pulmonary nodule ventrally to the bifurcation of the right cranial and middle main bronchi (Lung window)

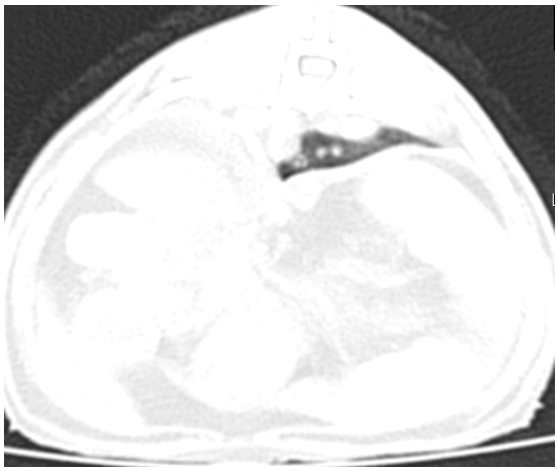

Figure 12.10 - Transverse CT image demonstrating subpleural thickening at the dorsal aspect of the left caudal lung lobe (Lung window)

Case 13. Ependymal Cyst

Signalment and History

A 3-year-old entire male Springer Spaniel exhibited an episode of pelvic limb weakness and abnormal behaviour associated with a reluctance to eat 1 month prior to presentation. This appeared to resolve without any further treatment. Two days before presentation, the dog had an acute onset of weakness and mild ataxia of the pelvic limbs after playing with another dog. He was also circling to the left. The following day, he appeared worse, able to stand but reluctant to move around and very quiet, with decreased appetite. A head tilt to the left was noted. On the day of presentation he was walking around, then suddenly collapsed on his hind limbs. The referring vet noted that the dog was paraparetic, non-ambulatory and appeared painful. He was given a dose of methadone, and referred to the neurology service of the Small Animal Hospital, University of Glasgow. The dog had no travel or ear disease history, and was currently vaccinated and dewormed.

Clinical Signs

a) Increased capillary refill time of 2 seconds.
b) Responsive but very quiet.
c) Tetraparetic, non-ambulatory.
d) Oriented to the left and attempted to circle to the left when supported.
e) Increased patellar reflexes bilaterally.

Regarding the clinical signs, the localization of the lesion was made to the left forebrain. Magnetic resonance imaging (MRI) of the brain was performed.

Magnetic Resonance Imaging Examination

1. **Equipment** - See Appendix 1
2. **Restraint** - The dog was under general anaesthesia and placed on dorsal recumbency.

MRI Report

A large well-defined rounded structure, of approximately 13x14x17mm, is visible at the level of the 4th ventricle, on the midline, slightly more to the left. It is markedly hyperintense on T2-weighted (T2w) images (Figs.13.1, 13.3 and 13.5), hypointense and moderately heterogeneous on T1-weighted (T1w) (Fig.13.7) and FLAIR (Fig.13.6) sequences, without signal void on T2*-weighted images, suggesting it is fluid filled. A

peripheral rim enhancement is visible on post-contrast T1-weighted images (Figs.13.2, 13.4 and 13.8). This cystic lesion wedged between the cerebellum and brainstem, markedly compresses the cerebellum dorsally and moderately the brainstem ventrally at the level of the reticular formation, slightly more on the right side. A moderate to marked ill-defined T2 and FLAIR hyperintense area is visible in the ventral margin of the cerebellar parenchyma and the left dorsal part of the brainstem, most likely consistent with oedema/inflammation. A moderate dilation of the lateral and 3rd ventricles and mesencephalic aqueduct is noted (Fig.13.9), associated with a mild periventricular oedema around the rostral end of the right lateral ventricle, and a loss of the cerebrospinal fluid signal at the periphery of the cortex are noted, consistent with an increased intracranial pressure.

Differential Diagnosis

Large cystic-like mass lesion at the level of the 4th ventricle showing mass effect inducing moderate to marked cerebellar oedema and increased intracranial pressure. Regarding the signal intensities on all sequences, differential diagnosis includes epidermoid, choroid plexus, or ependymal cysts most likely. A dermoid cyst and a subarachnoid cyst are considered less likely due to the lack of hyperintensity on T1-weighted images and the peripheral rim enhancement, respectively. An abscess or a cystic neoplastic process (e.g. meningioma) is less likely.

Further Investigations

Haematology was within normal limits.

Biochemistry showed a moderate increase of the pre-prandial biliary acids (18.9μmol/L; reference range <10μmol/L) and the creatine kinase (578U/L; reference range <150U/L).

Outcome

The overall prognosis for the dog was guarded given the MRI findings. The owners elected for euthanasia given the poor diagnosis and difficult treatment options. A post-mortem examination was performed. An ependymal cyst at the level of the 4th ventricle, with squamous cell metaplasia, severe subacute suppurative ventriculitis, obstructive hydrocephalus and increased intracranial pressure secondary to compression of the cerebellum and medulla oblongata were found on histology.

Discussion

Ependymal cyst, also called glioependymal cyst, is a subcategory of benign, neuroepithelial cysts, which are lined by ciliated epithelial cells resting directly upon brain parenchyma or a layer of astroglia rather than a basement membrane or connective tissue wall.[1,2,3] The exact pathogenesis remains unclear, however it has been suggested that ependymal cysts develop during embryogenesis subsequent to aberrant migration and entrapment of foetal ependymal cells.[1,2,3] They may also arise in any area of brain that has been damaged by haemorrhage, infarction, infection, trauma, or surgery.[1] Ependymal cysts share morphologic and immunohistochemical properties with the normal lining ependymal cells of the ventricular system.[2] Thus they are typically lined by simple flattened, cuboidal to low columnar epithelium, with a high percentage of ciliated epithelial cells. Areas of attenuation with flattened non-ciliated epithelium may also be present. The lumen contains cerebrospinal fluid (CSF)-like fluid mixed with epithelial degenerative and secretory products, however connection with the ventricular system is most commonly not present.[2,3]

In humans ependymal cysts are rare, benign lesions that most commonly occur in the supratentorial brain parenchyma, in the central white matter of the temporo-parietal and frontal lobes, and less frequently within the lateral ventricles or occipital lobes.[1,2,4] They have also been reported in the subarachnoid spaces, brainstem, cerebellum or within the spinal cord.[1,2,3] Progressive enlargement of ependymal cysts is postulated as the reason for development of clinical signs in middle-aged patients, by impingement upon critical neural structures. However the mechanism of enlargement is unclear, as the cysts are generally do not communicate with the ventricles and lack choroid plexus cells.[1,2,3] Some mechanisms by which fluid can accumulate within ependymal cysts include transcellular transport, active secretion, and passive transport.[4] These lesions may also be incidental findings detected by autopsy or during imaging procedures.[2] Two cases of intraparenchymal ependymal cysts have also been reported in adult monkeys[2,3] as incidental finding, whereas one case of cerebellar ependymal cyst has been described in a young dog, presenting with neurological signs from birth[1].

The magnetic resonance imaging (MRI) characteristics of ependymal cysts are of CSF-like fluid filled cystic lesions within the brain parenchyma, most often within the white matter, close to the ventricular system but without obvious communication, hypointense on T1-weighted images, hyperintense on T2-weighted images, which suppress on fluid-attenuation-inversion-recovery (FLAIR) sequences. No contrast enhancement or a peripheral rim enhancement may be visible. The cyst might be found within the

ventricular system or the subarachnoid space as described above. Depending on the cyst size, the amount of adjacent structures compression and the growing rate, perilesional oedema may be visible on T2-weighted and FLAIR sequences as hyperintense area within surrounding parenchyma, however it is generally a slow growing lesion. The MRI findings are not pathognomonic and definitive diagnosis is made by histopathology and immunohistochemistry.

Other intra-cranial cysts of central nervous system (CNS) origin (i.e. choroid plexus cysts, arachnoid cysts) or non-CNS origin (i.e. colloidal, epidermoid, dermoid, and Rathke's cleft cysts) may be encountered and differentiated from ependymal cysts, the most common intracranial cysts being choroid plexus and arachnoid cysts.[2,3]

Choroid plexus cysts occur from in-folding of the epithelial lining of the choroid plexus in early development, creating a fluid filled cavity.[5] They are non-ciliated neuroepithelial-derived lesions, containing choroid plexus cells, surrounding by adjacent connective tissue.[2,3,5] They are generally located within the ventricular system, however the neck of this cyst may occasionally be pinched off, separating it from the rest of the ventricular system. Choroid plexus cysts are predominantly incidental findings in people, in contrast to dog. These cysts have also been reported in adults following head trauma or intraventricular shunting.[5] Choroid plexus cysts are generally hyperintense to normal grey matter on T2-weighted images and hypointense on pre-contrast T1-weighted images. However, they appear hyperintense on FLAIR and diffusion weighted imaging (DWI) sequences, likely due to the high protein and at times gelatinous characteristics of the content, relative to normal CSF. Rim contrast enhancement is frequently seen on T1-weighted post-contrast images due to the presence of blood vessels within the cyst wall, however uniform contrast enhancement has been described in one dog with a choroid plexus cyst within the 4th ventricle.[5]

Arachnoid cysts derive from a splitting of the arachnoid membrane and are demarcated by fibrous connective tissue lined by meningothelial cells.[1,2,3,6] Intracranial arachnoid cysts are usually considered a primary malformation although they may develop secondary to meningoencephalitis, trauma, or subarachnoid haemorrhage. The most common intracranial arachnoid cysts encountered in dogs and cats are quadrigeminal cyst. On MRI, signal characteristics of fluid within an arachnoid cyst is identical to CSF on all sequences unless there has been haemorrhage within the cyst. Post-contrast enhancement of the wall is not expected unless concurrent meningoencephalitis.[6]

Epidermoid and dermoid cysts are rare benign lesions derived from aberrant migration of non-neuronal ectoderm during the neural tube closure.[2,6,7] They are lined by

squamous epithelium with varying amounts of intra-luminal keratin and gradually enlarge as desquamated keratinocytes, keratinaceous debris, and cholesterol accumulate in the lumen.[6,7,8] Dermoid cysts also contain epidermal adnexal structures such as hair follicles, sebaceous and apocrine glands, and fat.[6,7] They are mostly found within the cerebellopontine angle or the fourth ventricle, however clinical signs may not manifest until late in life, secondary to the slow lesion expansion, and epidermoid cysts are occasionally an incidental finding at necropsy. Because of their location, secondary obstructive hydrocephalus may be encountered.[6,7,8] Epidermoid cysts are usually iso- to hypointense in T1-weighted images and hyperintense in T2-weighted images, but remain iso- to hyperintense in FLAIR sequences and may be heterogeneous. They can have unusual signal intensity depending on the content and be hyperintense in T1-weighted images where there is high lipid content due to cholesterol deposition.[8] Dermoid cysts tend to be heterogeneous and predominantly hyperintense on both T1- and T2-weighted images and may have a low signal on fat suppression sequences, due to their fat content. Regions of low signal may reflect hair or calcification within the cyst. A peripheral rim enhancement on T1-weighted post-contrast images may be observed in both epidermoid and dermoid cysts.[6,8]

Rathke's cleft cysts, also called adenohypophyseal cysts, arise from the normal cleft between the neuro- and adenohypophysis, occupying the pituitary fossa.[2,6] They have ciliated and/or squamous epithelium[2] and appear as thin-walled cavitary lesions containing fluid that is hypointense in T1-weighted images and hyperintense in T2-weighted images. The central portion of a Rathke's cleft cyst may not null on FLAIR images because of its mucinous content. A peripheral rim enhancement may or not be present. Clinical signs are secondary to compression of adjacent structure, however endocrine disorders may also be present, such as dwarfism.[6]

Brain abscesses and cystic or necrotic neoplastic or infectious processes (e.g. cystic meningioma, choroid plexus tumour, gliomas, toxoplasmosis, cysticercosis, or aberrant nematode parasite migration) are other differential diagnosis, however adjacent tissue reaction consisting of inflammation, oedema and/or necrosis is usually seen in such lesions, in contrary to slow-growing intracranial cyst. The main differential diagnoses for the ependymal cyst are choroid plexus, arachnoid and epidermoid cysts.[2,6]

Immunohistochemistry is generally used to differentiate between types of benign intra-cranial cysts. The cyst-lining epithelial cells of ependymal cyst often express S100 protein, which indicates neuroectodermal origin, GFAP (Glial Fibrillary Acidic Protein), a marker for neural cells, and cytokeratin, which indicate the epithelium origin.

GFAP is expressed normally in foetal but not adult ependymal cells so the degree of expression may depend on the differentiation state of the cyst lining. In contrast, choroid plexus cysts express pancytokeratin but are negative for S-100 and GFAP and arachnoid cysts are negative for S-100 and GFAP but positive for epithelial membrane antigen.[2,3]

Several surgical methods for treatment have been described in human, including open craniotomy with total excision, shunting, fenestration of the cyst into the subarachnoid space, and stereotactic aspiration. In the case of haemorrhagic cysts with mass effect, surgical resection might be the most effective strategy. The clinical course and outcome are usually benign and favourable, respectively.[4]

References

1-Wyss-Fluehmann G, Konar M, Jaggy A, Vandevelde M, Oevermann A. Cerebellar ependymal cyst in a dog. **Vet Pathol** 2008; 45(6): 910-913.

2-Bergin IL, Campbell B, Agnew DW. Ependymal cyst in a cynomolgus macaque (*Macaca fascicularis*). **J Med Primatol** 2008; 37(5): 239-244.

3-Chang KS, Lee SR, Kim SW, Cho ZH, Son HY, Kim D, Chang KT. Ependymal cyst in the cerebrum of an African green monkey (*Chlorocebus aethiops*). **J Comp Pathol** 2011; 145(2-3): 235-239.

4-Ho NC, Wu HY. Ependymal cyst with hemorrhage in the cerebellopontine angle. **J Clin Neurosci** 2009; 16(1): 127-129.

5-Bewer DM, Cerda-Gonzalez S, Dewey CW, Coates JR. Diagnosis and surgical resection of a choroid plexus cyst in a dog. **J Small Anim Pract** 2010; 51(3): 169-172.

6-MacKillop E. Magnetic resonance imaging of intracranial malformations in dogs and cats. **Vet Radiol Ultrasound** 2011; 52(S): 42-51.

7-De Decker S, Davies E, Benigni L, Wilson H, Pelligand L, Rayner EL, Shihab N, Volk HA. Surgical treatment of an intracranial epidermoid cyst in a dog. **Vet Surg** 2012; 41(6): 766-771.

8-Steinberg T, Matiasek K, Brühschwein A, Fischer A. Imaging diagnosis – Intracranial epidermoid cyst in a Doberman Pinscher. **Vet Radiol Ultrasound** 2007; 48(3): 250-253.

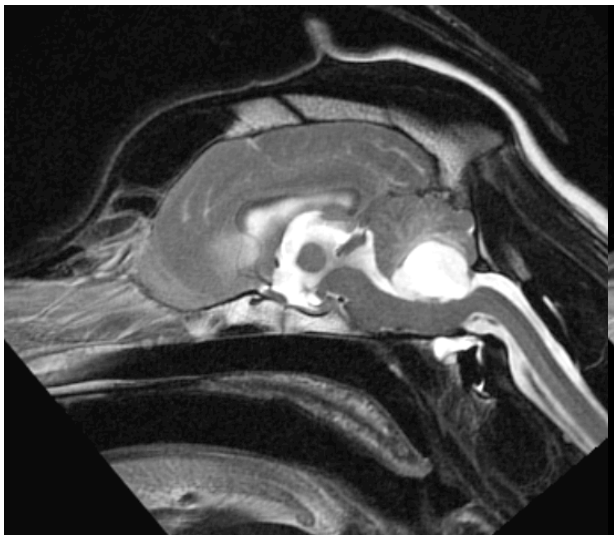

Figure 13.1 - T2w sagittal image of the cyst-like lesion at the level of the 4th ventricle (Mid brain)

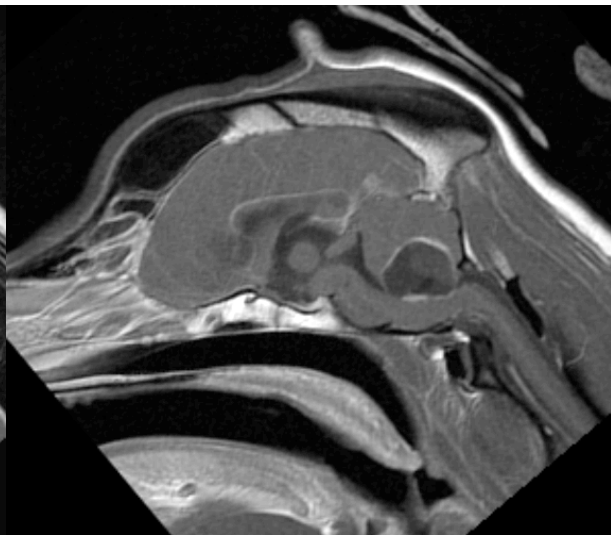

Figure 13.2 - T1w sagittal post-contrast image of the cyst-like lesion at the level of the 4th ventricle showing peripheral rim enhancement (Mid brain)

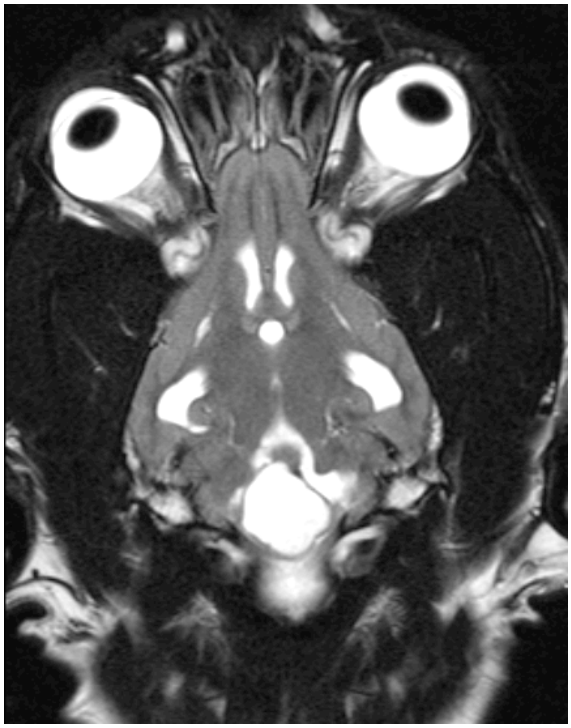

Figure 13.3 - T2w dorsal image of the cyst-like lesion at the level of the 4th ventricle

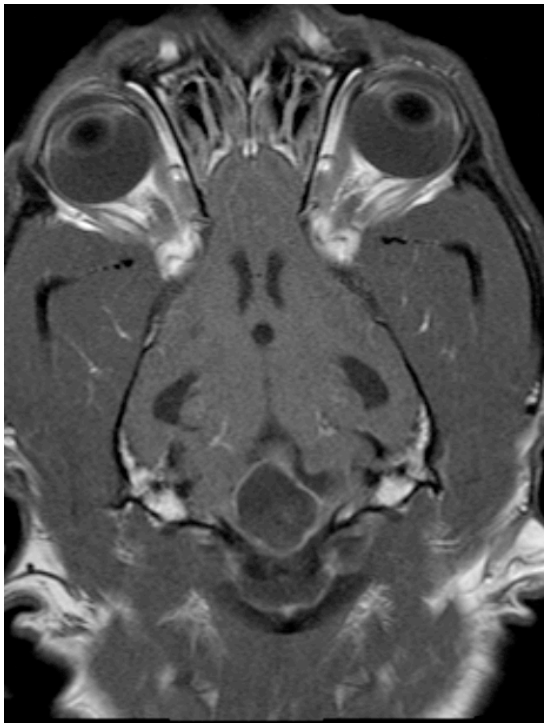

Figure 13.4 - T1w dorsal post-contrast image of the cyst-like lesion at the level of the 4th ventricle showing peripheral rim enhancement

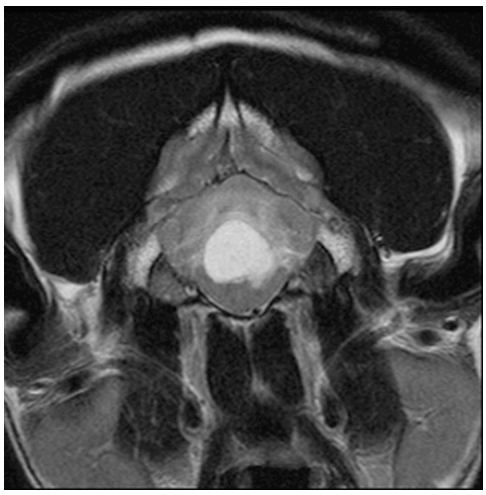

Figure 13.5 - T2w transverse image of the cyst-like lesion at the level of the 4th ventricle

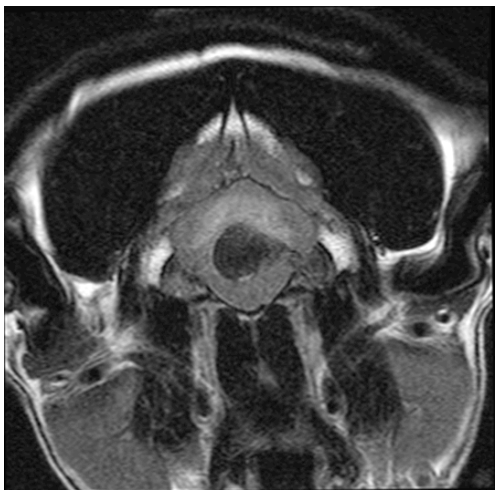

Figure 13.6 - FLAIR transverse image of the cyst-like lesion at the level of the 4th ventricle

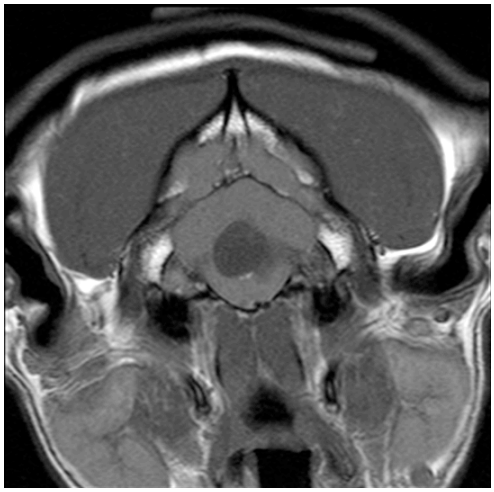

Figure 13.7 - T1w transverse image of the cyst-like lesion at the level of the 4th ventricle

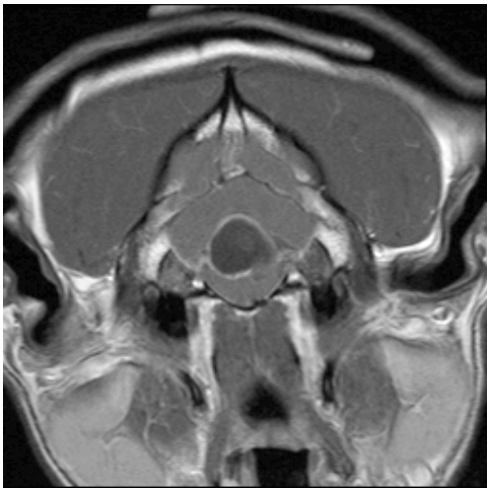

Figure 13.8 - T1w transverse post-contrast image of the cyst-like lesion at the level of the 4th ventricle showing peripheral enhancement

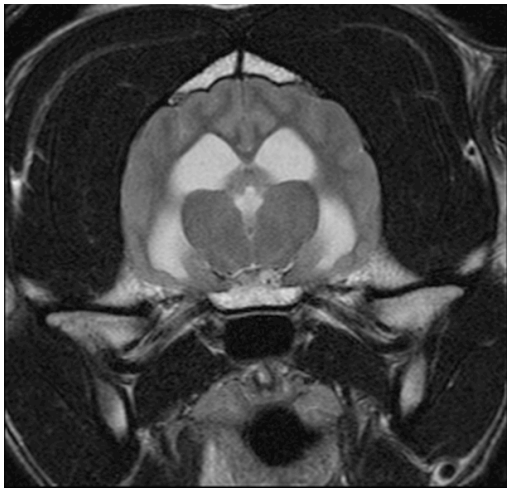

Figure 13.9 - T2w transverse image showing moderate dilation of the lateral ventricles

Case 14. Oesophageal Foreign Body

Signalment and History

A 7-year-old male neutered Cairn Terrier had started to regurgitate, have a reduced appetite and had been lethargic after having eaten a ham bone 1 week before presentation. The dog had been retching continually. Investigations had been done prior to referral to the Small Animal Hospital, University of Glasgow. No abnormality was detected on abdominal radiographs. Oesophagoscopy revealed a mass-like lesion in the distal oesophagus. The dog was fully vaccinated and wormed and had never been on any long-term medication.

Clinical Signs

a) Quiet but alert and responsive
b) Gulping
c) Increased abdominal component to breathing

Radiographic Examination

1. **Equipment** - See Appendix 1
2. **Restraint** - The dog was sedated. Positioning was achieved using wedges of dressing material, cradles and rope ties.

Area	View	kV	mAs	Grid
Thorax	Right Lateral (Fig.14.1)	63	9	O
	Dorso-Ventral (Fig.14.2)	63	9	O
Abdomen	Ventro-Dorsal (Fig.14.3)	66	7.1	O
	Right Lateral (Fig.14.4)	66	7.1	O

Radiographic Appraisal

The images are well processed. Both thoracic radiographs (Figs.14.1 and 14.2) are well centred and positioned. The cranial part of the abdomen and the diaphragm are missing on both abdominal views (Figs.14.3 and 14.4), otherwise the radiographs are well positioned. A radio-opaque band is visible perpendicular to the length of the view on the ventro-dorsal radiograph of the abdomen (Fig14.3), at the level of L6, associated with the presence of a thinner one more caudally. These changes are consistent with a superposition of the borders of the cradle positioning device. Primary markers are present on all views, although secondary right markers have been added to the thoracic radiographs. Exposure settings have been added on all radiographs, although 2 different exposure settings are visible on the right lateral view of the thorax. The radiographs are of diagnostic quality.

Radiological Report

A large wedge shaped slightly heterogeneous soft tissue opacity, approximately 20x25mm, is visible, at the 7th intercostal space on the right lateral thoracic view (Fig14.2) dorsal to the caudal vena cava and superimposed onto the 8th-9th vertebral bodies on the dorso-ventral thoracic view (Fig.14.2). The location of this structure on both thoracic radiographs may suggest a caudal mediastinal location, including the distal oesophagus. A mild diffuse bronchial pattern is noted, consistent with the age or a mild chronic bronchitis. A moderate diffuse interstitial pattern is visible on the dorso-ventral view most likely consistent with the expiratory status.

A mild to moderate volume of gas is visible in the stomach and some small intestinal loops, without dilation.

New bone formation is visible at the ventral aspect of the vertebral bodies from T4 to T6, consistent with moderate spondylosis. Mild irregular margins of the caudal aspect of one humeral head are visible, consistent with mild degenerative changes, likely incidental.

Differential Diagnosis

Regarding the shape and location, an oesophageal foreign body is most likely. Differential diagnosis includes oesophageal abscess, granuloma or neoplastic process but a more rounded shape might be expected, and the history tends to rule these out. A focus of pneumonia or a pulmonary foreign body, abscess, granuloma or neoplastic process is considered less likely.

Further Investigations

Haematology revealed a mild neutrophilia and monocytosis.

Biochemistry showed a mild reduction in urea, presumed secondary to reduced appetite.

Outcome

The dog underwent a further oesophagoscopy. A fragment of bone was removed from the distal oesophagus. Following removal, inspection of the oesophagus showed some haemorrhages at the site. Post-removal treatment included omeprazole (10mg PO SID for 7 days) and Peptac® liquid (Ivax - Sodium bicarbonate/Sodium alginate/Calcium carbonate - 3ml PO TID for 7 days, 1 hour prior to feeding) and to be fed soft food.

Discussion

Oesophageal foreign bodies are reputed to be relatively common in dogs. However, these represented less than 0.09% of the emergency presentations in one study[1] and

about 0.4% of the canine hospital population in another one[2]. These reports suggest that oesophageal foreign bodies are not that common.

Dogs presenting with oesophageal foreign bodies are most frequently small breeds under 10kg (from 62[1] to 84[3] % depending on the study), with Terriers (e.g. West Highland White Terrier, Yorkshire Terriers) being overrepresented. However, large breeds may also be encountered[2]. Dogs are generally young to middle age.

Bones are the most common oesophageal foreign bodies reported in dogs, followed by cartilage and rawhide[1], although fish hooks, dental chew treat[3], toys, balls, wooden sticks[5] or other pieces of plastic or metal may be found.[1,2,3,4,5]

Common clinical signs include ptyalism, retching, gagging, regurgitation or vomiting, anorexia, odynophagia, dysphagia, respiratory distress, cough and lethargy.[1,2,3,4,5] Occasionally, dogs show no clinical signs, and are presented as emergency cases because they have been seen ingesting foreign material.[1,2] The severity of the clinical signs depends on type and size of the foreign body, its location, the duration of obstruction, and the presence or absence of secondary aspiration pneumonia, oesophageal stricture or wall perforation with subsequent paraoesophageal abscess, pleuritis, mediastinitis, pneumomediastinum or pneumothorax. The gap between ingestion and presentation can vary from hours to weeks, although the time to presentation from onset clinical signs is generally less than 1 day.[1,2] Oesophageal foreign bodies are generally definitively detected or highly suspected on lateral chest radiographs, as a radiopaque structure (soft tissue, bone or metallic opacities) relatively well-defined, more or less geometrical in shape. However, small and non-radiopaque foreign bodies may be difficult to identify on survey radiographs and may require a positive contrast oesophagram[1,5]. However, if endoscopy is available the use of barium is contraindicated, as the barium will limit visualization. The most commonly reported location is the caudal oesophagus between the heart base and diaphragm (in 59[1] to 74[3] % of the cases). Further sites include the cranial oesophagus just caudal to the pharynx, the thoracic inlet and the heart base.[1,2,3,4] Other radiographic signs may include gas within the oesophagus, which can contrast with the foreign body, oesophageal dilation, most of the time orad to the obstructing material, evidence of aspiration pneumonia and rarely signs of oesophageal perforation, encompassing pneumomediastinum, pneumothorax or mediastinal/pleural effusion.

Given the possible complications, oesophageal foreign bodies can become life threatening and removal should be done promptly. Preferentially, per oral removal is achieved using rigid or flexible endoscope, with the aid of large rigid grasping forceps

or endoscopic grasping forceps, or the foreign body can be pushed into the stomach with the endoscope or a rigid stomach tube. The majority of dogs are generally successfully treated with endoscopy alone, with a median rate of oral removal of 78%[3]; however the skill of the operator to handle the endoscope is an important component of the success rate. Gastrotomy can be secondary performed if the foreign body is thought be at risk of causing gastrointestinal obstruction after being pushed into the stomach. Indications for transthoracic oesophagotomy retrieval include immovable foreign body, high risk of causing or worsening perforation of the oesophagus by attempting removal and the presence of a large oesophageal perforation or necrotic area.[4] However, it has been reported that oesophageal perforations up to 12mm may heal spontaneously and that a delayed surgical repair of 48 to 72 hours following perforation has higher mortality rates than if managed non-surgically with medical therapy alone.[4] In contrast a recent study[4] shows an overall survival rate of 93% following oesophagotomy retrieval of foreign bodies. Fluoroscopic guidance removal has also been described[2].

Reported complications associated with oesophageal foreign bodies include oesophagitis (most common), oesophageal tear, aspiration pneumonia, and oesophageal stricture formation. Less common and more severe complications include pneumothorax, pneumomediastinum, pleural effusion, pleuritis, mediastinitis, mediastinal or paraoesophageal abscess, pyothorax, haemothorax, pneumonitis, broncho-oesophageal fistula, aorto-oesophageal fistula, cardiopulmonary arrest and death.[1,2,3,4,6] The complication rate of oesophageal foreign body removal varies between 8 to 38%.[2] Repeat chest radiographs, positive contrast oesophagram[1,2] or the use of endoscopic ultrasonography[6] may help to assess further complications after oesophageal foreign body removal. Dogs with a longer duration of clinical signs, longer anaesthesia times and foreign bodies located in the caudal oesophagus are more likely to have moderate or severe oesophagitis.[1] An association between increased risk of complications, death or euthanasia and bone or dental chew treat foreign bodies, bodyweight under 10kg and duration of the foreign body for more than 3 days has been described.[2] A mortality rate of approximately 10% has been reported, but long-term complications after foreign body removal are uncommon.[1,2,4,5]

References

1-Thompson HC, Cortes Y, Gannon K, Bailey D, Freer S. Esophageal foreign bodies in dogs: 34 cases (2004-2009). **J Vet Emerg Crit Care** 2012; 22(2): 253-261.

2-Gianella P, Pfammatter NS, Burgener IA. Oesophageal and gastric endoscopic foreign body removal: complications and follow-up of 102 dogs. **J Small Anim Pract** 2009; 50(12): 649-654.

3-Leib MS, Sartor LL. Esophageal foreign body obstruction caused by a dental chew treat in 31 dogs (2000-2006). **J Am Vet Med Assoc** 2008; 232(7): 1021-1025.

4-Sale CS, Williams JM. Results of transthoracic esophagotomy retrieval of esophageal foreign body obstructions in dogs: 14 cases (2000-2004). **J Am Anim Hosp Assoc** 2006; 42(6): 450-456.

5-Burgos-Rodriguez AG, Forrester SD, Larson MM, Harper TA, Karnik PS. What is your diagnosis? Esophageal foreign body. **J Am Vet Med Assoc** 2003; 223(1): 43-44.

6-Gaschen L, Kircher P, Hoffmann G, Luckschander N, Schmoekel H, Spreng D, Lang J. Endoscopic ultrasonography for the diagnosis of intrathoracic lesions in two dogs. **Vet Radiol Ultrasound** 2003; 44(3): 292-299.

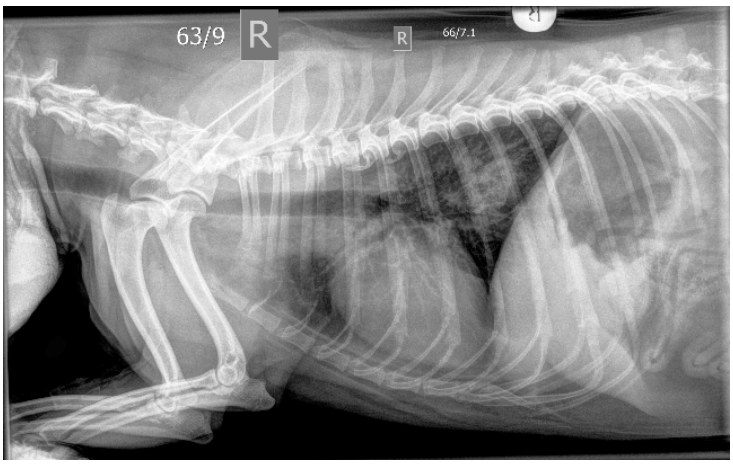

Figure 14.1 - Right lateral thoracic radiograph

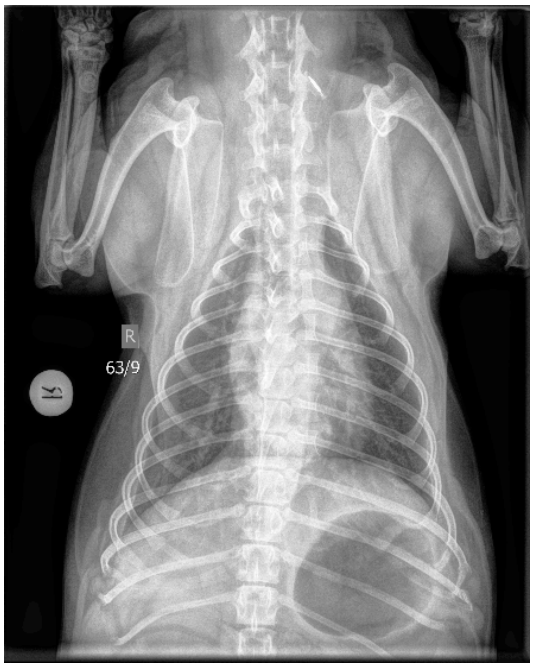

Figure 14.2 - Dorso-ventral thoracic radiograph

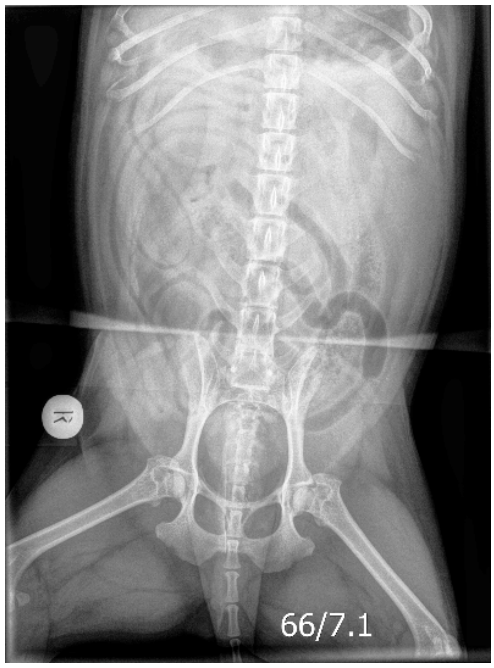

Figure 14.3 - Ventro-dorsal abdominal radiograph

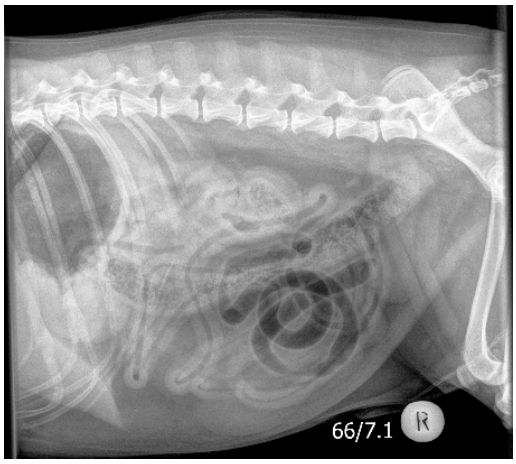

Figure 14.4 - Right lateral abdominal radiograph

Case 15. Bilateral Radial Hemimelia

Signalment and History

A 5-month-old male Domestic Short Hair was born with bilateral forelimb deformities associated with marked medial curvature of the antebrachia. The hind limbs appeared normal. The cat used to sit very upright, and could stand on two hind legs like a biped. The owner reported that the cat seemed to be adapting to walk on its elbows, but as it grew, some black areas had developed on the skin around carpus. A kink in its tail was also reported.

Clinical Signs

a) Possibly slight enlarged submandibular lymph nodes
b) Deformities of forelimbs – marked bilateral carpal varus
c) Deformities of the tail

Radiographic Examination

1. **Equipment** - See Appendix 1
2. **Restraint** - The cat was sedated. Positioning was achieved using wedges of dressing material.

Radiographic Appraisal

Only the lateral views of both radii are available (Figs.15.1 and 15.2), which limited the assessment of the humero-ulnar and ulno-carpal joints. The distal interphalangeal joints of the left forelimb are not in the primary beam. A marked rotation of both legs is noted, most likely linked to the abnormality. The digits of one limb are present in the beam of the left forelimb radiograph. Otherwise the radiographs are relatively well centred. Primary markers are present. Exposure setting has not been added on radiographs. The radiographs are diagnostic, though cranio-caudal views may have allowed a better assessment.

Radiological Report

No radius is present. A small radiopaque ill-defined area is visible distal to the left distal humeral epiphysis and cranially to the proximal ulna, which could be consistent with radial hypoplasia with the presence of a small portion of the left proximal radius (Fig.15.2). The proximal part of both ulnae has caudal bowing and the distal diaphyses are widened, with a thickening of the cranial cortex and a moderate sclerosis of the distal metaphysis. A slight cranio-distal displacement of both distal humeral epiphyses

relative to the proximal ulnae is consistent with humero-ulnar subluxation. Bilateral varus deviation of carpii is noted, associated with a mild medio-proximal displacement of the carpii relative to the ulnae and a rotation of both carpii around the longitudinal axis, more marked on the right side. A bilateral agenesis of the first digit is noted. A marked surrounding soft tissue swelling is visible, especially around the ulna-carpal joints.

Diagnosis

Bilateral pre-axial longitudinal intercalary radial hemimelia, associated with bilateral first digit agenesis.

Outcome

The cat was discharged with recommendation to be kept indoors, preferably in padded surfaces and beddings. Follows up were performed 1 and 3 months later to consider possible surgical treatment. The owner reported that the cat had a very good quality of life and was very playful. His weight bearing had improved, the cat being less plantigrade, and no obvious skin damage was present around his carpi or forearms. Surgical intervention was judged unnecessary at this stage.

Discussion

Pre-axial longitudinal intercalary radial hemimelia is the most common type of hemimelia in dogs and cats.[1] Hemimelia is a dysostosis, a congenital bone dysmorphology, characterised by the complete or partial absence of one or more bones of the limbs. All appendicular bones can be affected, and many different permutations of this condition have been recognized. Hemimelia is called “terminal” if all or part of the middle and distal bones of a limb are absent. It is called “intercalary” if all or parts of the middle bones of a limb are absent. These two main groups can be subdivided into “longitudinal hemimelia”, which indicates the absence of one or more bones along the pre-axial (medial) or post-axial (lateral) side of a limb, and “transverse hemimelia”, which refers to the complete absence of bone across the limb’s width.[1,2,3]

Radial hemimelia suggests an abnormality in the development of the medial ray of the limb bud, which is responsible for the formation of the radius, middle carpal bones, and the first digit. During the early stages of foetal development, somatic mesodermal cells, which take part in the origin of muscle, connective tissue and bone, migrate to and multiply beneath the surface ectoderm, resulting in bulges on the embryos surface called limb buds. After limb bud formation, the surface ectoderm thickens at the apex of each

limb bud to form a specialised zone, the apical ectodermal ridge that directs development of the bud. Elongation and further development of the presumptive limb are largely regulated by the continued interaction between the apical ectodermal ridge and underlying mesoderm. The localised lack of interaction between the apical ectodermal ridge and the mesodermal cells ultimately results in a failure of bone to develop in that region.[1,2]

Radial hemimelia is usually noticed soon after birth. This condition is usually unilateral, although a bilateral absence may be encountered. Typical clinical signs in affected animals include forelimb shortening, marked varus deformity of the ulna-carpal joint and caudal bowing of the ulna with flexion deformity associated with limited range of motion of the humero-ulnar and ulno-carpal joints. The gait of these animals is abnormal as they walk with the entire forearm in contact with the floor. No pain is usually noted unless arthritis or fracture secondary to the malformation is present. A severe muscle atrophy and muscle contraction over the entire length of the forelimb can also be noted, due to the flexor muscles being not balanced by extensor muscles.[2,3]

Radiographs of the affected limb may be used to confirm the diagnosis. The entire radius or part of it is absent and parts of the ulna are sometimes missing as well. Other radiographic findings include varus deformity of the ulno-carpal joint, shortening and caudal curvature of the ulna associated with enlargement of its diameter, humero-ulnar joint subluxation, absence of the radial carpal bone, first digit agenesis, and metacarpal synostosis.[1,2,3]

Treatment options are directed to prevent muscle contracture and atrophy, bone deformity and joint ankylosis and improve the animal's quality of life.[1,2] An early reduction of limb deformity by stabilisation of the ulno-carpal joint in a normal weight bearing position by means of a fortified Robert Jones bandage is recommended in animals younger than 4 to 5 months.[1] Additional conservative or surgical treatment may be considered, if the limb function is not acceptable after splinting. Conservatively treated animals, consisting of supportive care, usually have a good quality of life. Surgical treatment may consist of declawing of selected digits to prevent injury, reconstruction (ulno-carpal arthrodesis, bone graft to fill the skeletal defect, humero-ulnar arthrodesis, corrective ulnar osteotomy), or amputation (in case of unilateral condition).[1,2,3,4]

Multiple congenital abnormalities may be associated with radial hemimelia such as polydactyly[2] and vertebral abnormalities[3]. The heritability of radial hemimelia has been

suggested but *in utero* environmental causes are another possible cause of congenital radial hemimelia.[1,2,3]

References

1-Towle HAM, Breur GJ. Dysostoses of the canine and feline appendicular skeleton. **J Am Vet Med Assoc** 2004; 225(11): 1685-1692.

2-Lockwood A, Montgomery R, McEwen V. Bilateral radial hemimelia, polydactyly and cardiomegaly in two cats. **Vet Comp Orthop Traumatol** 2009; 22(6): 511-513.

3-Pisoni L, Cinti F, Del Magno S and Joechle M. Bilateral radial hemimelia and multiple malformations in a kitten. **J Feline Med Surg** 2012; 14(8): 598-602.

4-Rahal SC, Volpi RS, Ciani RB, Vulcano LC. Use of the Ilizarov method of distraction osteogenesis for the treatment of radial hemimelia in a dog. **J Am Vet Med Assoc** 2005; 226(1): 65-68.

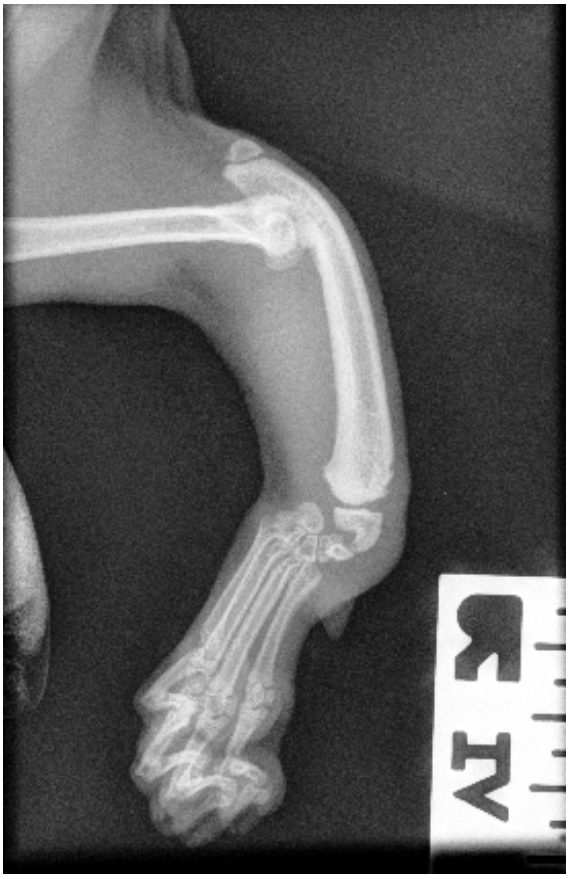

Figure 15.1 - Medio-lateral radiograph of the right forearm

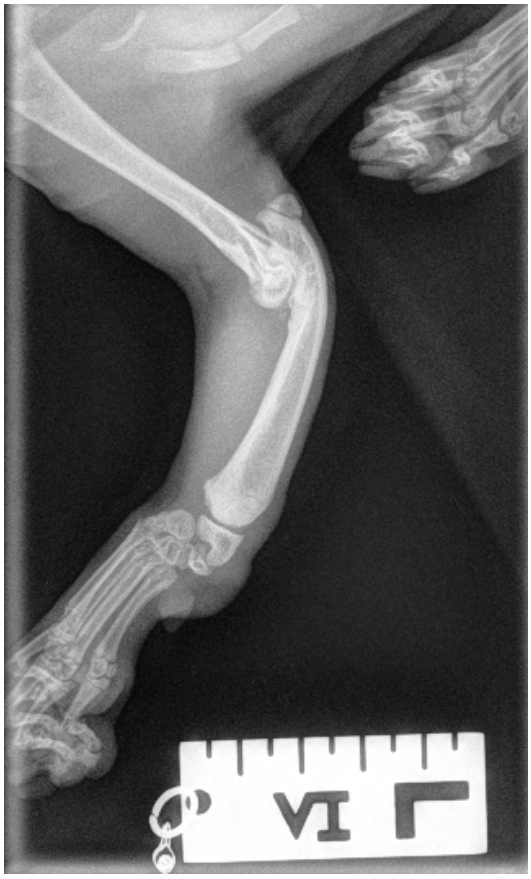

Figure 15.2 - Medio-lateral radiograph of the left forearm

Appendix

Appendix 1 - Diagnostic Imaging Equipment

The images come from the equipment of the Small Animal Hospital, University of Glasgow - see above.

Radiography

Siemens Multix Top Digital XR

Ultrasound

Logic E9, General Electric Healthcare, 5 to 8 MHz multi-frequency probe.

Computed tomography

Siemens Somatom Spirit dual slice CT Scanner

Magnetic resonance imaging

Siemens Magnetom Essenza 1,5 Tesla MRI Scanner

Fluoroscopy

C-Arm Philips BV Libra